Studies on intermolecular interaction of acetic acid: hydrogen-bonding and charge-transfer interaction in neat liquid, aqueous solutions, and gas phase clusters with benzene cations

Doctoral Dissertation

by

Kentaroh KOSUGI

Department of Structural Molecular Science

School of Mathematical and Physical Science

The Graduate University for Advanced Studies

2000

Abstract

Intermolecular interaction is a principal subject of chemistry for understanding the nature of substances and chemical reactions. For example, hydrogen-bonding interactions in such as O-H···O, N-H···O and N-H···N pairs are very important as well as hydrophobic interaction in structural biology. In recent years, other types of intermolecular interactions are recognized to play important roles in biological macromolecules. It is found that not only the typical hydrogen bonds that involve electronegative nitrogen and oxygen atoms but also the C-H···O hydrogen bond must be considered in the determination of protein structures. In addition to the C-H···O hydrogen bond, intermolecular interaction between a positively charged ion and an electron rich organic molecule (cation-π interaction) is frequently seen on the protein surfaces which is exposed to aqueous solvation effecting on the protein structures. Charge transfer is an essential factor in an accurate description of the cation-π interaction. These studies suggest that quantitative understanding of the charge transfer interactions between fundamental molecules of biological importance is indispensable particularly for the study of protein structures and functions.

Carboxyl group is a common functional group in living bodies. It is contained in numbers of biologically important molecules; therefore a deep understanding of many biological phenomena should be based on the knowledge on the intermolecular interaction of carboxylic groups with each

other or with other molecules. It is known that molecules with carboxylic groups show specific hydrogen-bonding interactions with each other or with other hydrogen-donating or -accepting molecules. Intermolecular interaction of acetic acid has long been studied as a prototype system of carboxylic compounds. Because acetic acid has four hydrogen-donor sites (a hydroxyl hydrogen and three methyl hydrogens) and two acceptor sites (a hydroxyl oxygen and a carbonyl oxygen) in a molecule, various kinds of hydrogen-bondings can be expected in various situations. In addition to the hydrogen bond formation, non-bonding orbitals of acetic acid can interact with virtual orbitals of positive charged ions as electron-donors.

In order to understand the nature of intermolecular interaction of carboxyl group, the present study is devoted to investigating the structures of liquid acetic acid, acetic acid aqueous solutions, and acetic acid-benzene cation complexes.

In chapter II, liquid structure of acetic acid is studied experimentally and theoretically. Experimentally, Raman spectra of acetic acid at various temperatures between 287 and 348 K are measured in the region of 15–3700 cm^{-1}. Theoretically, ab initio molecular orbital calculations are performed on the Raman activities of seven cluster species of acetic acid molecules. The Raman spectrum (in $R(\bar{\nu})$ representation) of crystalline acetic acid at 287 K shows six distinct bands in the 15–300 cm^{-1} region. These bands broaden on the melting of the crystal, while their peak positions remain almost unchanged on the melting. These spectral changes are reproduced in the case that the liquid spectrum mainly arises from a variety of sizes of

chain clusters as the fragments of the crystalline networks. The C=O stretching band becomes broadened toward higher wavenumbers and exhibits an asymmetric shape with increasing temperature. The wavenumbers calculated for the C=O stretching vibrations suggest that the strongly hydrogen-bonded C=O groups of the chain clusters show the prominent C=O band and its asymmetric shape is due to the presence of weakly hydrogen-bonded C=O groups of the same cluster species. The spectral analyses in both the low-wavenumber and the C=O stretching regions suggest that liquid acetic acid is mainly composed of the chain clusters, not the cyclic dimer. Assignments of the low-frequency Raman bands observed in the vapor and crystalline states are discussed on the basis of the calculated wavenumbers.

In chapter III, liquid structures of acetic acid aqueous solutions are studied using Raman spectroscopy and ab initio molecular orbital calculation. With the addition of water into liquid acetic acid, the C=O stretching vibration band of acetic acid shows high frequency shift from 1665 cm^{-1} to 1715 cm^{-1}. This means that the hydrogen-bond of the C=O group of acetic acid is not so strong as those seen in liquid acetic acid or in CCl_4 solution (in which the band appears at 1668 cm^{-1}). A bent type hydrogen-bond is accountable for this observation. On the other hand, the increase of acetic acid in water drastically decreases the intensity of the hydrogen-bonded O-H stretching Raman band of water at 3200 cm^{-1}. This suggests that acetic acid breaks the hydrogen-bond networks of water. Low frequency $R(\bar{\nu})$ spectra of acetic acid/water binary solutions are reexamined with new experimental

data and ab initio molecular orbital analysis of intermolecular vibrational modes. The $R(\bar{\nu})$ spectrum of the aqueous mixture at $x_A = 0.5$ bears a very close resemblance to that of the acetic acid/methanol mixture with $x_A = 0.5$, indicating that the molecular complexes responsible to the Raman spectra are acetic acid clusters. The calculated low-frequency Raman feature of a side-on type dimer with bent-type hydrogen-bonds based on ab initio molecular orbital theory reproduces the observed Raman pattern nicely. Any evidence of the formation of stable acid-water pairs is not found in the low frequency Raman spectra. Furthermore, an isosbestic point is seen in the region of $0.1 \leq x_A$ (mole fraction of acetic acid) ≤ 0.5, and another one is also observed in $0.5 \leq x_A \leq 1.0$. The observed spectra in the region of $0 < x_A < 0.5$ are reproduced simply by linear combinations of the pure water spectrum and the spectrum at $x_A = 0.5$. These results strongly suggest the presence of the two microphases with homogeneously associated molecules: a water cluster phase and an acetic acid cluster phase. The spectral change in $0.5 < x_A < 1.0$ is attributed to the coexistence of the acetic acid cluster phase in aqueous environment and the acid associated phase characteristic of liquid acetic acid.

The author demonstrates geometrical and electronic structures of acetic acid-benzene cation complex, $(CH_3COOH)\cdot(C_6H_6)^+$, experimentally and theoretically in chapter IV. Experimentally, a vibrational spectrum of $(CH_3COOH)\cdot(C_6H_6)^+$ in the supersonic jet is measured in the 3000-3680 cm^{-1} region using an ion-trap photodissociation spectrometer. An electronic spectrum is also observed with this spectrometer in the 12000-29600 cm^{-1}

region. Theoretically, ab initio molecular orbital calculations are performed for geometry optimization and evaluation of vibrational frequencies and electronic transition energies. The vibrational spectrum shows two distinct bands in the O-H stretching vibrational region. The frequency of the strong band (3577 cm^{-1}) is close to that of the O-H stretching vibration of acetic acid (3583 cm^{-1}) and the weak one is located at 3617 cm^{-1}. On the basis of geometry optimizations and frequency calculations, the strong band is assigned to the O-H stretching vibration of the *cis*-isomer of acetic acid in the hydrogen-bonded complex (horizontal *cis*-isomer). The weak one is assigned to the vertical *trans*-isomer where the *trans*-isomer of acetic acid interacts with the π-electron system of the benzene cation. The weakness of the high frequency band in the photodissociation spectrum is attributed to the binding energy larger than the photon energy injected. Only hot vertical *trans*-isomers can be dissociated by the IR excitation. The electronic spectrum exhibits two bands with intensity maxima at 17500 cm^{-1} and 24500 cm^{-1}. The calculations of electronic excitation energies and oscillator strengths suggest that charge transfer bands of the vertical *trans*-isomer can be observed in this region in addition to a local excitation band of the horizontal *cis*-isomer. The 17500 cm^{-1} band is attributed to the charge transfer transition of the vertical *trans*-isomer and the 24500 cm^{-1} band is assigned to the π-π transition of the horizontal *cis*-isomer. The calculations also suggest that the charge transfer is induced through the intermolecular C$\cdots$O=C bond formed between a carbon atom of benzene and the carbonyl oxygen atom of acetic acid.

In chapter V, geometrical structures of acetic acid monomer-benzene dimer cation cluster, $(CH_3COOH)\cdot(C_6H_6)_2^+$, and acetic acid dimer-benzene dimer cation cluster, $(CH_3COOH)_2\cdot(C_6H_6)_2^+$, are investigated. A vibrational spectrum of $(CH_3COOH)\cdot(C_6H_6)_2^+$ in the supersonic jet is measured in the 2800-3700 cm^{-1} region using the ion-trap photodissociation spectrometer. An electronic spectrum of this cluster cation is also observed with this spectrometer and a time-of-flight type spectrometer in the 6000-24500 cm^{-1} region. For $(CH_3COOH)_2\cdot(C_6H_6)_2^+$, vibrational and electronic spectra are observed in the regions of 2740-3700 cm^{-1} and 6000-27000 cm^{-1}, respectively. In order to clarify the assignment of vibrational bands, vibrational spectra of the deuterated cluster cations, $(CD_3COOD)\cdot(C_6H_6)_2^+$ and $(CD_3COOD)_2\cdot(C_6H_6)_2^+$, are measured. The electronic spectrum of $(CH_3COOH)\cdot(C_6H_6)_2^+$ show a broad and strong band in the near-IR region and another band at 22750 cm^{-1}. This spectral feature resembles that of benzene dimer cation, $(C_6H_6)_2^+$ which has a strong charge resonance (CR) band in the near-IR region and a local excitation (LE) band with an absorption cross section one order smaller than the CR band. This fact suggests that the ion core of $(CH_3COOH)\cdot(C_6H_6)_2^+$ is $(C_6H_6)_2^+$. In the vibrational spectrum of $(CH_3COOH)\cdot(C_6H_6)_2^+$, a strong band is located at 3084 cm^{-1} and two weak bands are observed at 3585 and 3627 cm^{-1}. From comparison between the vibrational spectra of $(CH_3COOH)\cdot(C_6H_6)_2^+$ and $(CD_3COOD)\cdot(C_6H_6)_2^+$, the strong band is assigned to the C–H stretching vibration of $(C_6H_6)_2^+$. As mentioned above, the frequency of the free O–H stretching vibration of acetic acid monomer in the gas phase is 3583 cm^{-1}.

Thus, the band at 3585 cm^{-1} is assigned to the free O–H stretching vibration of the *cis*-isomer of acetic acid in $(CH_3COOH)\cdot(C_6H_6)_2^+$. The band at 3627 cm^{-1} is attributed to the O–H stretching vibration of the *trans*-isomer of acetic acid, because its frequency is predicted to be 51 cm^{-1} (without scaling) higher than that of the *cis*-isomer at the CASSCF(4,3)/6-31G(d,p) level. In the electronic spectrum of $(CH_3COOH)_2\cdot(C_6H_6)_2^+$, CR and LE bands are also observed. Therefore, the ion core of $(CH_3COOH)_2\cdot(C_6H_6)_2^+$ is $(C_6H_6)_2^+$. The vibrational spectrum of $(CH_3COOH)_2\cdot(C_6H_6)_2^+$ show very broad band from 3400 cm^{-1} to 2740 cm^{-1} with several peaks and no band is observed in the free O–H stretching vibrational region. On the basis of the vibrational spectrum of $(CD_3COOD)_2\cdot(C_6H_6)_2^+$ measured in the present study and the reported IR spectrum of the cyclic dimer of acetic acid in argon matrix, the vibrational spectrum of $(CH_3COOH)_2\cdot(C_6H_6)_2^+$ is regarded as a superposition of those of $(C_6H_6)_2^+$ and the acetic acid cyclic dimer. This indicates that $(C_6H_6)_2^+$ weakly interacts with the cyclic dimer of acetic acid in $(CH_3COOH)_2\cdot(C_6H_6)_2^+$.

Contents

Abstract iii
Contents xi

CHAPTER I General introduction 3
I.A. Preface 5
I.B. Scope for chapters 8

CHAPTER II Liquid structure of acetic acid studied by Raman spectroscopy and ab initio molecular orbital calculations 13
II.A. Introduction 15
II.A.1. C–H···O hydrogen bond 15
II.A.2. Crystal structure of acetic acid 18
II.A.3. Liquid structure of acetic acid 22
II.A.4. Aims of the present study 24
II.B. Experimental 25
II.C. Computational Details 27
II.D. Results 28
II.D.1. Calculated structures and hydrogen-bonded energies of cluster species 28
II.D.2. Observed low-frequency Raman spectra 44
II.D.3. Calculated low-frequency Raman spectra 49
II.D.4. Observed Raman spectra in intramolecular mode region 55
II.D.5. Calculated vibrational frequency of C=O stretching modes 59
II.E. Discussion 61
II.E.1. Calculated hydrogen-bonding energies of cluster species: cooperative interactions 61
II.E.2. $R(\bar{\nu})$ representation of Raman spectra of acetic acid: comparison between low-frequency vibrations of liquid and those of crystalline 63
II.E.3. Comparison between observed low-frequency Raman spectra and those calculated for dimer species and crystalline-like chain clusters 66
II.E.4. Comparison between observed and calculated Raman spectra in the C=O stretching retion 72
II.F. Conclusion 76

CHAPTER III Raman spectroscopic study on acetic acid clusters in aqueous solutions: dominance of acid-acid association producing microphases 83
III.A. Introduction 85
III.A.1. Microphases in binary solutions 85
III.A.2. Liquid structure of acetic acid aqueous solutions 87
III.A.3. Aims of the present study 88
III.B. Experimental 89
III.C. Computational Details 90
III.D. Results 91
III.D.1. Raman spectra in the C=O stretching vibrational region 92
III.D.2. Raman spectra in the O–H and C–H stretching vibrational region 95
III.D.3. Low-frequency Raman spectra 97
III.D.4. Ab initio molecular orbital calculations 101
III.E. Discussion 106
III.E.1. Spectral shifts of Raman-active intramolecular vibrations 106
III.E.2. Low-frequency Raman spectra 113
III.E.3. Analysis of low-frequency spectra 118
III.E.4. Hydrophobic hydration 122
III.E.5. Three-state model and density change 124
III.E.6. Rayleigh wing spectra and microphase formation 126
III.F. Conclusion 131

CHAPTER IV Charge transfer interaction in acetic acid-benzene cation complex . 137
IV.A. Introduction 139
IV.A.1. Photodissociation spectroscopy 139
IV.A.2. Benzene monomer ion 142
IV.A.3. Charge transfer cation complexes of aromatic molecules 145
IV.A.4. Aims of the present study 147
IV.B. Experimental 149
IV.C. Computational details 152
IV.D. Results 154
IV.D.1. Observed vibrational spectrum 154
IV.D.2. Calculated structures and binding energies at the CASSCF(7,7)/6-31G(d,p) level 157

IV.D.3. Calculated structures and binding energies at the B3LYP/6-31G(d,p) level 167
IV.D.4. Calculated frequencies and IR intensities of the C-H and O-H stretching vibrations at the B3LYP/6-31G(d,p) level 169
IV.D.5. Observed electronic spectrum 171
IV.D.6. Calculated electronic states 173
IV.E. Discussion 183
IV.E.1. Geometrical structures of $(CH_3COOH)\cdot(C_6H_6)^+$ isomers 183
IV.E.1.1. Assignment of vibrational spectrum in the C–H stretching region 183
IV.E.1.2. Assignment of vibrational spectrum in the O–H stretching region 185
IV.E.1.3. Energetic and geometrical differences among cluster species 187
IV.E.1.4. Comparison between the CASSCF and DFT calculations 191
IV.E.1.5. Comparison between calculated and observed vibrational spectra 193
IV.E.2. Electronic states of $(CH_3COOH)\cdot(C_6H_6)^+$ isomers 195
IV.E.2.1. Assignment of electronic spectrum 195
IV.E.2.2. Comparison between calculated and observed electronic spectra 196
IV.F. Conclusion 199

CHAPTER V Photodissociation spectroscopic study on $(CH_3COOH)\cdot(C_6H_6)_2^+$ and $(CH_3COOH)_2\cdot(C_6H_6)_2^+$ in the gas phase 209
V.A. Introduction 211
V.A.1. benzene cluster ions 211
V.A.2. Aims of the present study 214
V.B. Experimental 215
V.C. Results 219
V.C.1. Electronic spectrum of $(CH_3COOH)\cdot(C_6H_6)_2^+$ 219
V.C.2. Vibrational spectrum of $(CH_3COOH)\cdot(C_6H_6)_2^+$ 221
V.C.3. Electronic spectrum of $(CH_3COOH)_2\cdot(C_6H_6)_2^+$ 224
V.C.4. Vibrational spectrum of $(CH_3COOH)_2\cdot(C_6H_6)_2^+$ 226
V.D. Discussion 229
V.D.1. Structure of $(CH_3COOH)\cdot(C_6H_6)_2^+$ 229
V.D.2. Structure of $(CH_3COOH)_2\cdot(C_6H_6)_2^+$ 233
V.E. Conclusion 238

Studies on intermolecular interaction of acetic acid: hydrogen-bonding and charge-transfer interaction in neat liquid, aqueous solutions, and gas phase clusters with benzene cations

Doctoral Dissertation

by

Kentaroh KOSUGI

Department of Structural Molecular Science

School of Mathematical and Physical Science

The Graduate University for Advanced Studies

2000

CHAPTER I

General introduction

I.A. Preface

Intermolecular interaction is a principal subject of chemistry for understanding the nature of substances and chemical reactions; intermolecular interaction governs how molecules align themselves in substances and how molecules come closer and collide in chemical reactions. In addition to the chemical importance, understanding of biological phenomena in molecular level requires knowledge of intermolecular interaction. For example, hydrogen-bonding interactions in such as O–H···O, N–H···O and N–H···N pairs are very important as well as hydrophobic interaction in structural biology. Hydrogen bonds play pivotal structural and functional roles in biological macromolecules. They are the key to many phenomena such as the formation and stabilization of secondary structure, protein folding and stability, molecular recognition, and enzymatic reactions.

In recent years, other types of intermolecular interactions are also recognized to play important roles in biological macromolecules. It is found that not only the typical hydrogen bonds that involve electronegative nitrogen and oxygen atoms but also the C–H···O hydrogen bond must be considered in the determination of protein structures. This study in the biological field can be motivated by the progress in structural chemistry. The concept of the C–H···O hydrogen bond was not familiar to chemists before 1982. In order to explain the boiling and melting points that is higher than those expected, the concept of the C–H···O hydrogen bond had

been proposed. However, there had been controversy because of lack of systematical investigation based on observed data. On the basis of analysis of great number of neutron diffraction crystal structures, the existence of C–H···O hydrogen bond in crystalline is shown in 1982. Today, there is a consensus that C–H···O hydrogen bonds have significant implications in many diverse areas of structural chemistry.

In addition to the C–H···O hydrogen bond, intermolecular interaction between a positively charged ion and an electron rich organic molecule (cation-π interaction) is becoming important in the last decade. The cation-π interaction is frequently seen on the protein surfaces which is exposed to aqueous solvation effecting on the protein structures. Charge transfer is an essential factor in an accurate description of the cation-π interaction. These studies suggest that quantitative understanding of the charge transfer interactions between fundamental molecules of biological importance is indispensable particularly for the study of protein structures and functions.

Carboxyl group is a common functional group in living bodies. It is contained in numbers of biologically important molecules; therefore a deep understanding of many biological phenomena should be based on the knowledge on the intermolecular interaction of carboxylic groups with each other or with other molecules. It is known that molecules with carboxylic groups show specific hydrogen-bonding interactions with each other or with other hydrogen-donating or -accepting molecules. Intermolecular interaction of acetic acid has long been studied as a prototype system of carboxylic compounds. Because acetic acid has four hydrogen-donor sites (a

hydroxyl hydrogen and three methyl hydrogens) and two acceptor sites (a hydroxyl oxygen and a carbonyl oxygen) in a molecule, various kinds of hydrogen-bondings can be expected in various situations. In addition to the hydrogen bond formation, non-bonding orbitals of acetic acid can interact with virtual orbitals of positive charged ions as electron-donors.

In the present study, we investigate intermolecular interaction of acetic acid by spectroscopic methods and ab initio molecular orbital calculation in view of the C–H···O hydrogen-bonding and the charge transfer interaction. Liquid structures of neat acetic acid, acetic acid aqueous solutions are studied by Raman spectroscopy and ab initio molecular orbital calculations. Intermolecular interactions of acetic acid with the benzene monomer and dimer cations in gas phase are also investigated by photodissociation spectroscopy and ab initio molecular orbital calculations. More detailed information of the present study is mentioned in the following section.

I.B. Scope for chapters

In order to understand the nature of intermolecular interaction of carboxyl group, the present study is devoted to investigating the structures of liquid acetic acid, acetic acid aqueous solutions, and acetic acid-benzene cation complexes.

In chapter II, liquid structure of acetic acid is studied experimentally and theoretically. Experimentally, Raman spectra of acetic acid at various temperatures between 287 and 348 K are measured in the region of 15–3700 cm^{-1}. In addition to liquid acetic acid, we observe the intermolecular and intramolecular vibrational spectra of crystalline acetic acid by Raman spectroscopy, and discuss the similarity in band positions of the spectra of liquid and crystalline acetic acid. Theoretically, ab initio molecular orbital calculations are performed on the Raman activities of seven cluster species of acetic acid molecules including fragments of the crystalline structure of acetic acid. We compare the observed and calculated Raman spectra and discuss the liquid structure that is responsible for the observed vibrational spectra.

In chapter III, liquid structures of acetic acid aqueous solutions are studied using Raman spectroscopy and ab initio molecular orbital calculation. We measure both the intermolecular and intramolecular vibrational spectra of acetic acid aqueous solutions with various mole fractions of acetic acid, x_A, between 0 (pure water) and 1 (pure liquid acetic acid) by Raman spectroscopy. In addition to the analysis of the observed spectra, we perform ab initio

molecular orbital calculations and obtain optimized geometries, dipole moments, vibrational frequencies, and Raman intensities of four dimer species. On the basis of these observed spectra and calculated values, we discuss the liquid structure of acetic acid aqueous solution and show the microphase formation in this system.

In chapter IV, the author demonstrates geometrical and electronic structures of acetic acid-benzene cation complex, $(CH_3COOH)\cdot(C_6H_6)^+$, experimentally and theoretically. Experimentally, a vibrational spectrum of $(CH_3COOH)\cdot(C_6H_6)^+$ in the supersonic jet is measured in the 3000-3680 cm^{-1} region using an ion-trap photodissociation spectrometer. An electronic spectrum is also observed with this spectrometer in the 12000-29600 cm^{-1} region. Theoretically, ab initio molecular orbital calculations are performed for geometry optimization and evaluation of vibrational frequencies and electronic transition energies. In order to obtain information on the intermolecular interaction that is dominant in this system, we discuss the geometrical structure of $(CH_3COOH)\cdot(C_6H_6)^+$ on the basis of the vibraitonal spectrum, calculated binding energies and vibrational frequencies. Next, the electronic structure of $(CH_3COOH)\cdot(C_6H_6)^+$ is investigated by comparing the observed and calculated electronic spectra.

In chapter V, geometrical structures of acetic acid monomer-benzene dimer cation cluster, $(CH_3COOH)\cdot(C_6H_6)_2^+$, and acetic acid dimer-benzene dimer cation cluster, $(CH_3COOH)_2\cdot(C_6H_6)_2^+$, are investigated. A vibrational spectrum of $(CH_3COOH)\cdot(C_6H_6)_2^+$ in the supersonic jet is measured in the 2800-3700 cm^{-1} region using the ion-trap photodissociation spectrometer.

An electronic spectrum of this cluster cation is also observed with this spectrometer and a time-of-flight type spectrometer in the 6000-24500 cm^{-1} region. For $(CH_3COOH)_2 \cdot (C_6H_6)_2^+$, vibrational and electronic spectra are observed in the regions of 2740-3700 cm^{-1} and 6000-27000 cm^{-1}, respectively. In order to clarify the assignment of vibrational bands, vibrational spectra of the deuterated cluster cations, $(CD_3COOD) \cdot (C_6H_6)_2^+$ and $(CD_3COOD)_2 \cdot (C_6H_6)_2^+$, are measured. First, the ion cores of these cluster cations are investigated. Next, the geometrical structures of the cluster cations are discussed.

CHAPTER II

Liquid structure of acetic acid studied by Raman spectroscopy and ab initio molecular orbital calculations

This chapter is based on Chem. Phys. Lett. **291**, 253 (1998)

and J. Phys. Chem. **103**, 8595 (1999).

II.A. Introduction

II.A.1. C–H···O hydrogen bond

The concept of a C–H···O hydrogen bond has become more and more important for our understanding of how molecules align themselves in crystals [1] and how protein structures are stabilized [2]. In 1937, Glasstone suggested that complexes of haloforms with ketones (X_3C–H···O=C<) have a definite existence. [3] Jeffrey correlated the relatively high melting point of dimethyl oxalate (54°C) with methyl carbonyl interactions in the crystal. [4] Pauling observed that the boiling point of acetyl chloride (51°C) is substantially higher than that of trifluoroacetyl chloride (<0°C). He attributed this discrepancy to hydrogen bond formation even though the expected hydrogen-bonding groups are not present. [5] Sutor assumed a van der Waals distance of 2.6 Å for the H···O contact and claimed that C–H···O hydrogen bonds exist in caffeine (H···O, 2.07 Å), theophylline (2.25 Å), and other compounds. [6,7] Donohue, however, argued that the 2.6-Å value was inappropriate. Quoting Ramachandran's values for "normally allowed" (2.4 Å) and "outer limit" (2.2 Å) O···H distances [8], he claimed that no special bonding effects are needed to explain Sutor's C–H···O geometries. An article by Cohen on the structural chemistry of quinines hints that C–H···O bond strengths need not be well-correlated with O···H distances and identifies C–H···O interactions as "lateral" in crystal structures of planar molecules. [9]

A landmark study by Taylor and Kennard in 1982 provided conclusive evidence of the existence of C–H···O hydrogen bonds in crystals. [10] These authors showed that C–H···O contacts are electrostatic and that they occur within certain distance (C···O, 3.0–4.0 Å) and angle (C–H···O, 90–180°) ranges. Desiraju identified these directional preferences in several crystal structures of planar oxygenated compounds. [11] The choice between several competing packing arrangements of these planar compounds may be understood only by a consideration of the directional properties of weak C–-H···O bonds present in these structures.

Today, there is a consensus that C–H···O bonds have significant implications in many diverse areas of structural chemistry. Thousands of crystal structures must contain short C···O distances, many of which could arise from C–H···O bonds, because of the frequent occurrence of oxygen in organic compounds. The significance of the C–H···O interaction in a particular structure increases with the number relative to the stronger O–-H···O and N–H···O interactions. Further, the energy of the C–H···O bond (1–2 kcal/mol) is just in the range where it can compete with conformational forces in small molecules and with forces responsible for the three dimentional structure of macromolecules. Accordingly, a preferred molecular conformation in an organic solvent may yield to an unfavorable conformation in aqueous media because of additional C–H···O stabilization, while an appropriate C–H···O bond may clinch the site of protein folding.

In the field of molecular biology, the concept of the C–H···O hydrogen bond became important following crystallographic studies mentioned above.

Hydrogen bonds are a major feature of protein structure. The biological importance of hydrogen bonds, which play pivotal structural and functional roles in macromolecules, cannot be overemphasized. [12] They are the key to many phenomena, including the formation and stabilization of secondary structure [13], protein folding and stability [14,15], molecular recognition [16], and enzymatic reactions which utilize general acid and general base catalysis, involving the transfer of protons along very specific trajectories [17,18]. In 1995, Derewenda and his co-workers find strong evidence that a large percentage of short C···O contacts constitute cohesive interactions by analyzing the short C–H···O interactions in a sample of known protein structures representing different categories of tertiary folds. [2] Moreover, the stereochemical study of C–H···O=C contacts reveals that these interactions exhibit stereochemical features typical of hydrogen bonds.

II.A.2. Crystal structure of acetic acid

The crystal structure of acetic acid has been studied using X-ray and neutron diffraction techniques since the middle of twentieth century [19-21]. In 1958, Jones and Templeton first observed X-ray diffraction of a single crystal of acetic acid at 278 K and reported that the acetic acid molecules are hydrogen-bonded into roughly planar chains in the crystalline state [19]. The crystal structure that involve C–H···O=C and O–H···O=C hydrogen bonds is depicted in Figure II-1. In their study, the lengths of the single and double bonds between carbon and oxygen atoms are 1.29 Å and 1.24 Å, respectively, while the length of the single bond between two carbon atoms is 1.54 Å. The C–C–O, C–C=O and O=C–O angles are determined to be 115.6°, 122.3° and 122.1°, respectively. The difference between the C–O and C=O distances is only 0.05 Å. According to the studies of compounds with unionized carboxyl groups, it was pointed out that the difference is usually at least 0.1 Å [22]. In early 1970's, two groups reinvestigated the crystal structure of acetic acid by means of X-ray and neutron diffraction [20, 21]. The geometrical parameters were redetermined in the respective studies. However, the infinite chain structure was supported by both of these reinvestigations. Nahringbauer redetermined the bond lengths and the angles from two sets of three-dimensional single-crystal X-ray data collected at 278 K and 83 K [20]. In his study, the two carbon-oxygen distances are significantly different; the C–O bond length is 1.318 Å and that of the C=O bond is 1.220 Å at 278 K. Corresponding bond lengths at 83 K are 1.319 Å

and 1.229 Å. The C–C bond is relatively short, being 1.482 Å at 278 K and 1.478 Å at 83 K. The C–C–O, C–C=O and O=C–O angles are determined to be 113.8°, 124.2° and 122.0° at 278 K. Corresponding angles at 83 K are 113.8°, 125.1° and 121.1°. The intermolecular distance between the carbonyl oxygen and the hydroxyl oxygen is also reported to be 2.626 Å and 2.625 Å at 278 K and 83 K, respectively. These results have shown that the hydrogen bond lengths do not vary with the temperature, whereas minor changes occur in the packing of the hydrogen-bonded chains. Jönsson investigated the crystal structure of acetic acid based on three-dimensional neutron diffraction data recorded at 133 K [21]. The C–O, C=O and C–C lengths are 1.321 Å, 1.206 Å and 1.501 Å, respectively. Three C–H bond lengths of the methyl group is reported to be 1.050 Å, 1.052 Å and 1.078 Å. The O–H bond lengths of the hydroxyl group is 1.011 Å. The C–C–O, C–C=O and O=C–O angles are determined to be 113.8°, 124.9° and 121.9°. The intermolecular O···O distance is reported to be 2.631 Å. In addition, important intermolecular distances are determined from neutron diffraction data. The intermolecular distance between the carbonyl oxygen and the hydroxyl hydrogen is 1.642 Å. Those from the carbonyl oxygen to the methyl hydrogen and carbon are 2.409 Å and 3.429 Å, respectively. Although the distance between the carbonyl oxygen and the methyl group is longer than those of the O–H···O and N–H···O hydrogen bonds, Taylor and Kennard provided evidence for the existence of the C–H···O=C hydrogen bond by analyzing neutron diffraction data [10]. Ab initio and semiempirical molecular orbital studies on chain dimer that is the analog of the crystal

structure and the gas phase cyclic dimer with two O–H···O=C hydrogen bonds were reported by Turi and Dannenberg [23]. In their study, the hydrogen-bonding energies of the crystal chain dimer and the gas phase cyclic dimer are –11.8 and –6.0 kcal/mol at the MP2/6-31G(d,p) level after correction for both basis set superposition error and zero-point vibrational energies. They suggest that cooperativity or interactions in the second and third dimensions are important to determining the crystal structure. According to their study, the hydrogen-bonding enthalpy of a C–H···O bond is about 0.5–1.0 kcal/mol, while that of a simple O–H···O is 4.7 kcal/mol.

Formic acid is also shown to form similar infinite chains in the crystalline state [10], but other carboxylic acid, such as propionic and monofluoroacitic acids, exist in the cyclic dimers as in the gas phase [24-26].

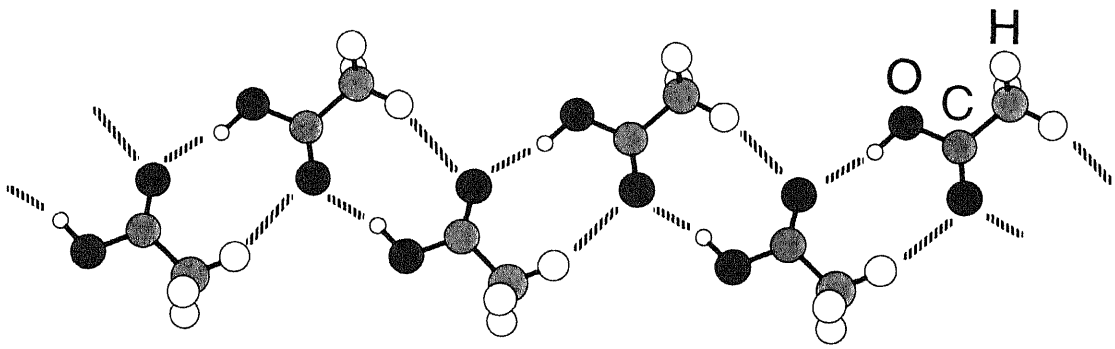

Figure II-1. Orientation of acetic acid molecules in the crystalline network structure

II.A.3. Liquid structure of acetic acid

The liquid structure of acetic acid is also considered to be determined mainly by hydrogen-bonding interactions. Information on the liquid structure is, however, more limited than that on the gas and the crystalline network structures, which can be derived from electron and X-ray diffraction measurements, respectively. Bertagnolli and Hertz have performed neutron and X-ray diffraction measurements on liquid acetic acid [27, 28]. They found the remarkable constancy of the hydrogen-bond length as the substance passes from the crystalline to the liquid state [27]. Comparison of the simulated results based on the crystal-like cyclic dimer structure and the chain structure existing in the crystalline state suggested that the cyclic dimer structure yields a better description of the structure of liquid acetic acid [28]. However, other structures, such as chain "fragments" of the crystalline networks, were not treated in the report [28].

Low-frequency vibrational spectroscopy is very useful for studies of local structures of solution systems, since it directly probes intermolecular vibrational bands. Far-IR and low-frequency Raman spectra of liquid acetic acid have been observed by several groups [29-33]. Waldstein and Blatz observed the low-frequency Raman spectra of liquid acetic acid and suggested that the cyclic dimers are predominant structures in the liquid state [30]. Their analysis was based on the normal coordinate calculations with empirical force constants [33]. Nielsen and Lund [31] assigned the three distinctive peaks of the Raman spectrum of the liquid to the three

fundamental modes of the cyclic dimer by means of depolarization ratios, isotope effects, and the calculations with empirical force fields [33-36]. Their assignments, however, were based on the assumption that all the bands observed in the liquid spectra arise from the cyclic dimer. To the best of our knowledge, no one has analyzed the low-frequency Raman spectra of acetic acid on the basis of the calculations for the chain fragments of the crystalline networks.

II.A.4. Aims of the present study

Although low-frequency Raman spectra of liquid acetic acid have been reported and it has been suggested that the cyclic dimer are predominant structures in the liquid phase, none of these spectra has been analyzed on the basis of the calculations for the chain fragments of the crystal structure, as mentioned above. Is it true that the whole intermolecular bonding that associates acetic acid molecules drastically changes with melting? To reinvestigate the liquid structure of acetic acid in view of the chain fragment of the crystal structure seems to be worth doing. In the present study, the structure of liquid acetic acid is reinvestigated experimentally and theoretically. To make complete analyses of not only intermolecular but also intramolecular vibrations, we examine the Raman spectra of acetic acid in a wide wavenumber region of 15-3700 cm^{-1}. We also perform ab initio molecular orbital calculations on the Raman spectra of some different cluster species of acetic acid molecules. The Raman band intensities of the cluster species are compared with the observed spectra to clarify the structure of liquid acetic acid.

II.B. Experimental

Spectroscopy grade acetic acid was purchased from Wako Pure Chemical Co. and used without further purification. Sample solutions were sealed in Φ = 6 mm Pyrex glass tubes after degassing of carbon dioxide by repeating the freezing and evacuation. Crystalline samples were grown in tapered glass tubes in a commercial refrigerator. Silicon rubber heaters wound on the sealed glass tube were used for the temperature control. The temperature of the sample was monitored by a thermocouple placed ≈ 1 mm down from the laser point. The Raman spectra were obtained with the 514.527 nm line from an Ar^+ ion laser (NEC). The Raman-scattered light at 90° was analyzed by an NR-1800 Raman spectrometer (JASCO) equipped with a triple monochromator and a thermoelectrically cooled photomultiplier tube (Hamamatsu Photonics R943-02) as shown in Figure II-2. The incident laser was linearly polarized, and neither a polarizer nor a polarization scrambler was used to keep the throughput of the spectrometer as high as possible. Polarization dependency of the sensitivity of the spectrometer was separately examined by using the Raman bands of carbon tetrachloride and cyclohexane and was found to be less than 10 %. The average power of the exciting light was ≈ 150 mW at the sample.

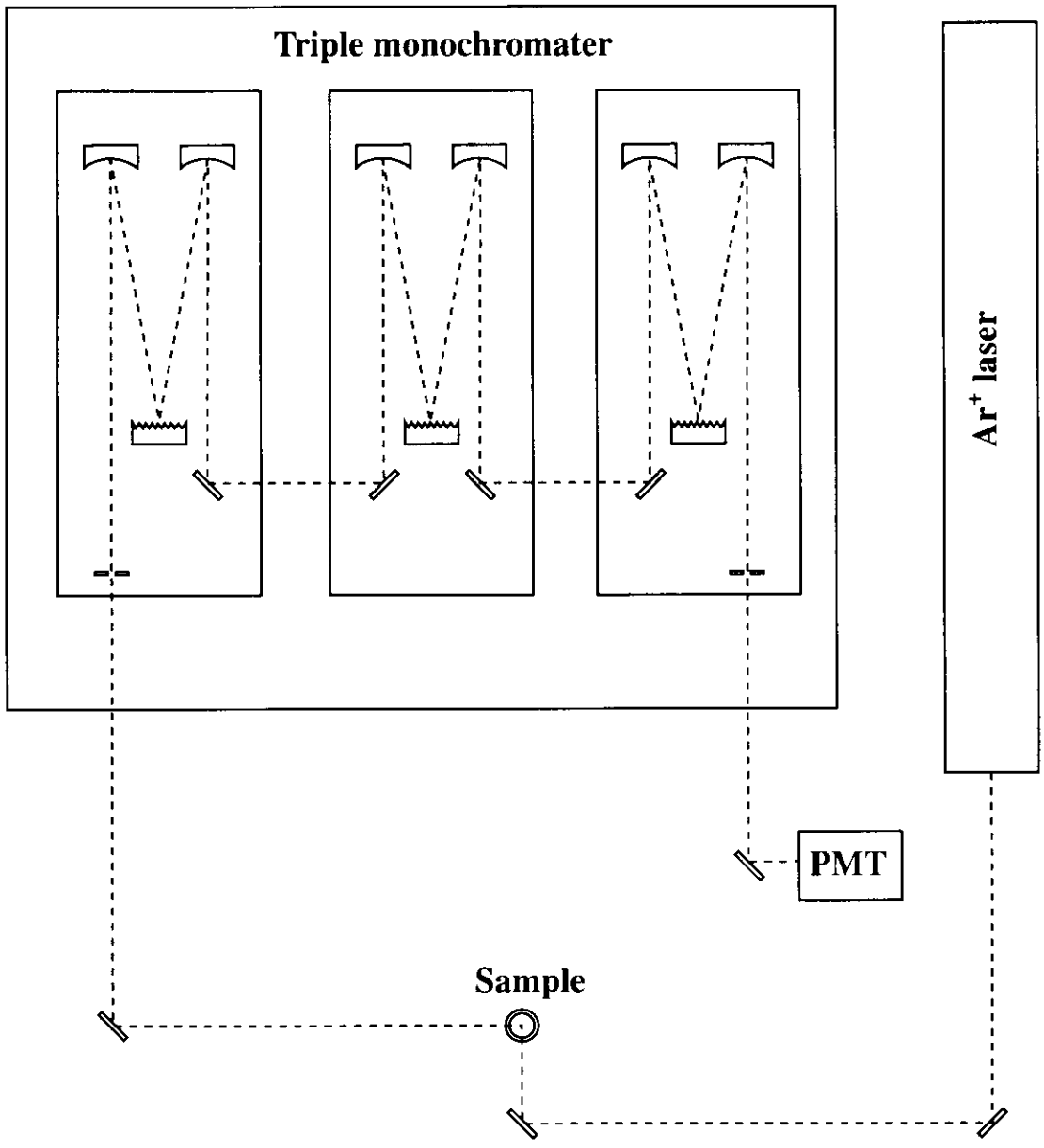

Figure II-2. Schematic diagram of Raman spectrometer equipped with a triple monochromator and a thermoelectrically cooled photomultiplier tube.

II.C. Computational Details

Ab initio MO calculations were performed by using the Gaussian 94 program package [37] on a DEC workstation (AlphaStation 500). All the calculations were carried out at the Hartree-Fock (HF) level. The 6-31G(d,p) basis set was employed. The 6-31++G(d,p) basis set, which contains one set of diffuse functions on all the atoms, was also employed except for pentamer.

At the HF level, the acetic acid molecules were optimized to have a C_s plane containing the heavy atoms and one of the methyl hydrogen at the side of the C=O group. The other two methyl hydrogens are located symmetrically above and under the carboxylic plane. A planar structure of C_s symmetry was assumed for each cluster species. Force calculations confirmed convergence to the minima on the potential energy surface because the wavenumbers of all the modes were real for the optimized structures of the monomers and the cluster species.

II.D. Results

II.D.1. Calculated structures and hydrogen-bonded energies of cluster species

The structures of the cluster species treated in this study are shown in Figure II-3. Two conformers must be considered for acetic acid: the hydroxyl hydrogen and the carbonyl oxygen be in the same side (*cis)* and the opposite side (*trans*). The ab initio MO calculations predict that *cis*-isomer of acetic acid is more stable than *trans*-isomer by 7.0 kcal/mol at the HF/6-31++G(d,p) level. Such an energy difference may arise from a weak internal hydrogen bond between the hydroxyl hydrogen and the carbonyl oxygen in the *cis* form. Since the *cis*-isomers are observed in both the gas and crystalline phases as dominant structures, the *trans*-isomers are considered not to be so important in the liquid state. Hence only the cluster species of the *cis*-isomers are treated in this study.

Four dimer species are taken into account for the calculation, all of which contain two intermolecular hydrogen bonds. Dimer 1 contains two O–H···O=C hydrogen bonds and has C_{2h} symmetry. This dimer is dominant in the gas phase at temperatures below 150°C [38, 39] and is called the cyclic dimer as mentioned before. In dimer 2, one of the O–H···O=C hydrogen bonds in dimer 1 is replaced by a C–H···O=C hydrogen bond. This dimer can be regarded as the dimer unit of the chain structure in the crystal shown in Figure II-1. Dimer 3 contains one O–H···O=C hydrogen bond and one

additional intermolecular hydrogen bond between the acidic hydrogen and the oxygen atom of the OH group. This structure is suggested to be formed in aqueous solutions on the basis of several experimental facts [40-43]. Dimer 4 is a cyclic complex with two C–H···O=C hydrogen bonds and has C_{2h} symmetry. Various kinds of cluster species of acetic acid molecules can be formed in combination with these four dimer species. Trimer, tetramer, and pentamer, all of which structures are calculated as the chain fragments of the hydrogen-bonded networks of the crystal (Figure II-3).

Total energies of monomer and cluster species at the optimized geometries are shown in Table II-I. Values of zero-point vibrational energy (ZPVE) correction are listed in Table II-II. Total energies after ZPVE correction are also shown in Table II-I.

Total energies of acetic acid monomer are –227.822171 and –227.755443 hartree before and after ZPVE correction of 0.066729 hartree, respectively, at the HF/6-31G(d,p) level. Those calculated at the HF/6-31++G(d,p) level are –227.829486 and –227.762979 hartree before and after ZPVE correction of 0.066508 hartree, respectively.

As mentioned above, we performed geometry optimization and frequency calculation for four dimer species. The most stable dimer species is the cyclic dimer with two O–H···O=C hydrogen bonds, dimer 1. Total energies of dimer 1 are –455.681057 and –455.533134 hartree before and after ZPVE correction of 0.135905 hartree, respectively, at the HF/6-31G(d,p) level. Those calculated at the HF/6-31++G(d,p) level are –455.681057 and –455.545575 hartree before and after ZPVE correction of 0.135483 hartree,

respectively.

The dimer species that is the fragment of crystalline structure, dimer 2, is the second most stable with total energies of –455.658343 and –455.523143 hartree before and after ZPVE correction of 0.135200 hartree, respectively. At the HF/6-31++G(d,p) level, total energies of dimer 2 are –455.671431 and –455.536712 hartree before and after ZPVE correction of 0.134720 hartree, respectively.

The dimer species next to dimer 2 in total energy is dimer 3. Total energies of dimer 3 are –455.656067 and –455.521044 hartree before and after ZPVE correction of 0.135023 hartree, respectively, at the HF/6-31G(d,p) level. Those obtained at the HF/6-31++G(d,p) level are –455.668915 and –455.534353 hartree before and after ZPVE correction of 0.134562 hartree, respectively.

The least stable dimer species is dimer 4. Total energies of dimer 4 are –455.649703 and –455.515239 hartree before and after ZPVE correction of 0.134464 hartree, respectively, at the HF/6-31G(d,p) level. Those calculated at the HF/6-31++G(d,p) level are –455.663286 and –455.529358 hartree before and after ZPVE correction of 0.133928 hartree, respectively.

Total energies of crystalline fragment trimer cluster are –683.494903 and –683.291393 hartree before and after ZPVE correction of 0.203510 hartree, respectively, at the HF/6-31G(d,p) level. Those obtained at the HF/6-31++G(d,p) level are –683.513827 and –683.310999 hartree before and after ZPVE correction of 0.202828 hartree, respectively.

Total energies of crystal-like chain tetramer cluster are –911.331729 and

–911.059931 hartree before and after ZPVE correction of 0.271798 hartree, respectively, at the HF/6-31G(d,p) level. Those obtained at the HF/6-31++G(d,p) level are –911.356500 and –911.085571 hartree before and after ZPVE correction of 0.270929 hartree, respectively.

Total energies of crystal-like chain pentamer cluster are –1139.168621 and –1138.828547 hartree before and after ZPVE correction of 0.340074 hartree, respectively, at the HF/6-31G(d,p) level. Those obtained at the HF/6-31++G(d,p) level are –1139.199235 and –1138.860214 hartree before and after ZPVE correction of 0.339021 hartree, respectively.

Let us evaluate the strengths of intermolecular interactions of cluster species from hydrogen-bonding energy that is defined as difference between the total energy of the clusters and that of acetic acid monomer multiplied by the number of acetic acid molecule in the cluster. Table II-III shows hydrogen-bonding energies of acetic acid clusters on the basis of total energies listed in Table II-I. The most stable dimer species (dimer 1) has much the largest hydrogen-bonding energy among the four dimer species. The hydrogen-bonding energies of dimer 1 are 5421 cm^{-1} (15.50 kcal/mol) and 4883 cm^{-1} (13.96 kcal/mol) before and after ZPVE correction, respectively, at the HF/6-31G(d,p) level. Those obtained at the HF/6-31++G(d,p) level are 4847 cm^{-1} (13.86 kcal/mol) and 4305 cm^{-1} (12.31 kcal/mol).

The crystalline fragment dimer, dimer 2, has the second strongest intermolecular interaction. Its hydrogen-bonding energies are 3073 cm^{-1} (8.79 kcal/mol) and 2690 cm^{-1} (7.69 kcal/mol) before and after ZPVE correction, respectively, at the HF/6-31G(d,p) level. Those obtained at the

HF/6-31++G(d,p) level are 2734 cm^{-1} (7.82 kcal/mol) and 2360 cm^{-1} (6.75 kcal/mol). Thus the hydrogen-bonding energy of the crystal-like dimer is only 55% of that of the cyclic dimer.

The hydrogen-bonding energies of dimer 3 which has two O–H···O hydrogen bonds between the carboxyl group of one component acetic acid and the hydroxyl group of the other acetic acid are 2573 cm^{-1} (7.36 kcal/mol) and 2229 cm^{-1} (6.37 kcal/mol) before and after ZPVE correction, respectively, at the HF/6-31G(d,p) level. Those obtained at the HF/6-31++G(d,p) level are 2182 cm^{-1} (6.24 kcal/mol) and 1843 cm^{-1} (5.27 kcal/mol).

Dimer 4 has two C–H···O=C hydrogen bonds which is usually weaker than the O–H···O hydrogen bond. As expected, the hydrogen-bonding energy of dimer 4 is considerably smaller than other three dimer species mentioned above. Its hydrogen-bonding energies are 1177 cm^{-1} (3.36 kcal/mol) and 955 cm^{-1} (2.73 kcal/mol) before and after ZPVE correction, respectively, at the HF/6-31G(d,p) level. Those obtained at the HF/6-31++G(d,p) level are 947 cm^{-1} (2.71 kcal/mol) and 746 cm^{-1} (2.13 kcal/mol).

For crystal-like chain clusters the incremental hydrogen-bonding energy is defined as increase of hydrogen-bonding energy that accompanies addition of one acetic acid molecule and two hydrogen bonds and listed in Table II-IV. The hydrogen-bonding energy of the chain trimer is 6231 cm^{-1} (17.81 kcal/mol) before ZPVE correction at the HF/6-31G(d,p) level. After ZPVE correction, that is 5501 cm^{-1} (15.73 kcal/mol) at the same level. These values are 3158 cm^{-1} (9.02 kcal/mol) and 2811 cm^{-1} (8.04 kcal/mol) larger than those of the crystal-like dimer. The values obtained at the HF/6-31++G(d,p)

level are 5568 cm^{-1} (15.92 kcal/mol) and 4842 cm^{-1} (13.84 kcal/mol) and these are 2834 cm^{-1} (8.10 kcal/mol) and 2482 cm^{-1} (7.09 kcal/mol) larger than those of dimer 2.

The hydrogen-bonding energy of the chain tetramer is 9447 cm^{-1} (27.01 kcal/mol) before ZPVE correction at the HF/6-31G(d,p) level. After ZPVE correction, that is 8375 cm^{-1} (23.95 kcal/mol) at the same level. These values are 3216 cm^{-1} (9.20 kcal/mol) and 2874 cm^{-1} (8.22 kcal/mol) larger than those of the crystal-like dimer. The values obtained at the HF/6-31++G(d,p) level are 8462 cm^{-1} (24.19 kcal/mol) and 7386 cm^{-1} (21.12 kcal/mol) and these are 2894 cm^{-1} (8.27 kcal/mol) and 2544 cm^{-1} (7.28 kcal/mol) larger than those of dimer 2.

The hydrogen-bonding energy of the chain pentamer is 12678 cm^{-1} (36.25 kcal/mol) before ZPVE correction at the HF/6-31G(d,p) level. After ZPVE correction, that is 11266 cm^{-1} (32.21 kcal/mol) at the same level. These values are 3231 cm^{-1} (9.24 kcal/mol) and 2891 cm^{-1} (8.26 kcal/mol) larger than those of the crystal-like dimer. The values obtained at the HF/6-31++G(d,p) level are 11370 cm^{-1} (32.51 kcal/mol) and 9946 cm^{-1} (28.44 kcal/mol) and these are 2908 cm^{-1} (8.31 kcal/mol) and 2560 cm^{-1} (7.32 kcal/mol) larger than those of dimer 2.

Calculated dipole moments of optimized structures of acetic acid monomer and clusters are collected in Table II-V. The dipole moments of acetic acid monomer are calculated to be 1.8288 and 1.9706 debye at the HF/6-31G(d,p) and HF/6-31++G(d,p) levels, respectively. The dipole moment of dimer 1 and dimer 4 is zero at both the levels. In these dimer

species, one component molecule is equivalent to the other, therefore two dipoles cancel out. On the other hand, two component molecules of dimer 2 and dimer 3 are not equivalent, therefore total dipole moments are not zero. The dipole moments of dimer 2 are 1.4017 and 1.3030 debye at the HF/6-31G(d,p) and HF/6-31++G(d,p) levels, respectively. Those of dimer 3 are 3.8011 and 4.0107 debye and more than twice of the values of monomer. The dipole moments of the chain trimer, tetramer, and pentamer are 3.2030, 4.0307, and 5.7149 debye, respectively, at the HF/6-31G(d,p) levels. Those at the HF/6-31++G(d,p) level are 3.1443, 3.8161, and 5.5207 debye.

The optimized geometrical parameters of the monomer and the dimer species at the HF/6-31G(d,p) level are collected in Table II-VI. Those calculated at the HF/6-31++G(d,p) level are listed in Table II-VII.

Table II-VIII shows the optimized structures of the chain fragments characteristic of hydrogen-bonding interactions. To simplify the analyses of the optimized parameters of the chain clusters, the averaged values for the constituent acetic acid molecules are shown in this table.

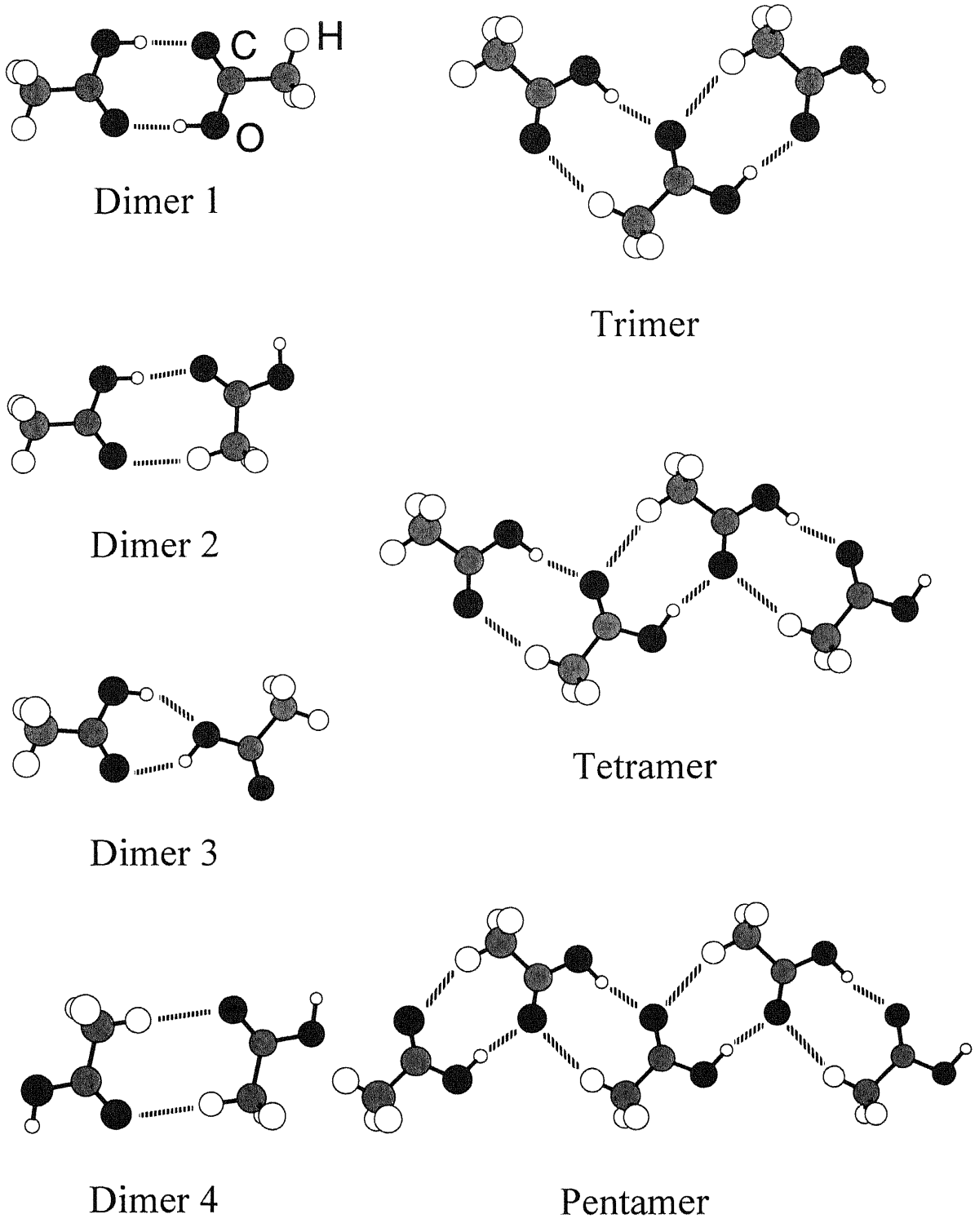

Figure II-3. Optimized geometries of acetic acid cluster species treated in this study.

TABLE II-I. Total energy of monomer and clusters of acetic acid

method		total energy / hartree	
		without corr.	after ZPVE
HF/6-31G(d,p)	monomer	–227.822171	–227.755443
	dimer 1	–455.669040	–455.533134
	dimer 2	–455.658343	–455.523143
	dimer 3	–455.656067	–455.521044
	dimer 4	–455.649703	–455.515239
	trimer	–683.494903	–683.291393
	tetramer	–911.331729	–911.059931
	pentamer	–1139.168621	–1138.828547
HF/6-31++G(d,p)	monomer	–227.829486	–227.762979
	dimer 1	–455.681057	–455.545575
	dimer 2	–455.671431	–455.536712
	dimer 3	–455.668915	–455.534353
	dimer 4	–455.663286	–455.529358
	trimer	–683.513827	–683.310999
	tetramer	–911.356500	–911.085571
	pentamer	–1139.199235	–1138.860214

TABLE II-II. Zero-point vibrational energy correction.

method		zero-point correction		
		/ hartree	/ cm^{-1}	/ kcal mol^{-1}
HF/6-31G(d,p)	monomer	0.066729	14645	41.873
	dimer 1	0.135905	29828	85.282
	dimer 2	0.135200	29673	84.839
	dimer 3	0.135023	29634	84.728
	dimer 4	0.134464	29512	84.377
	trimer	0.203510	44666	127.704
	tetramer	0.271798	59653	170.556
	pentamer	0.340074	74638	213.400
HF/6-31++G(d,p)	monomer	0.066508	14597	41.734
	dimer 1	0.135483	29735	85.017
	dimer 2	0.134720	29568	84.538
	dimer 3	0.134562	29533	84.439
	dimer 4	0.133928	29394	84.041
	trimer	0.202828	44516	127.276
	tetramer	0.270929	59463	170.012
	pentamer	0.339021	74407	212.739

TABLE II-III. Hydrogen-bonding energies of acetic acid aggregates.

	hydrogen-bonding energy			
	without correction		after ZPVE	
	/ cm^{-1}	/kcal mol^{-1}	/ cm^{-1}	/kcal mol^{-1}
HF/6-31G(d,p)				
dimer 1	5421	15.50	4883	13.96
dimer 2	3073	8.79	2690	7.69
dimer 3	2573	7.36	2229	6.37
dimer 4	1177	3.36	955	2.73
trimer	6231	17.81	5501	15.73
tetramer	9447	27.01	8375	23.95
pentamer	12678	36.25	11266	32.21
HF/6-31++G(d,p)				
dimer 1	4847	13.86	4305	12.31
dimer 2	2734	7.82	2360	6.75
dimer 3	2182	6.24	1843	5.27
dimer 4	947	2.71	746	2.13
trimer	5568	15.92	4842	13.84
tetramer	8462	24.19	7386	21.12
pentamer	11370	32.51	9946	28.44

TABLE II-IV. Incremental hydrogen-bonding energies of crystal-like chain clusters.

	incremental hydrogen-bonding energy			
	without correction		after ZPVE	
	/ cm^{-1}	/kcal mol^{-1}	/ cm^{-1}	/kcal mol^{-1}
HF/6-31G(d,p)				
trimer	–3158	–9.02	–2811	–8.04
tetramer	–3216	–9.20	–2874	–8.22
pentamer	–3231	–9.24	–2891	–8.26
HF/6-31++G(d,p)				
trimer	–2834	–8.10	–2482	–7.09
tetramer	–2894	–8.27	–2544	–7.28
pentamer	–2908	–8.31	–2560	–7.32

TABLE II-V. Dipole moment of optimized structures of monomer and clusters of acetic acid.

method		dipole moment / debye			
		X	Y	Z	Total
HF/6-31G(d,p)	monomer	–0.4711	–1.7671	0.0000	1.8288
	dimer 1	0.0000	0.0000	0.0000	0.0000
	dimer 2	1.3751	–0.2715	0.0000	1.4017
	dimer 3	0.4322	–3.7765	0.0000	3.8011
	dimer 4	0.0000	0.0000	0.0000	0.0000
	trimer	2.0294	–2.4781	0.0000	3.2030
	tetramer	–3.9124	0.9690	0.0000	4.0307
	pentamer	3.4928	–4.5233	0.0000	5.7149
HF/6-31++G(d,p)	monomer	–0.4074	–1.9280	0.0000	1.9706
	dimer 1	0.0000	0.0000	0.0000	0.0000
	dimer 2	1.2675	–0.3018	0.0000	1.3030
	dimer 3	0.4858	–3.9812	0.0000	4.0107
	dimer 4	0.0000	0.0000	0.0000	0.0000
	trimer	1.8181	–2.5654	0.0000	3.1443
	tetramer	–3.6928	0.9623	0.0000	3.8161
	pentamer	2.9673	–4.6555	0.0000	5.5207

TABLE II-VI. Calculated geometrical parameters[a] of acetic acid monomer and dimer species at the 6-31G(d,p) level.

Parameter	monomer	dimer 1	dimer 2 [b]		dimer 3 [c]		dimer 4
R(C=O)	1.187	1.201	1.193	1.196	1.195	1.185	1.190
R(C–O)	1.331	1.306	1.317	1.323	1.321	1.332	1.330
R(O–H)	0.948	0.962	0.957	0.949	0.952	0.956	0.948
R(C–C)	1.501	1.501	1.503	1.498	1.500	1.502	1.500
R(C–H) [d]	1.079	1.079	1.080	1.079	1.079	1.079	1.079
R(C–H) [e]	1.084	1.084	1.084	1.084	1.084	1.084	1.084
R(O···O) [f]		2.780	2.855			2.797	
R(O···O) [g]					2.960		
R(C···O) [h]				3.461			3.625
A(O–C=O)	122.36	123.60	123.59	121.24	123.03	122.52	121.74
A(C–C=O)	125.71	123.46	124.30	125.96	124.62	125.49	126.02
A(C–O–H)	108.25	111.05	110.80	108.69	110.02	111.04	108.27

[a] In units of angstrom (bond length) and degree (bond angle).

[b] First entry is the acetic acid molecule whose OH is the H-bond donor.

[c] First entry is the acetic acid molecule whose O=H is the H-bond acceptor.

[d] H is in the plane of the heavy atoms.

[e] H is out of the plane of the heavy atoms.

[f] Intermolecular O···O distance for the O–H···O=C hydrogen bond.

[g] Intermolecular O···O distance for the O–H···O–C hydrogen bond.

[h] Intermolecular C···O distance for the C–H···O=C hydrogen bond.

TABLE II-VII. Calculated geometrical parameters[a] of acetic acid monomer and dimer species at the 6-31++G(d,p) level.

Parameter	monomer	dimer 1	dimer 2 [b]		dimer 3 [c]		dimer 4
R(C=O)	1.189	1.203	1.195	1.197	1.196	1.187	1.192
R(C–O)	1.331	1.308	1.318	1.324	1.323	1.333	1.331
R(O–H)	0.949	0.962	0.958	0.949	0.952	0.956	0.948
R(C–C)	1.501	1.500	1.503	1.498	1.500	1.502	1.499
R(C–H) [d]	1.079	1.079	1.080	1.079	1.079	1.079	1.079
R(C–H) [e]	1.084	1.084	1.084	1.084	1.084	1.084	1.084
R(O···O) [f]		2.793	2.860			2.818	
R(O···O) [g]					2.999		
R(C···O) [h]				3.500			3.634
A(O–C=O)	122.16	123.28	123.23	121.20	122.70	122.39	121.69
A(C–C=O)	125.68	123.66	124.44	125.86	124.80	125.44	125.89
A(C–O–H)	108.93	111.28	111.08	109.23	110.30	111.34	108.86

[a] In units of angstrom (bond length) and degree (bond angle).

[b] First entry is the acetic acid molecule whose OH is the H-bond donor.

[c] First entry is the acetic acid molecule whose O=H is the H-bond acceptor.

[d] H is in the plane of the heavy atoms.

[e] H is out of the plane of the heavy atoms.

[f] Intermolecular O···O distance for the O–H···O=C hydrogen bond.

[g] Intermolecular O···O distance for the O–H···O–C hydrogen bond.

[h] Intermolecular C···O distance for the C–H···O=C hydrogen bond.

TABLE II-VIII. Averaged geometrical parameters[a] characteristic of hydrogen-bonding interaction in chain clusters of acetic acid.

Mothod	aggregate	R(C=O)	R(C–O)	R(O–H)	R(O···O)[b]	R(C···O)[c]
HF/6-31G(d,p)	dimer 2	1.195	1.320	0.953	2.855	3.461
	trimer	1.197	1.316	0.955	2.825	3.517
	tetramer	1.199	1.314	0.957	2.812	3.535
	pentamer	1.199	1.312	0.958	2.805	3.547
HF/6-31++G(d,p)	dimer 2	1.196	1.321	0.954	2.860	3.500
	trimer	1.199	1.317	0.956	2.829	3.557
	tetramer	1.200	1.315	0.957	2.816	3.577
	pentamer	1.201	1.313	0.958	2.807	3.591

[a] In units of angstrom (bond length) and degree (bond angle).

[b] Intermolecular O...O distance for the O-H···O=C hydrogen bond.

[c] Intermolecular C...O distance for the C-H···O=C hydrogen bond.

II.D.2. Observed low-frequency Raman spectra

Figure II-4 shows the low-frequency spectra of scattered light intensity ($I(\bar{\nu})$) for acetic acid taken at different temperatures around the melting point (289.8 K). Solid trace is the $I(\bar{\nu})$ spectrum observed at 287 K. Dotted trace shows the $I(\bar{\nu})$ spectrum at 288 K. Thick-dotted and thick-solid traces indicate the $I(\bar{\nu})$ spectra at 289 and 296 K, respectively. Both the spectra taken at 287 K and 288 K are due to crystalline acetic acid, the spectrum at 289 K to a mixture of solid and liquid acetic acid, and the spectrum at 296 K to liquid acetic acid. Although the range of the temperature difference is very small (less than 9 K), the features observed in the $I(\bar{\nu})$ spectra show marked changes with increasing temperature. In both the crystalline spectra taken at 287 and 288 K, we can see six distinct bands: three strong Raman peaks at 50, 124, and 181 cm^{-1}, weak two peaks at 78 and 90 cm^{-1}, and a shoulder at 41 cm^{-1}. The features of these two spectra are almost the same, although the intensity at the low-frequency tail (< 80 cm^{-1}) of Rayleigh scattering signal is slightly larger in the spectrum at 288 K. The intensity of the Rayleigh wing component of the mixture of solid and liquid acetic acid at 289 K increases in comparison with the crystalline spectra, while the peak intensities of the three strong Raman bands decrease eminently. In the liquid spectrum at 296 K, the Rayleigh wing component dramatically increases to make it difficult to distinguish the Raman bands from the Rayleigh background.

In order to obtain accurate information on low-frequency vibrations,

especially for the liquid spectra, we transform the $I(\bar{\nu})$ spectra into $R(\bar{\nu})$ spectra. The $R(\bar{\nu})$ spectra of acetic acid observed at 287, 288, 289, and 296 K are shown in Figure II-5.

Figure II-6 shows the temperature dependence of the $R(\bar{\nu})$ spectra of liquid acetic acid in the 15–400 cm^{-1} region. The intensity of each spectrum is normalized to the peak-intensity of the band at 50 cm^{-1}. The intensities of the bands at 120 and 170 cm^{-1} relative to the band at 50 cm^{-1} increase and show small shifts to lower wavenumbers as the temperature grows.

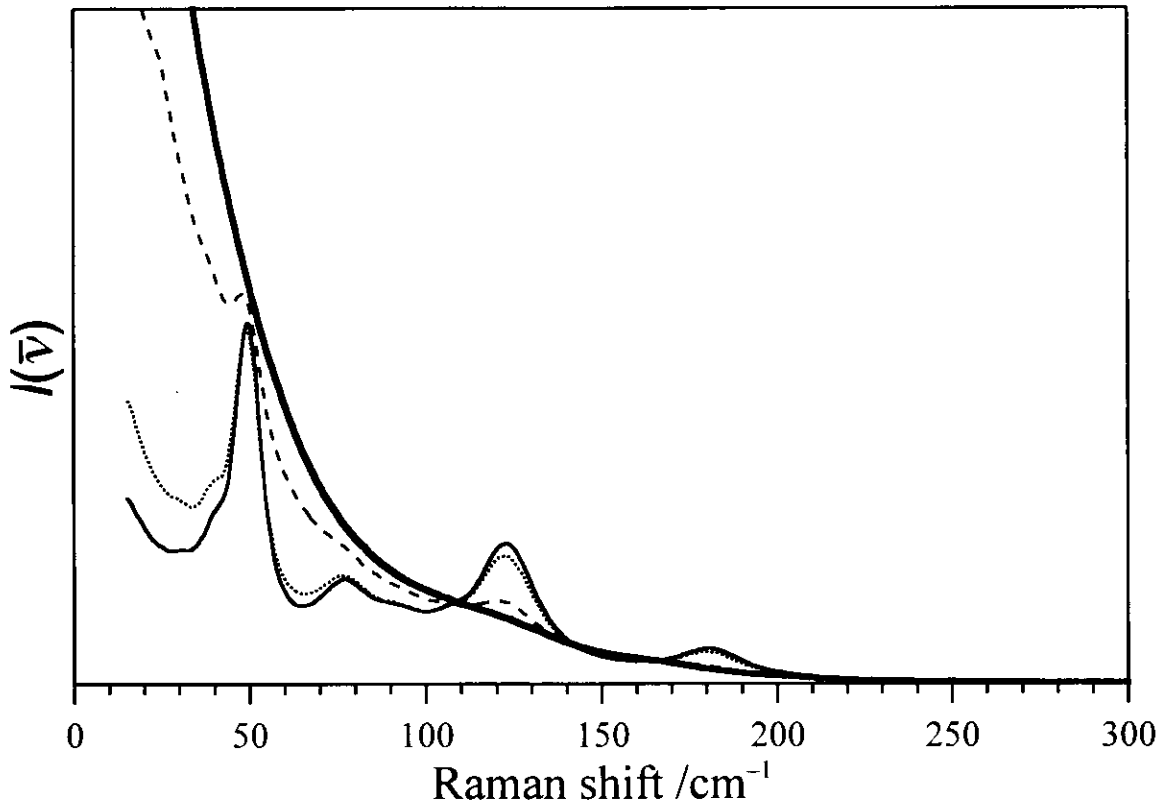

Figure II-4. Raman spectra of acetic acid in the 15-300 cm^{-1} region in $I(\bar{\nu})$ representaiton at didferent temperatures: solid trace, 287 K; dotted trace, 288 K; thick-dotted trace, 289 K; thich-solid trace, 296 K.

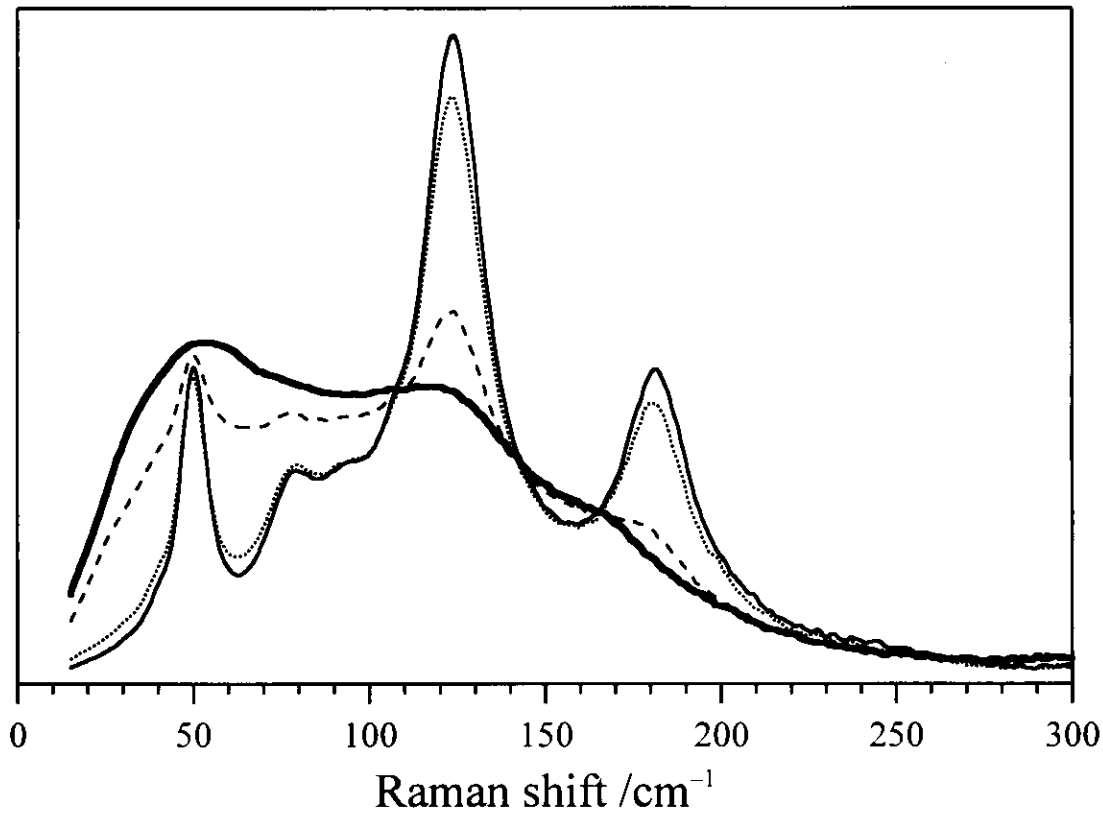

Figure II-5. Raman spectra of acetic acid in the 15-300 cm^{-1} region in $R(\bar{\nu})$ representaiton at didferent temperatures: solid trace, 287 K; dotted trace, 288 K; thick-dotted trace, 289 K; thich-solid trace, 296 K.

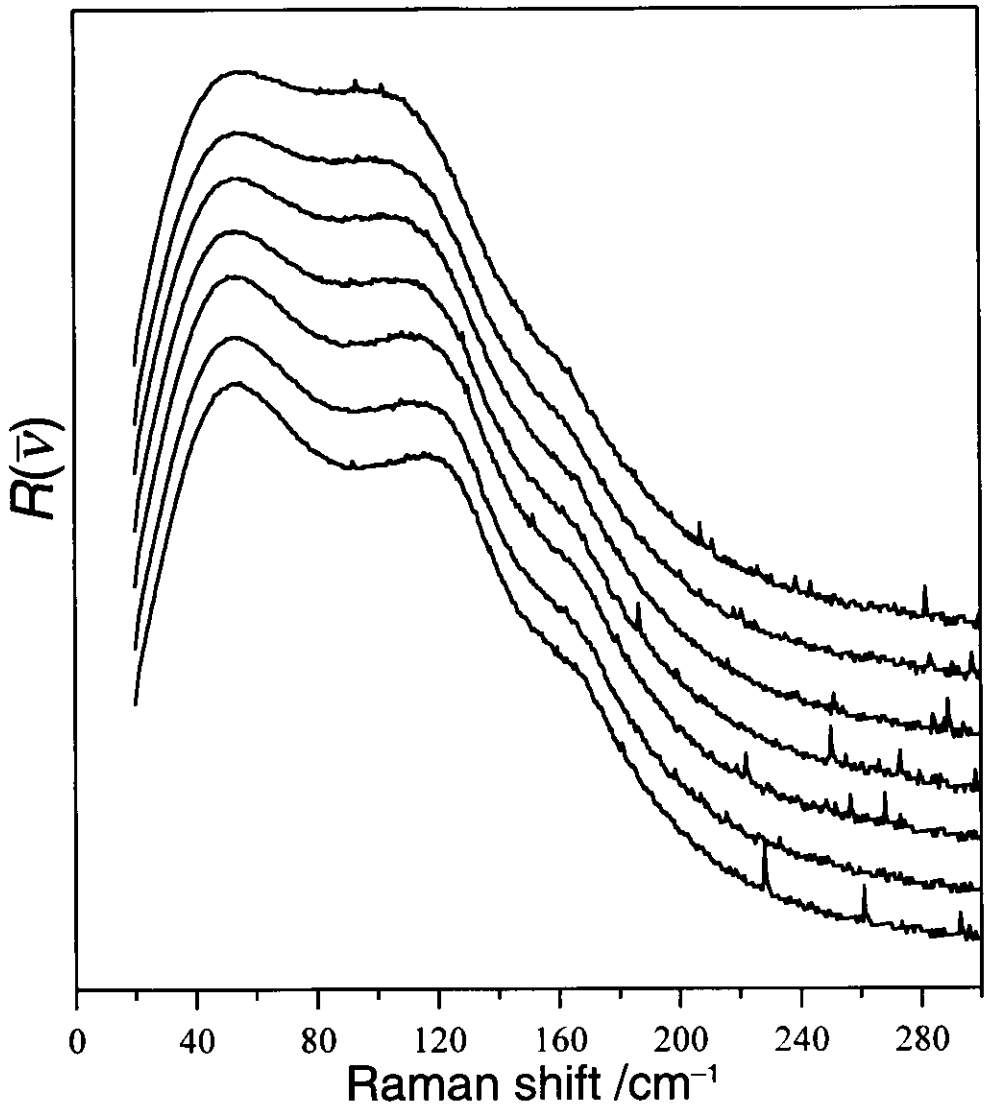

Figure II-6. The $R(\bar{\nu})$ spectra of liquied acetic acid in the 15-400 cm^{-1} region at the temperature of 296, 303, 1313, 323, 333, 343, and 348 K.
The intensity of each spectrum is normalized by reference to the peak intensity of the band at 50 cm^{-1}.

II.D.3. Calculated low-frequency Raman spectra

$R(\bar{\nu})$ spectra in the 0–300 cm^{-1} region calculated for the dimer species using HF/6-31G(d,p) are shown in Figure II-7. Table II-IX summarizes calculated vibrational wavenumbers and the assignment of these species in the 0–300 cm^{-1} region. The band positions observed in crystalline, liquid, and gaseous acetic acid [44, 45] are collected in Table II-X. We also calculated the $R(\bar{\nu})$ spectra for the cluster species at both the HF/6-31G(d,p) and HF/6-31++G(d,p) levels and found that the inclusions of diffuse functions do not seriously affect their peak positions and intensity patterns. In the Gaussian program, the Raman activity ($A(\bar{\nu})$, in units of $Å^4$ amu^{-1}) is defined as proportional to the sum of the square of the polarizability derivatives. Thus we obtained $R(\bar{\nu})$ spectra by plotting $A(\bar{\nu})$ against the calculated wavenumber. Torii and Tasumi have shown that the features observed in the $R(\bar{\nu})$ spectra of hydrogen-bonded amides are well reproduced at the HF level. [46, 47] The calculated low-wavenumbers are not multiplied by a scale factor, since a reliable value of a scale factor for intermolecular vibrations has not been established.

Figure II-8 shows the $R(\bar{\nu})$ spectra in the 0–300 cm^{-1} region calculated for the chain clusters at the HF/6-31G(d,p) level. The observed spectrum of the crystalline acetic acid at 287 K is also shown in the bottom. The calculated wavenumbers of the Raman active vibrations of the chain clusters in the 0–300 cm^{-1} region are collected in Table II-XI.

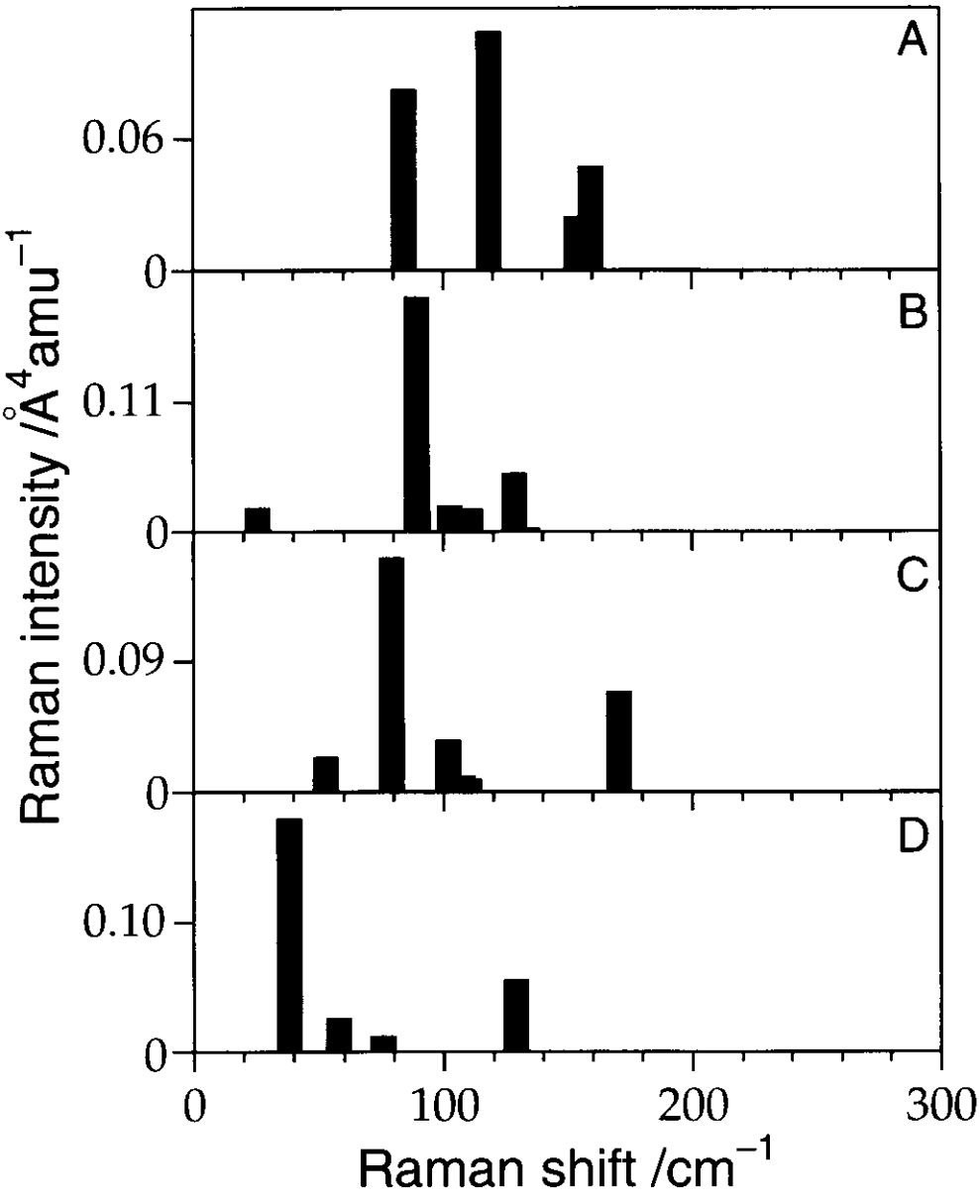

Figure II-7. The $R(\bar{\nu})$ spectra in the 0-300 cm^{-1} region calculated for (A) dimer 1, (B) dimer 2, (C) dimer 3, and (D) dimer 4 at the HF/6-31G(d,p) level.

TABLE II-IX. Calculated low wavenumbers (cm^{-1}) of acetic acid dimer species at the HF/6-31G(d,p) level.

dimer 1	dimer 2	dimer 3	dimer 4	assignment[a]
50.2 (0.00) [b]	38.1 (0.00)	13.1 (0.02)	19.4 (0.00)	o.o.p. ring bent
73.2 (0.00)	25.8 (0.17)	52.7 (0.11)	30.8 (0.00)	o.o.p. ring def.
84.1 (0.24)	102.5 (0.05)	101.8 (0.09)		(free) CH_3 tor.
92.1 (0.00)		110.1 (0.02)		(free) CH_3 tor.
	128.5 (0.10)		129.0 (0.12)	(H-bonded) CH_3 tor.
			140.6 (0.00)	(H-bonded) CH_3 tor.
118.5 (0.24)	89.3 (0.54)	79.2 (0.51)	38.2 (1.06)	o.o.p. ring bent
	89.7 (0.05)		67.6 (0.00)	C–H···O stretch
			75.7 (0.04)	C–H···O stretch
153.7 (0.04)	133.8 (0.01)	107.6 (0.03)		O–H···O stretch
153.8 (0.00)				O–H···O stretch
159.5 (0.08)	110.9 (0.05)	52.6 (0.09)	57.8 (0.11)	i.p. ring def.
		170.5 (0.12)		i.p. ring def.

[a] o.o.p. and i.p. are the abbreviations of out-of-plane and in-plane, respectively.

[b] The unit of Raman activity in the parentheses is $Å^4\ amu^{-1}$.

TABLE II-X. Low-frequency Raman bands observed in $R(\bar{\nu})$ spectra of gas, liquid, and crystalline acetic acid (in cm^{-1}).

gas	liquid	solid
106 (s)	50 (s)	41(w)
155 (w)	120 (s)	50 (s)
	170 (w)	78 (w)
		90 (w)
		124 (s)
		181 (s)

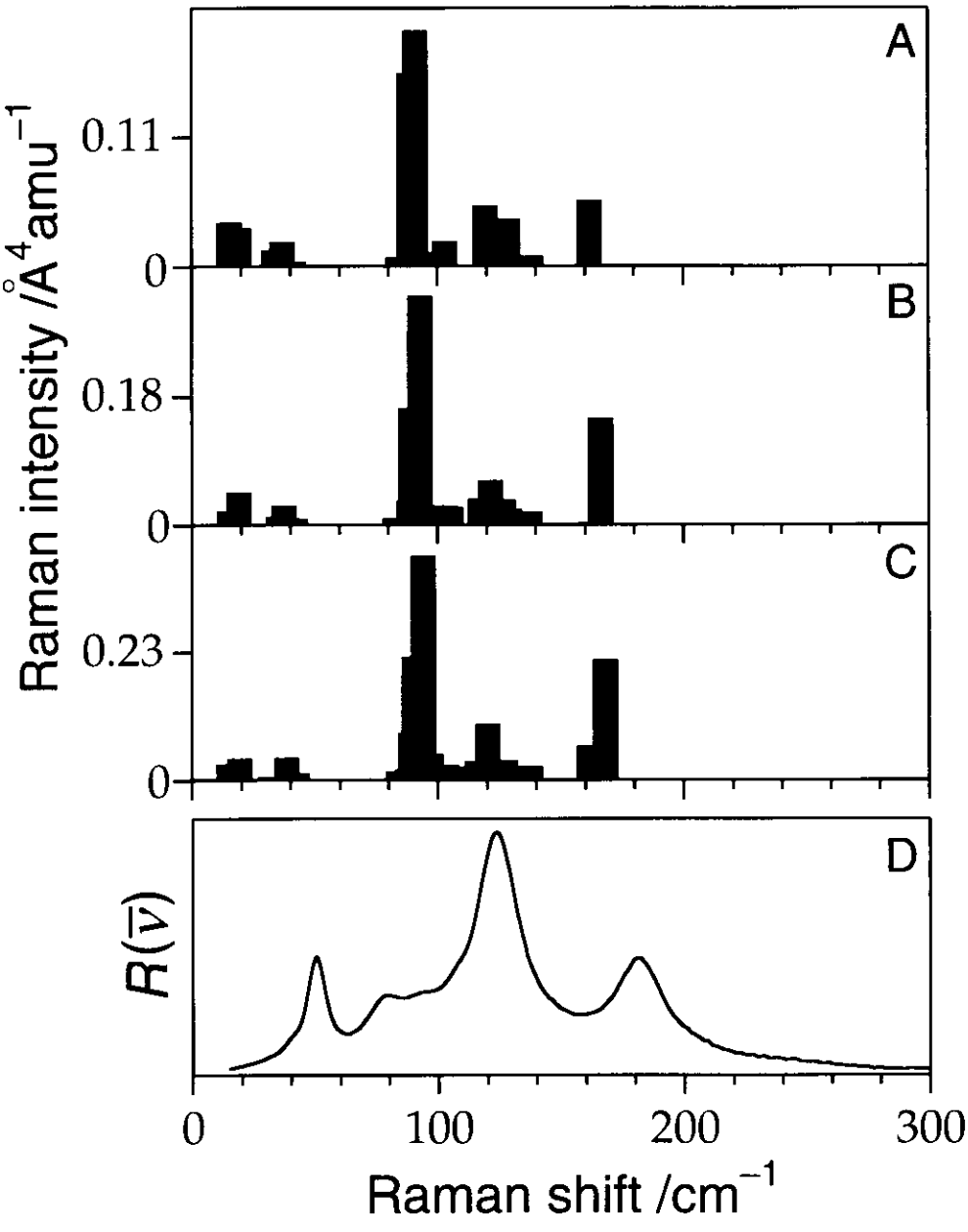

Figure II-8. The $R(\tilde{\nu})$ spectra in the 0-300 cm^{-1} region calculated for (A) trimer, (B) tetramer, and (C) pentamer at the HF/6-31G(d,p) level.
The observed $R(\nu)$ spectrum of crystalline acetic acid at 287 K is shown in (D) for comparison.

TABLE II-XI. Calculated Raman active low wavenumbers (cm^{-1}) of acetic acid trimer, tetramer, and pentamer at the HF/6-31G(d,p) level [a].

assignment	trimer	tetramer	pentamer
out-of-plane	15.3 (0.51)	15.1 (0.27)	4.3 (0.17)
	19.0 (0.36)	19.2 (0.52)	15.1 (0.39)
	36.6 (0.13)	37.4 (0.16)	19.3 (0.41)
	88.6 (0.46)	88.3 (0.10)	38.3 (0.23)
	91.0 (0.55)	89.0 (0.47)	88.9 (0.23)
		92.9 (0.88)	90.2 (0.60)
			94.3 (1.04)
in-plane	161.8 (0.10)	166.5 (0.27)	97.1 (0.12)
			161.5 (0.11)
			168.1 (0.37)
CH_3 torsion	119.6 (0.11)	121.6 (0.14)	120.5 (0.22)

[a] Vibrational modes Raman intensities of which are higher than 0.10 are shown in this table.

[b] The unit of Raman activity in the parentheses is $Å^4\ amu^{-1}$.

II.D.4. Observed Raman spectra in intramolecular mode region

Figure II-9 shows the Raman spectra of crystalline and liquid acetic acid in the intramolecular vibrational region (300–3700 cm^{-1}). Figure II-10 shows the enlargement of the two spectra in the C=O stretching region.

Temperature dependence of the $R(\bar{\nu})$ spectra of liquid acetic acid in the C=O stretching region is shown in Figure II-11. In the Raman intensity analyses at different temperatures, the best method to evaluate the relative Raman intensities is the use of an internal intensity reference. By adding a small amount of benzene to liquid acetic acid (benzene mole fraction χ_B = 0.06), we get a very strong Raman band of benzene at 992 cm^{-1} as an internal intensity reference in Figure II-11. A small amount of benzene was found to have no effect on the Raman spectra of liquid acetic acid in this temperature range (296–348 K).

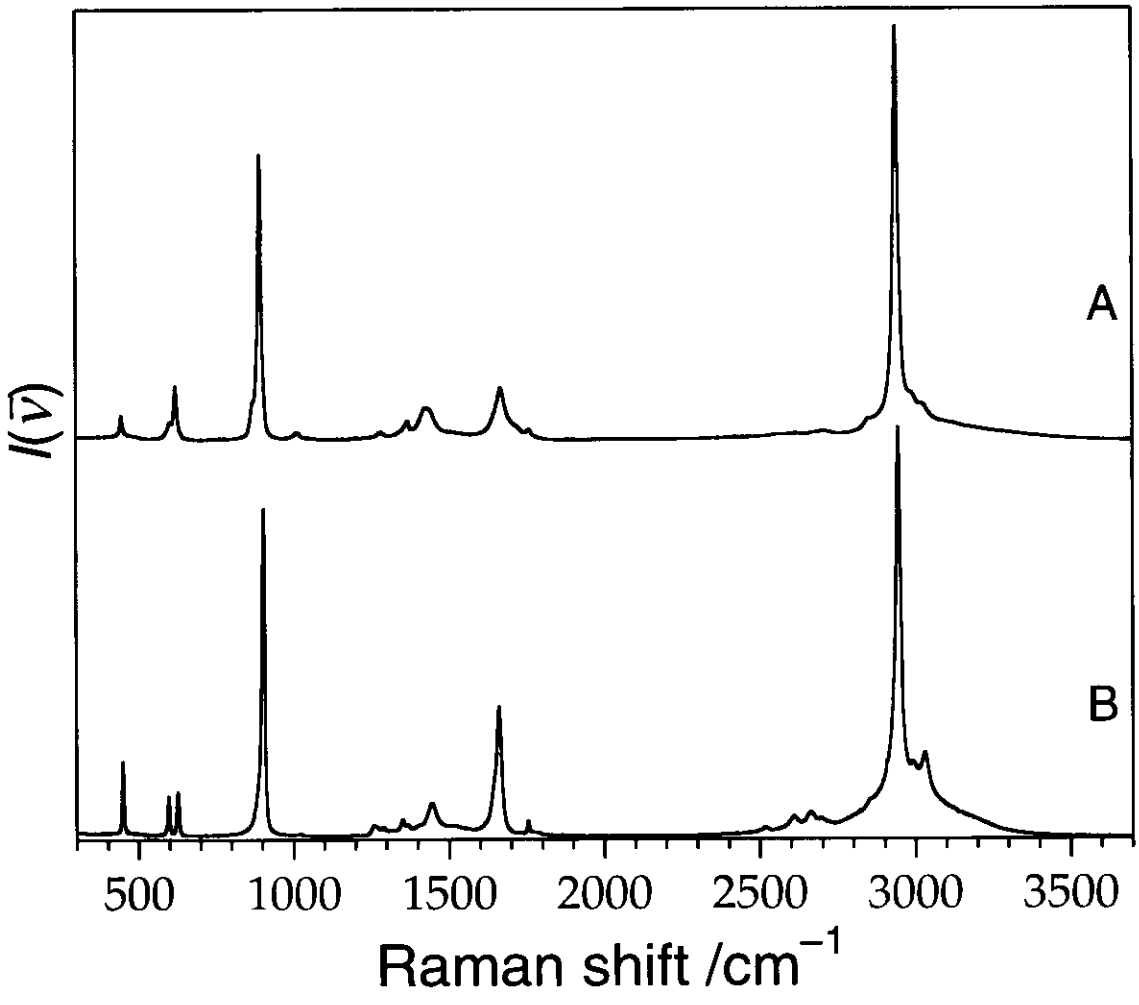

Figure II-9. The $I(\bar{\nu})$ spectra of (A) liquid and (B) solid acetic acid in the 300-3700 cm^{-1} region. The intensity of each spectrum is normalized by reference to the peak intensity of the C-H stretching band at 2950 cm^{-1}.

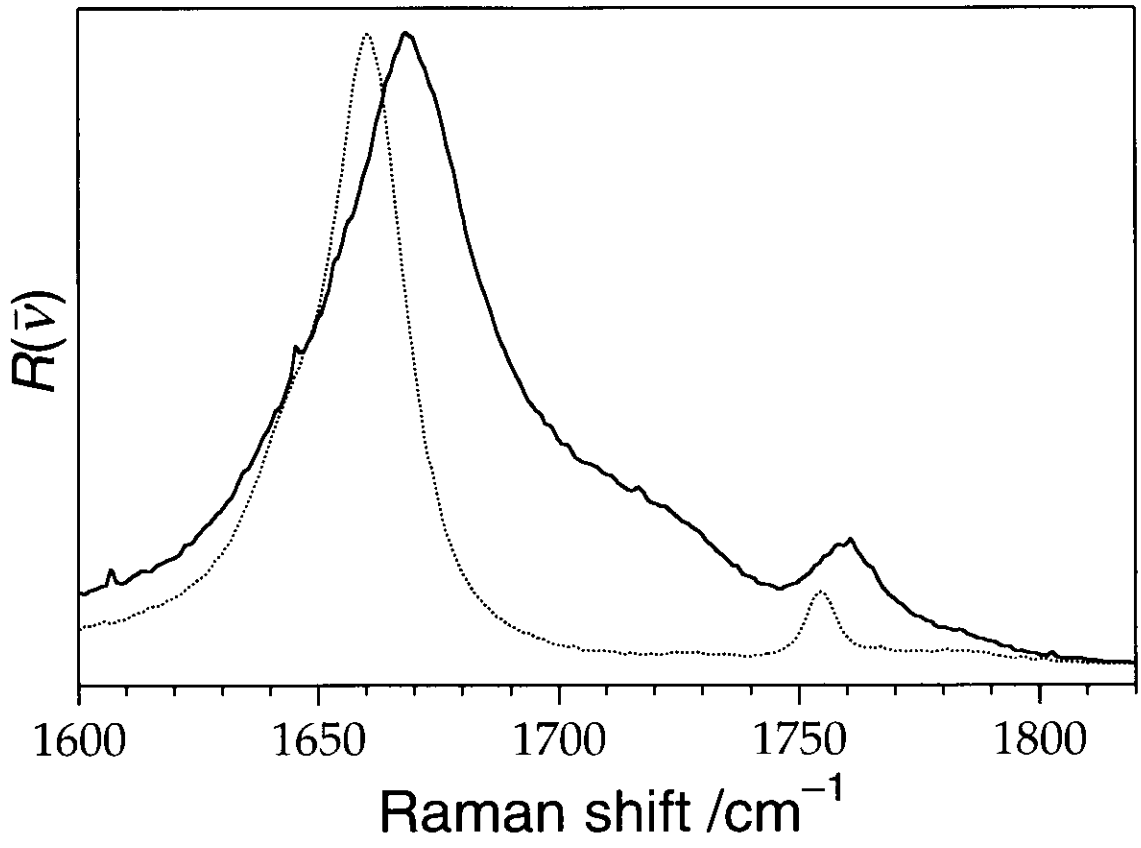

Figure II-10. The $R(\bar{\nu})$ spectra of acetic acid in the C=O stretching region (1600-1840 cm^{-1}). The solid and dotted traces are recorded in the liquied and solid states, respectively. The intensity of each spectrum is normalized by reference to the peak intensity of the strong C=O stretching band at ≈1665 cm^{-1}.

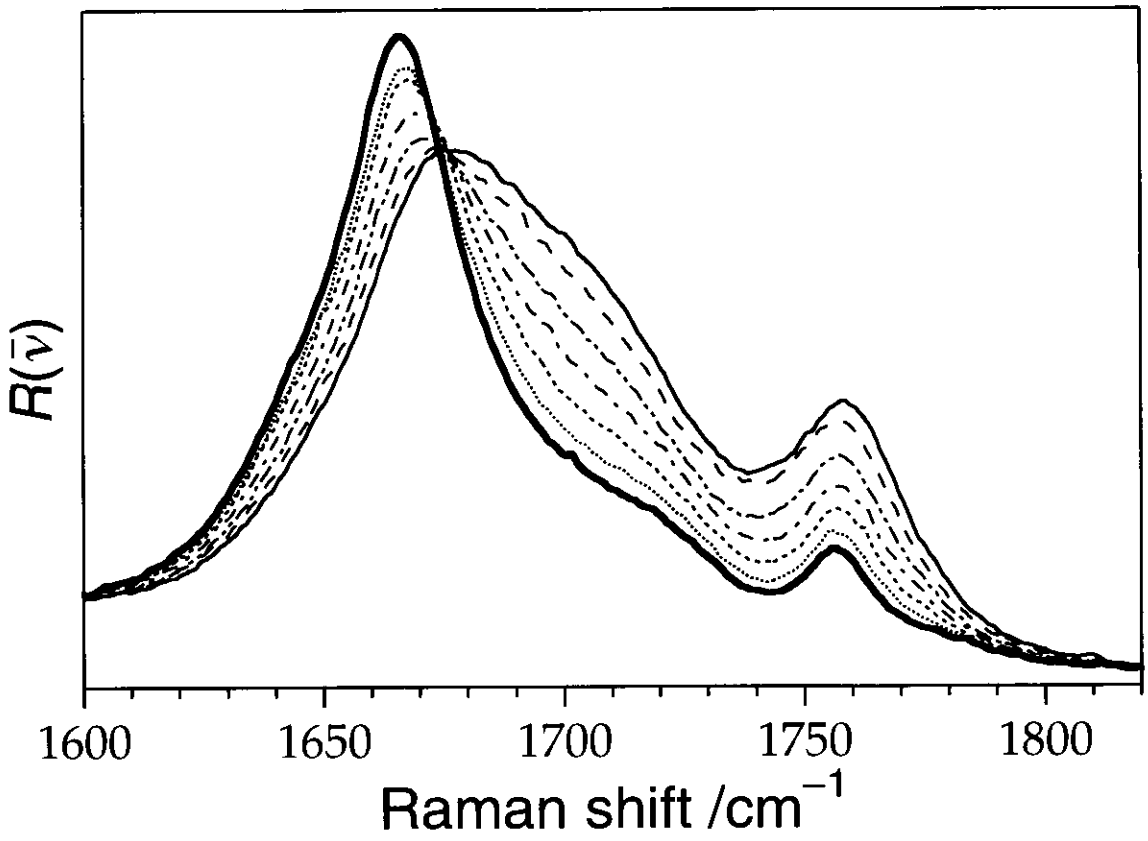

Figure II-11. The $R(\bar{\nu})$ spectra of liquid acetic acid in the C=O stretching region (1600-1840 cm^{-1}) at different temperatures. The intensity of each spectrum is normalized by reference to the intensity of a band of benzene at 992 cm^{-1}. Thick-solid trace, 296 K; dotted trace, 303 K; thick-dotted trace, 313 K; dot-dashed trace, 323 K; dot-dot-dashed trace, 333 K; broken trace, 343 k; solid trace, 348 K.

II.D.5. Calculated vibrational frequency of C=O stretching modes

Vibrational wavenumbers and Raman intensities of the C=O stretching modes calculated for the monomer and the cluster species at the HF/6-31G(d,p) level are listed in Table II-XII. The wavenumbers listed are not multiplied by a scale factor.

TABLE II-XII. Calculated wavenumbers (cm^{-1}) of C=O stretching modes of acetic acid monomer and cluster species at the HF/6-31G(d,p) level [a].

aggregate	(free) C=O str.	(H-bond) C=O str.
monomer	2038.8 (5.35) [b]	
dimer 1		1950.6 (5.60)
		1989.2 (0.00)
dimer 2	2014.4 (1.46)	1989.5 (8.29)
dimer 3	2045.2 (4.48)	2002.3 (6.13)
dimer 4		2016.4 (11.03)
		2027.5 (0.00)
trimer	2013.2 (4.45)	1956.0 (6.95)
		1997.3 (2.10)
tetramer	2011.9 (2.61)	1945.7 (9.14)
		1970.1 (0.44)
		1998.9 (5.58)
pentamer	2011.8 (3.57)	1940.9 (11.83)
		1956.5 (0.07)
		1977.5 (2.60)
		1999.6 (4.10)

[a] Wavenumbers are not multiplied by a scaling factor.

[b] The unit of Raman activity in the parentheses is $Å^4\ amu^{-1}$.

II.E. Discussion

II.E.1. Calculated hydrogen-bonding energies of cluster species: cooperative interactions

As for the chain fragments of the crystalline networks, the hydrogen-bonding energy increases with increasing aggregate size. Turi and Dannenberg have shown that this stabilization is due to the increase in the cooperative interactions between acetic acid molecules with increasing aggregation [23, 48]. They also estimated the hydrogen-bonding energy expected for the infinite chain by an asymptotical approach. At the HF/6-31G(d,p) level, this value was estimated to be –9.85 kcal/mol without corrections, and –8.4 kcal/mol after ZPVE [23, 48]. This indicates that, even for the pentamer, the calculated hydrogen-bonding energy is smaller than that for the infinite chain.

Dimer 1 has the shortest C–O bond length, the longest C=O and O-H bond lengths, and the shortest O···O distance for the O–H···O=C hydrogen bond. This indicates that the O–H···O=C hydrogen-bonding interaction of dimer 1 is the strongest, as far as the dimer species are concerned. Dimer 2 has a shorter C···O distance for the C–H···O=C hydrogen bond than dimer 4. This means that the C–H···O=C interaction of dimer 2 is stronger than that of dimer 4. The C-H bond lengths of all the dimer species are found to remain almost constant even in the presence of hydrogen-bonding interactions.

The trends of the geometrical change with increasing cluster size have been also found by Turi and Dannenberg [48]. The most interesting to note is that the O···O distance for the O–H···O=C hydrogen bond decreases with increasing the extent of aggregation, while the C···O distance for the C–H···O=C hydrogen bond increases. In other words, the O–H···O=C interaction becomes stronger and the C–H···O=C interaction becomes weaker as the chain length is extended. The increase in the cooperative interactions shown in Table II-IV is therefore the sum of two divergent components [48]. For all the hydrogen bonds, HF/6-31++G(d,p) predicts the longer intermolecular distance than HF/6-31G(d,p). This result is in accord with the fact that the hydrogen-bonding energy at the HF/6-31++G(d,p) level is lower than that at the HF/6-31G(d,p) level for all the aggregates shown in Table II-IV.

II.E.2. $R(\bar{\nu})$ representation of Raman spectra of acetic acid: comparison between low-frequency vibrations of liquid and those of crystalline

Such a large enhancement of the intensity at the tail of Rayleigh scattering on melting has been observed in other molecular crystals [49]. This phenomenon has been considered to arise from the increase in the density fluctuation with increasing temperature [50]. The problems caused by the very strong Rayleigh line can be partly overcome using the $R(\bar{\nu})$ representation [31, 46, 47, 49, 51, 52].

Temperature dependence of the $R(\bar{\nu})$ spectra of acetic acid is shown in Figure II-5. Liquid acetic acid at 296 K exhibits two peaks and one shoulder in the $R(\bar{\nu})$ spectrum, although they are hardly identified in the $I(\bar{\nu})$ spectrum in Figure II-4.

The two $R(\bar{\nu})$ spectra of crystalline acetic acid in Figure II-5 are essentially the same. On the other hand, the peak intensities observed in the spectrum of the mixture of solid and liquid acetic acid are much smaller than those in the crystalline spectra. In the liquid spectrum, all the bands broaden and the intensity in the low-wavenumber region around 50 cm^{-1} increases, although the positional changes of the two prominent bands at 50 and 124 cm^{-1} are very small on the melting of the crystal. X-ray and neutron scattering measurements have suggested that the hydrogen-bonded atomic distances are preserved during melting [27]. The constancy of the peak position in Figure II-5 appears to be in agreement with the X-ray and neutron scattering observations. The band at 181 cm^{-1} seems to shift

slightly to a lower wavenumber on the melting. Figure II-12 shows the curve fitting analysis for the $R(\bar{\nu})$ spectrum of liquid acetic acid at 296 K. The fit to the liquid spectrum shown in Figure II-12 is based on a model composed of six Gaussian lineshapes and a flat background. Inclusion of two Gaussian components at 75 and 92 cm^{-1} is needed to reproduce the liquid spectrum in the 50–200 cm^{-1} region satisfactorily. It should be noted in Figure II-12 that the fitting analysis shows the presence of the hidden component with a peak at $\approx$ 185 cm^{-1}, the integrated intensity of which is comparable to that of the discernible component at 165 cm^{-1}. This result suggests that the positional change of the 181 cm^{-1} band is also small on the melting. It may be therefore said that the band positions observed in the crystalline spectrum remain almost unchanged on the melting of the crystal.

As shown in Figure II-6, we observed the $R(\bar{\nu})$ spectra at various temperature from 296 to 348 K. However the widths of bands become broader with increasing the temperature, making it difficult to analyze the temperature dependence of the six Gaussian components individually.

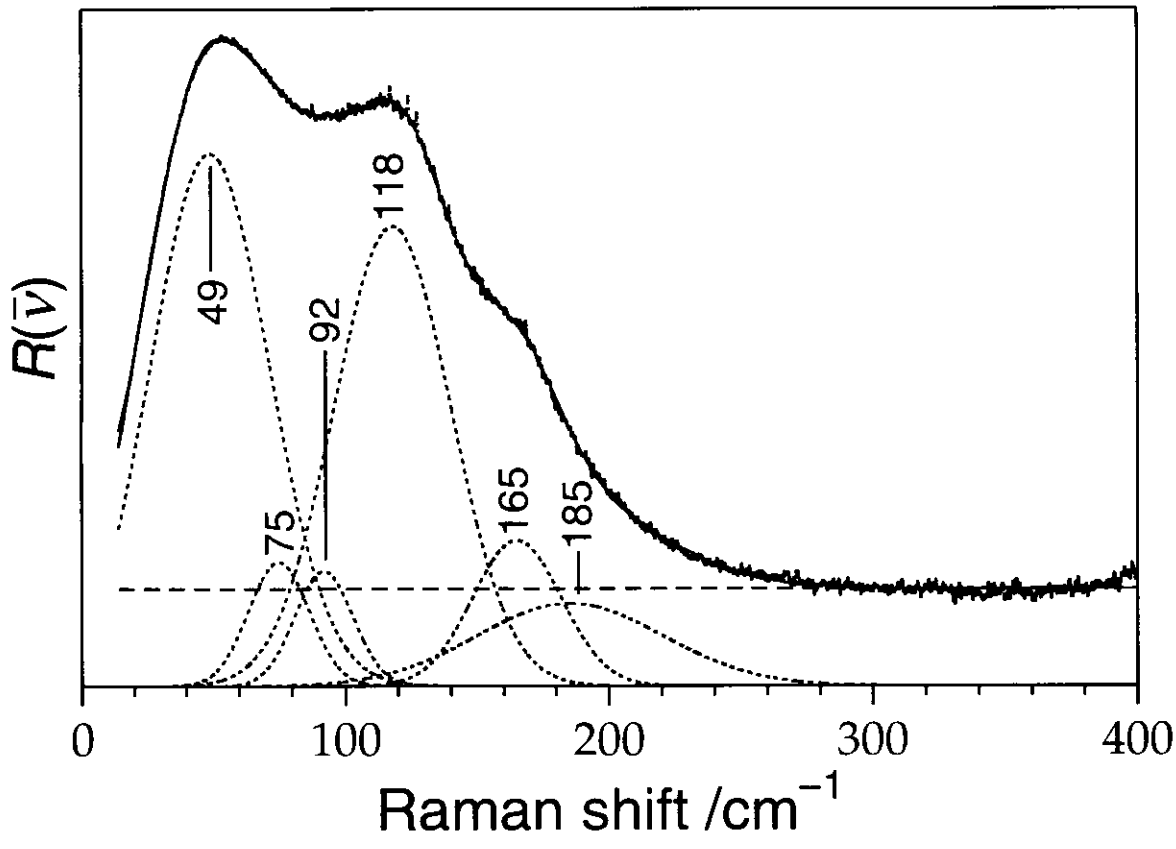

Figure II-12. Curve fitting analysis using Gaussian components for $R(\bar{\nu})$ spectrum of liquid acetic acid in the 15-400 cm^{-1} region: dotted trace, observe; solid curve, fitted spectrum with six Gaussian components (thick-dotted curves) and a flat background (broken line). The numbers in the figure indicate peak potions of the Gaussian components.

II.E.3. Comparison between observed low-frequency Raman spectra and those calculated for dimer species and crystalline-like chain clusters

The reported low-frequency Raman spectra of the cyclic dimer in the gas phase at 21 °C showed two broad bands at 106 and 155 cm^{-1}, the former of which was larger in intensity than the latter [44, 45]. On the other hand, the ab initio MO calculations for dimer 1 provide four Raman active vibrations in the 0–400 cm^{-1} region. As shown in Figure II-7-A, the two bands at 84.1 and 118.5 cm^{-1} are comparably strong and the other two bands at 153.7 and 159.5 cm^{-1} are weak. This may suggest that the broad band at 106 cm^{-1} observed in the vapor state is composed of the two bands, which are assigned to the CH_3 torsion and the out-of-plain ring bent modes, and the 155 cm^{-1} band is also divided in the two bands, which are the hydrogen-bond stretching and the in-plane ring deformation modes. With the help of the normal coordinate calculations with empirical force constants [33-36], Nielsen and Lund assigned the three peaks at 55, 115, and 165 cm^{-1} in the liquid spectrum to the three fundamental modes of the cyclic dimer, in-plane ring deformation, out-of-plane bent, and hydrogen-bond stretching vibrations, respectively [31]. The ab initio MO calculation for dimer 1, however, predicts that the wavenumber of the in-plane ring deformation mode is the highest among the intermolecular modes.

For all the dimer species in Table II-IX, the out-of-plane motion of oxygen atoms produces the strongest Raman intensities among the intermolecular modes. Dimer 1 has the highest wavenumber of the strongest Raman active

mode among the calculated dimer species, while dimer 4 has the lowest one. This result is in accord with the fact that the O–H···O=C hydrogen-bonding interaction of dimer 1 is the strongest and the C–H···O=C interaction of dimer 4 is the weakest among other intermolecular bonds in Table II-VI and II-VII. The free CH_3 torsions of dimer 2 and dimer 3 are calculated to be lower in wavenumber than the hydrogen-bonded CH_3 torsions of dimer 2 and dimer 4, but higher than the CH_3 torsions of dimer 1. This result may arise from the situation that the C–H···O=C hydrogen-bonds hinder the CH_3 torsional motions and the strong O–H···O=C hydrogen-bond of dimer 1 weakens an internal hydrogen bond between the methyl hydrogen in the carboxylic plane and the carbonyl oxygen.

Ab initio calculation provides intermolecular vibrational wavenumbers 10 ~ 20 % lower than the observed wavenumbers. All the calculated spectra in Figure II-8 are decomposed into roughly four groups: strong or medium intensity bands in the 20–40 cm^{-1} region, strong bands at ≈ 90 cm^{-1}, weak bands in the 100–140 cm^{-1} region, and medium intensity bands at ≈ 165 cm^{-1}. The intensity pattern in the spectrum of pentamer is shown to be in reasonable agreement with that in the spectrum of crystalline acetic acid, except for the positions of the weak bands calculated in the 100–140 cm^{-1} region. Although these weak bands are calculated to be higher in wavenumber than the strongest Raman active modes for the chain clusters, small bands at 78 and 90 cm^{-1} are observed on the lower-wavenumber side of the strongest Raman band in the crystalline spectrum.

As shown in Table II-XI, the strong Raman bands at ≈ 90 cm^{-1} and the

bands in the region of 20–40 cm^{-1} of the chain clusters arise from the out-of-plain rotational motions of component molecules. The bands at ≈ 165 cm^{-1} is attributable to the in-plain ring deformation and stretching vibrations. Although further higher-wavenumber shifts are expected, these assignments can be applied to the crystalline spectrum straightforwardly. The three peaks in the crystalline spectrum at 41, 50 and 124 cm^{-1} are ascribed to the out-of-plane motions and the peak at 181 cm^{-1} is to the in-plain ring motion. The calculated bands at ≈ 90 and 165 cm^{-1} shift to higher wavenumbers as the aggregate size grows. Increase in the hydrogen-bonding interaction with increasing aggregation makes the force constants larger resulting in higher-wavenumber shifts. This behavior is consistent with the fact that the hydrogen-bonding energies for the chain clusters are smaller than that for the infinite chain as suggested in previous section. Stacking of the infinite two dimensional chains along the out-of-plane axis through weak C-H···O hydrogen bonds may also cause significant effect on the peak positions of the observed crystalline spectrum. These interactions may increase the hydrogen-bonding energy and lead to the shifts of the peak positions to higher wavenumbers [48].

In Figure II-8, the peak positions and the relative intensities in the spectra of the chain clusters show only slight changes with increasing aggregation, except that the intensity of the strong band at ≈ 90 cm^{-1} relative to that of the band at ≈ 20 cm^{-1} apparently increases as the aggregate size grows. Although no band is seen at ≈ 165 cm^{-1} in the spectrum of dimer 2 (Figure II-7-B), the intensity pattern calculated for dimer 2, which is the

dimer unit of the chain structure, is also similar to those for the other chain clusters. If a variety of sizes of the chain clusters are generated on the melting of the crystal, the weighted summation of the components therefore makes the spectrum quite broad with similar peak positions to those of the crystalline spectrum. This behavior is in agreement with the experimental observation that the melting of the crystal leads to the broadening of the $R(\bar{\nu})$ spectrum, while does not affect the peak positions so much. Depolarization ratios of the out-of plane vibrations in Table II-XI are calculated to be 0.75 (depolarized) and those of the in-plane vibrations to be less than 0.75 (polarized). This result is consistent with the polarized Raman observation that the 50 and 124 cm^{-1} bands in the liquid are polarized and the 181 cm^{-1} band depolarized [31]. Since the spectral features calculated for either dimer 1 or dimer 4 does not coincide with the observed spectrum, it is hard to consider that the liquid spectrum mainly arises from either of these dimer species. If dimer 1 is dominant in the liquid as in the gas phase, the bands at 106 and 155 cm^{-1} observed in the gas phase should correspond to the 120 and 170 cm^{-1} bands in the liquid, respectively (Table II-X). This assumption is inconceivable because, on going from the gaseous state to the liquid state, it is unlikely that the O–H···O=C interaction of dimer 1 becomes stronger and the intermolecular vibrational bands shift to higher wavenumbers. The spectral shape for dimer 3 is not much different from those for the chain clusters. This seems to indicate that dimer 3 also contributes to the $R(\bar{\nu})$ spectrum of liquid acetic acid. The side-on dimer structures, such as dimer 3, have also been

suggested as predominant species in aqueous solutions [41-43, 53]. If liquid acetic acid consists primarily of the side-on dimer structures, the spectral shape of liquid acetic acid should be unchanged with the presence of water. However, the $R(\bar{\nu})$ spectra of acetic acid–water binary solutions cannot be reproduced by linear combinations of the pure water spectrum and the spectrum of liquid acetic acid [43]. Actually, the $R(\bar{\nu})$ spectrum of acetic acid–water 1:1 mixture is well reproduced by the spectrum of dimer 3 [43]. This result indicates that the side-on dimer structure is not dominant in the liquid state. In consequence, comparison of the calculated and observed low-frequency Raman spectra suggests that the liquid spectrum in the low-wavenumber region is mainly due to the chain clusters as the fragments of the crystalline networks. The present results do not directly support the dominance of the cyclic dimers in the liquid, contrary to the previous low-wavenumber studies [29-33]. Since the intensity pattern is almost unchanged with increasing temperature up to 348 K (Figure II-6), a marked structural change in the liquid does not occur within the range of the temperature examined in this study.

The liquid spectrum shown in Figure II-12 seems to be reproduced by taking account of the components in the crystalline spectrum plus one additional Gaussian component at 165 cm^{-1}. It is also seen that the Gaussian component at 185 cm^{-1} is much broader than the others. The observed liquid spectrum, however, cannot be reproduced properly without adding such two or more Gaussian components in the region of 150–300 cm^{-1}. The broadness of the observed spectrum cannot completely exclude the

contribution of other structural isomers as minor components.

II.E.4. Comparison between observed and calculated Raman spectra in the C=O stretching retion

As shown in Figure II-9, the features of the crystalline spectrum are observed to be similar to those of the liquid spectrum. The two prominent peaks at ≈ 900 and ≈ 2950 cm^{-1} are ascribed to the C–C and C–H stretching bands, respectively. The medium intensity band at ≈ 1665 cm^{-1} is safely attributable to the C=O stretching band since there is no other Raman active vibrations due to acetic acid in the 1600–1900 cm^{-1} region.

It is clearly seen in Figure II-10 that, on going from the crystalline to liquid states, the C=O band shifts slightly to a higher wavenumber (1660 cm^{-1} in the crystalline spectrum and 1666 cm^{-1} in the liquid spectrum) and becomes broadened on the higher-wavenumber side exhibiting an obviously asymmetric shape. Such a high-wavenumber component was found not to mainly arise from the Raman noncoincidence effect [46] from polarized Raman studies. The small band at ≈ 1755 cm^{-1} is seen in both the spectra [54].

In Figure II-11, the intensity of the prominent band at 1666 cm^{-1} is shown to decrease and that of the asymmetric component to increase as the temperature grows. The integrated intensity of the asymmetric component becomes apparently larger than that of the prominent C=O band at 348 K. The intensity of the 1758 cm^{-1} band also becomes larger with increasing temperature. Such spectral changes with the temperatures should reflect the nature of the liquid structure of acetic acid.

Ng et al. suggested that the 1758 cm^{-1} band is due to the end C=O groups of a linear dimer and linear polymers, and the asymmetric shape around 1710 cm^{-1} in the liquid is mainly due to the monomer species [55, 56]. However, the free (end) C=O groups calculated for the chain clusters have wavenumbers lower than that for the monomer. As for the chain clusters (dimer 2, trimer, tetramer, and pentamer), the calculated C=O stretching Raman active vibrations are classified into three groups: strongly hydrogen-bonded C=O groups in the 1940–1960 cm^{-1} region, weakly hydrogen-bonded C=O groups in the 1975–2000 cm^{-1}, and free C=O groups at ≈ 2012 cm^{-1}. These three groups show strong, strong or medium, and weak Raman intensities, respectively. This result appears to be in agreement with the liquid spectra in Figure II-11, namely the prominent band observed at 1666 cm^{-1} arises from the strongly hydrogen-bonded C=O groups of the chain clusters, and the asymmetric shape around 1710 cm^{-1} and the small band at 1758 cm^{-1} arise from the weakly hydrogen-bonded and end C=O groups of the chain clusters, respectively.

The C=O band arising from the cyclic dimer is observed at 1681.5 cm^{-1} in the gaseous state at 21 °C [44]. This result suggests that the prominent C=O band at 1666 cm^{-1} in the liquid is not due to dimer 1 because the O–H···O=C interaction is considered not to become stronger and the C=O band not to shift to a lower wavenumber on going from the gas to liquid phases. As for dimers 2, 3, and 4, the C=O modes are calculated to be 50–100 cm^{-1} higher in wavenumber than the strongest Raman active C=O mode of the pentamer. This result indicates that the strong C=O band in the liquid

arises from none of these dimer species, since the prominent C=O band in the liquid spectrum is observed to be similar in peak position to that in the crystalline spectrum. If the C=O bands arising from dimers 1, 3 and 4 mainly contribute to the intensity of the asymmetric band, the structural change from the chain fragments to other cluster species should be considered in the liquid because the integrated intensity of the asymmetric band is larger than that of the prominent band at 348 K. However, as mentioned in previous section, temperature dependence of the low-frequency Raman spectra suggests that the marked structural change in the liquid does not occur up to 348 K. Thus their contributions to the asymmetric band can be thought to be small. In other words, the high temperature components must have intermolecular configuration similar to the low temperature one.

From the results mentioned above, we assign the strong C=O band at 1666 cm^{-1} in the liquid spectrum to the strongly hydrogen-bonded C=O groups of the chain clusters and the asymmetric shape around 1710 cm^{-1} to the weakly hydrogen-bonded C=O groups of the same cluster species. The relative intensity change in Figure II-11 is therefore considered to reflect the decrease in the number of the long chain clusters and the increase in the small chain clusters with increasing temperature. The weak band at 1758 cm^{-1} may be attributed to the end C=O groups of the chain clusters. This band is also observed around 1758 cm^{-1} in the spectrum of acetic acid–carbon tetrachloride mixture with acetic acid mole fraction of 0.1 [57]. A similar weak band has been observed in the Raman spectra of liquid acetone and

acetone–carbon tetrachloride mixture and ascribed to a combination of two intramolecular modes [58]. In order to provide a definitive conclusion on this point, however, measurements at lower temperatures are essential.

II.F. Conclusion

Local structure of liquid acetic acid is studied on the basis of the temperature dependence of the Raman spectra and ab initio MO calculations on some cluster species. The melting of the crystal leads to a broadening of the low-frequency Raman spectrum, while it does not affect their peak positions. This constancy of the spectral positions is in accord with the similar observation in X-ray and neutron scattering measurements. These spectral changes are well understood in the case that the liquid spectrum mainly arises from a variety of sizes of chain clusters produced on the melting of the crystal. With increasing temperature, the C=O stretching band becomes broadened toward higher wavenumbers and exhibits an asymmetric shape. The wavenumbers calculated for the C=O stretching modes suggest that the prominent C=O band is attributable to the strongly hydrogen-bonded C=O groups of the chain clusters and the asymmetric shape to the weakly hydrogen-bonded C=O groups of the same cluster species. The spectral analyses in the low-wavenumber and the C=O stretching regions suggest that the chain clusters as the fragments of the crystalline networks are the predominant structures of liquid acetic acid. The spectral changes with the temperature increase do not directly support the dominance of the cyclic dimer structure in the liquid.

References for chapter II

[1] G. R. Desiraju, Acc. Chem. Res. **24**, 290 (1991).

[2] Z. S. Derewenda, L. Lee, and U. Derewenda, J. Mol. Biol. **252**, 248 (1995).

[3] S. Glasstone, Trans. Faraday Soc. **33**, 200 (1937).

[4] M. W. Dougill and G. A. Jeffrey, Acta Crystallogr. **6**, 831 (1953).

[5] L. Pauling, The Nature of the Chemical Bond, 3rd ed., Cornell University Press, Ithaca, p 459 (1960).

[6] D. J. Sutor, Nature **68**, 195 (1962).

[7] D. J. Sutor, J. Chem. Soc. 1105 (1963).

[8] G. N. Ramachandran, C. Ramakrishnan, and V. Sasisekharan, J. Mol. Biol. **7**, 95 (1963).

[9] J. Bernstein, M. D. Cohen, and L. Leiserowitz, In The Chemistry of Quinonoid Compounds, S. Patai, Ed., Interscience, New York, p 37 (1974).

[10] R. Taylor and O. Kennard, J. Am. Chem. Soc. **104**, 5063 (1982).

[11] J. A. R. P. Sarma and G. R. Desiraju, J. Chem. Soc., Perkin Trans. 2 1195, (1987).

[12] G. A. Jeffrey and W. Saenger, Hydrogen Bonding in Biological Structures, Springer-Verlag, NY.

[13] D. Bordo and P. Argos, J. Mol. Biol. **243**, 504 (1994).

[14] K. A. Dill, Biochemistry **29**, 7133 (1990).

[15] A. R. Fersht and L. Serrano, Curr. Opin. Struct. Biol. **3**, 75 (1993).

[16] A. R. Fersht, J-P. Shi, J. Knill-Jones, D. M. Lowe, A. J. Wilkinson, D. M.

Blow, P. Brick, P. Carter, M. M. Y. Waye, and G. Winter, Nature **314**, 235 (1985).

[17] W. W. Cleland and M. M. Kreevoy, Science **264**, 1887 (1994).

[18] P. A. Frey, S. A. Whitt, and J. B. Tobin, Science **264**, 1927 (1994).

[19] R. E. Jones and D. H. Templeton, Acta Crystallogr. **11**, 484 (1958).

[20] I. Nahringbauer, Acta Chem. Scand. **24**, 453 (1970).

[21] P. –G. Jönsson, Acta Crystallogr. **B27**, 893 (1971).

[22] I. Nahringbauer, Acta Chem. Scand. **23**, 1653 (1969).

[23] L. Turi and J. J. Dannenberg, J. Phys. Chem. **97**, 12197 (1993).

[24] F. J. Strieter, D. H. Templeton, R. F. Scheuerman, and R. L. Sass, Acta Crystallogr. **15**, 1233 (1962).

[25] J. A. Kanters and J. Kroon, Acta Crystallogr. **B28**, 1946 (1972).

[26] R. S. Payne, R. J. Roberts, R. C. Rowe, and R. Docherty, J. Comput. Chem. **19**, 1 (1998).

[27] H. Bertagnolli and H. G. Hertz, Phys. Status Solidi A, **49**, 463 (1978).

[28] H. Bertagnolli, Chem. Phys. Lett. **93**, 287 (1982).

[29] U. A. Zirnit and M. M. Sushchinskii, Opt. Spectrosc. **16**, 490 (1964).

[30] P. Waldstein and L. A. Blatz, J. Phys. Chem., **71**, 2271 (1967).

[31] O. Faurskov Nielsen and P.-A. Lund, J. Chem. Phys., **78**, 652 (1983).

[32] A. E. Stanevich, Opt. Spectrosc., **16**, 243 (1964).

[33] R. J. Jakobsen, Y. Mikawa, J. W. Brasch, Spectrochim. Acta, **23A**, 2199 (1967).

[34] T. Miyazawa and K. S. Pitzer, J. Am. Chem. Soc., **81**, 74 (1959).

[35] S. Kishida and K. Nakamoto, J. Chem. Phys., **41**, 1558 (1964).

[36] K. Fukushima and B. J. Zwolinski, J. Chem. Phys., **50**, 737 (1969).

[37] M.J. Frisch, G.W. Trucks, H.B. Schlegel, P.M.W. Gill, B.G.. Johnson, M.A. Robb, J.R. Cheeseman, T. Keith, G.A. Petersson, J.A. Montgomery, K. Raghavachari, M.A. Al-Laham, V.G. Zakrzewski, J.V. Ortiz, J.B. Foresman, J. Cioslowski, B.B. Stefanov, A. Nanayakkara, M. Challacombe, C.Y. Peng, P.Y. Ayala, W. Chen, M.W. Wong, J.L. Andres, E.S. Replogle, R. Gomperts, R.L. Martin, D.J. Fox, J.S. Binskey, D.J. Defrees, J. Baker, J.P. Stewart, M. Head-Gordon, C. Gonzalez, and J.A. Pople, *GAUSSIAN 94*, Revision C.3, Gaussian Inc., Pittsburgh, PA, 1995.

[38] J. Karle, L. O. Brockway, J. Am. Chem. Soc. **66**, 574 (1944).

[39] J. L. Derissen, J. Mol. Struct. 7, 67 (1971).

[40] G. R. Nash and C. B. Monk, J. Chem. Soc. 4274 (1957).

[41] E. E. Schrier, M. Pottle, and H. A. Scheraga, J. Am. Chem. Soc. **86**, 3444 (1964).

[42] K. Yamamoto and N. Nishi, J. Am. Chem. Soc. **112**, 549 (1990).

[43] N. Nishi, T. Nakabayashi, and K. Kosugi, J. Phys. Chem. **103**, 10851 (1999).

[44] J. E. Bertie and K. H. Michaelian, J. Chem. Phys., 77, 5267 (1982).

[45] J. E. Bertie, H. H. Eysel, D. N. S. Permann, and D. H. J. Kalantar, J. Raman Spectrosc. **16**, 137 (1985).

[46] H. Torii and M. Tasumi, J. Phys. Chem. B, **102**, 315 (1998).

[47] H. Torii and M. Tasumi, Int. J. Quantum Chem., 70, 241 (1998).

[48] L. Turi and J. J. Dannenber, J. Am. Chem. Soc., **116**, 8714 (1994).

[49] O. Faurskov Nielsen, D. H. Christensen, O. J. Have Rasmussen, Mol.

Struct., **242**, 273 (1991).

[50] T. Ishibashi and H. Hamaguchi, J. Chem. Phys., **106**, 11 (1997).

[51] M. H. Brooker and O. Faurskov Nielsen, and E. Praestgaard, J. Raman Spectrosc., **19**, 71 (1988).

[52] K. Egashira and N. Nishi, J. Phys. Chem. B, **102**, 4054 (1998).

[53] G. R. Nash and C. B. Monk, J. Chem. Soc., 4274 (1957).

[54] The Raman measurements of an isotopic molecule ($CH_3C^{18}OOH$) confirm that all the bands observed in the 1600-1820 cm^{-1} region are due to the C=O vibrations.

[55] J. B. Ng and H. F. Shurvell, J. Phys. Chem., **91**, 496 (1987).

[56] J. B. Ng, B. Petelenz, and H. F. Shurvell, Can. J. Chem., **66**, 1912 (1988).

[57] T. Nakabayashi and N. Nishi, unpublished results.

[58] M. Musso, M. G. Giorgini, G. Doge, and A. Asenbaum, Mol. Phys., **92**, 97 (1997).

CHAPTER III

Raman spectroscopic study on acetic acid clusters in aqueous solutions: dominance of acid-acid association producing microphases

This chapter is based on Chem. Phys. Lett. **291**, 253 (1998) and J. Phys. Chem. **103**, 10851 (1999).

III.A. Introduction

III.A.1. Microphases in binary solutions

The liquid structure of ethanol/water binary solution had been attributed to the complex formation between ethanol and water molecules, because of absence of macroscopic phase separation and the ability of the hydroxyl group to act as proton donor and acceptor. It is well known that one cannot see macroscopic phase separation in ethanol/water binary solution. This situation is also seen in other binary solutions such as methanol/water, 1-propanol/water, 2-propanol/water, and acetic acid/water mixtures. On the other hand, the hydroxyl group of alcohol plays roles of proton donor and acceptor in hydrogen-bonding; the hydroxyl hydrogen interacts with an electronegative atom such as oxygen, while the hydroxyl oxygen forms an intermolecular hydrogen bond with a hydrogen atom of a neighboring molecule.

Low-frequency vibrational spectroscopy is very useful for studies of local structures of solution systems because it directly probes intermolecular vibrational bands. Egashira and Nishi observed low-frequency Raman spectra of ethanol/water solutions of various concentrations. [1] They also measured those of liquid ethanol and pure water. This system shows a single isosbestic point over the whole mixing ratios and the observed spectra are reproduced with linear combinations of the pure water spectrum and the pure ethanol spectrum. This indicates that the mixtures are composed of

microphases of water associates and ethanol associates and there is little contribution to the spectra from ethanol/water complexes. We observed the low-frequency Raman spectra of 1-propanol/water binary solutions and pure liquid 1-propanol. [2] This system also shows a single isosbestic point over the whole mixing ratios. We also measured the low-frequency Raman spectra of 2-propanol/water mixtures and pure liquid 2-propanol and shows that the system also exhibits a single isosbestic point over the whole mixing ratios. [2] These results suggest that microscopic phase separation and little complex formation between alcohol and water occur in both the 1-propanol/water and 2-propanol/water systems, while macroscopic phase separation can be seen.

III.A.2. Liquid structure of acetic acid aqueous solutions

Low-frequency Raman spectroscopy provides information on local structure of solutions coupled with hindered translational and librational motions. Waldstein and Blatz reported the low-frequency Raman spectra of liquid acetic acid and its solution in water. [3] However, we could not observe any spectrum similar to those they reported as shown in the following section. They also stated that predominant associated species in the aqueous mixture is probably an open dimer of acetic acid. The Rayleigh wing spectra have been presented with $R(\tilde{\nu})$, the intrinsic Raman scattering activity. [1,4-8] The Raman signals originating from dipole-induced dipole interaction are dominated with the interaction between the neighboring molecules. [1,4] In fact, Madden and Impey succeeded to reproduce the observed $R(\tilde{\nu})$ spectrum of water from molecular dynamics (MD) simulation using the MCY potential with 125 molecules. [4] They found that the 185 cm^{-1} component is prominently correlated with the bi-molecular in-plane mode of hydrogen bonded water molecules. The vibrational frequencies and Raman intensities of such bimolecular modes can be estimated by ab initio molecular orbital method with a reliable basis set.

III.A.3. Aims of the present study

The vibrational frequencies and Raman intensities of intermolecular modes can be estimated by ab initio molecular orbital method with a reliable basis set as mentioned above. In this study, we investigate the liquid structure of acetic acid aqueous solutions experimentally and theoretically. Experimentally we observe both the intermolecular and intramolecular vibrational spectra by Raman spectroscopy. Theoretically ab initio molecular orbital calculations are performed on geometrical structures, dipole moments, vibrational frequencies, and Raman intensities of acetic acid-acetic acid, acetic acid-water, and acetic acid-methanol cluster species. We demonstrate the usefulness of the theoretical calculation of intermolecular vibrational modes for the assignment of low frequency Raman spectra of binary solutions.

III.B. Experimental

High purity water was prepared by a Puric-Z water purifier (Organo Co. Ltd.). Acetic acid of spectroscopy grade (more than 99.7 v/v %; Wako Pure Chemical Industries) was used without further purification. Acetic acid aqueous solutions were sealed in 6 mm Pyrex glass tubes after degassing of carbon dioxide by repeating the freezing and evacuation. Raman spectra were measured in the low frequency region (14-400 cm^{-1}) at 293 K with a NR-1800 Raman Spectrophotometer (JASCO) equipped with a triple monochromator and a cooled photomultiplier tube (Hamamatsu Photonics R943-02). Scattered light was measured at an angle of 90° relative to the exciting laser beam. The 514.527 nm (19,435 cm^{-1}) line from an argon ion laser (NEC) was used with a power of 150 mW at the sample.

III.C. Computational Details

Ab initio MO calculations were performed by using the Gaussian 94 program package [9] on a DEC workstation (AlphaStation 500). All the calculations were carried out at the Hartree-Fock (HF) level. The 6-31G(d,p) basis set was employed. The 6-31++G(d,p) basis set, which contains one set of diffuse functions on all the atoms, was also employed except for pentamer.

At the HF level, the acetic acid molecules were optimized to have a C_s plane containing the heavy atoms and one of the methyl hydrogen at the side of the C=O group. The other two methyl hydrogens are located symmetrically above and under the carboxylic plane. A planar structure of C_s symmetry was assumed for each cluster species. Force calculations confirmed convergence to the minima on the potential energy surface because the wavenumbers of all the modes were real for the optimized structures of the monomers and the cluster species.

III.D. Results

III.D.1. Raman spectra in the C=O stretching vibrational region

The frequency of the C=O stretching vibration reflects the intermolecular bonding at the carbonyl oxygen of acetic acid. In order to obtain information on intermolecular interaction, we observed Raman spectra of acetic acid under various circumstances in the C=O stretching vibrational region. The spectra are shown in Figure III-1. The thick solid curve in Figure III-1 indicates Raman spectrum of acetic acid in a crystalline sample at 286 K. The thin solid line shows that of acetic acid aqueous solution. The spectrum of acetic acid/carbon tetrachloride mixture is also shown in Figure III-1. The mole fraction of acetic acid is 0.1 in both the solutions, and the temperature of the solutions is 297 K. A vertical arrow at 1770 cm^{-1} indicates the position where high-temperature liquid acetic acid at 343 K shows a high-temperature band attributed to the free (or nonbonded) C=O. The strongest band in the spectrum of crystalline acetic acid is located at 1660 cm^{-1} and other weak band is seen at 1754 cm^{-1}. In the spectrum of aqueous solution, a broad band is observed. The center of the broad band is located at 1710 cm^{-1}. In the spectrum of acetic acid/carbon tetrachloride, the strongest band appears at 1668 cm^{-1} and a weak band is located at 1760 cm^{-1}.

Figure III-2 shows Raman spectra of acetic acid aqueous solutions with x_A = 0.0075, 0.015, and 0.05 in the region of 1200–1900 cm^{-1}. The spectra of water and crystalline acetic acid at 286 K (AA) are also shown for

comparison. The intensity of AA is reduced to approximately 1/15. The bottom spectrum is obtained by subtracting the water spectrum from the spectrum of the aqueous solution at $x_A = 0.015$.

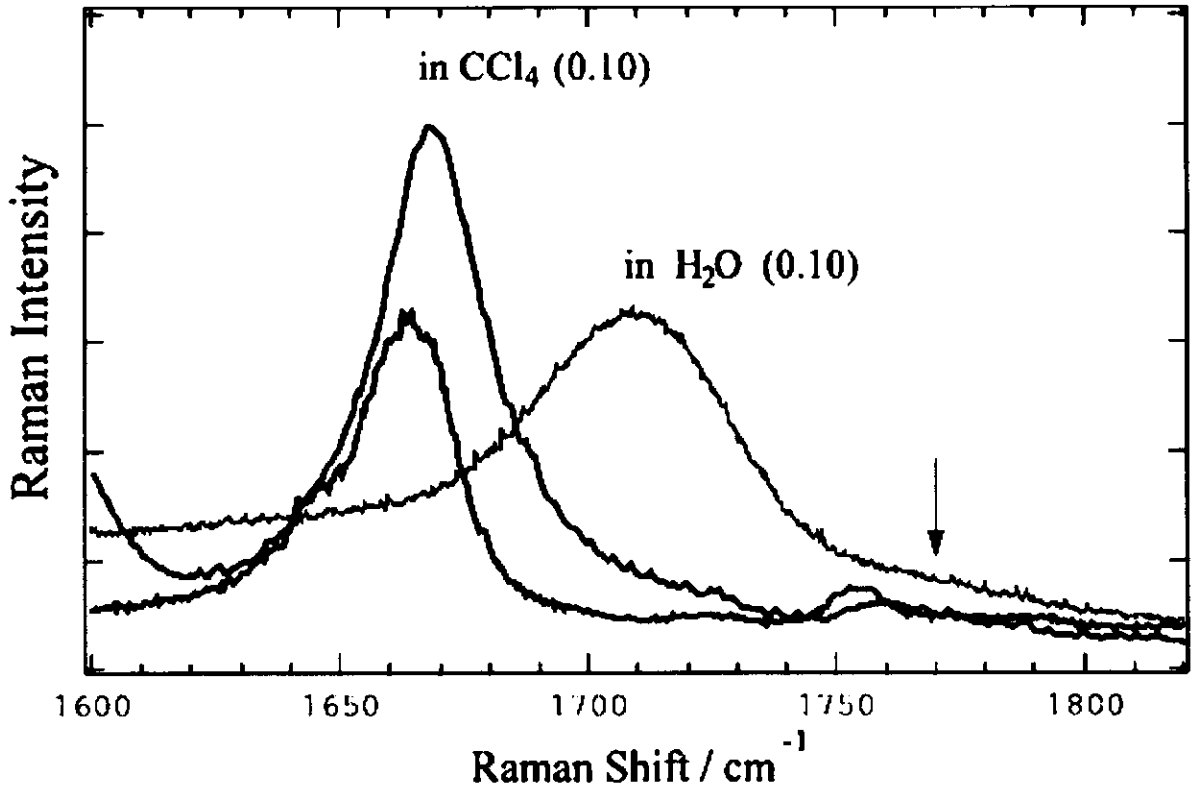

Figure III-1. Raman spectral shifts of the C=O stretching vibration band of acetic acid in a crystalline sample at 286 K (thick solid line), in water (thin solid line), and in CCl_4 (dotted line). The mole fraction of acetic acid is 0.1 in both the solutions, and the temperature of the solutions is 297 K. A vertical arrow at 1770 cm^{-1} indicates the position where high-temperature liquid acetic acid at 343 K shows a high-temperature band attributed to the free (or nonbonded) C=O.

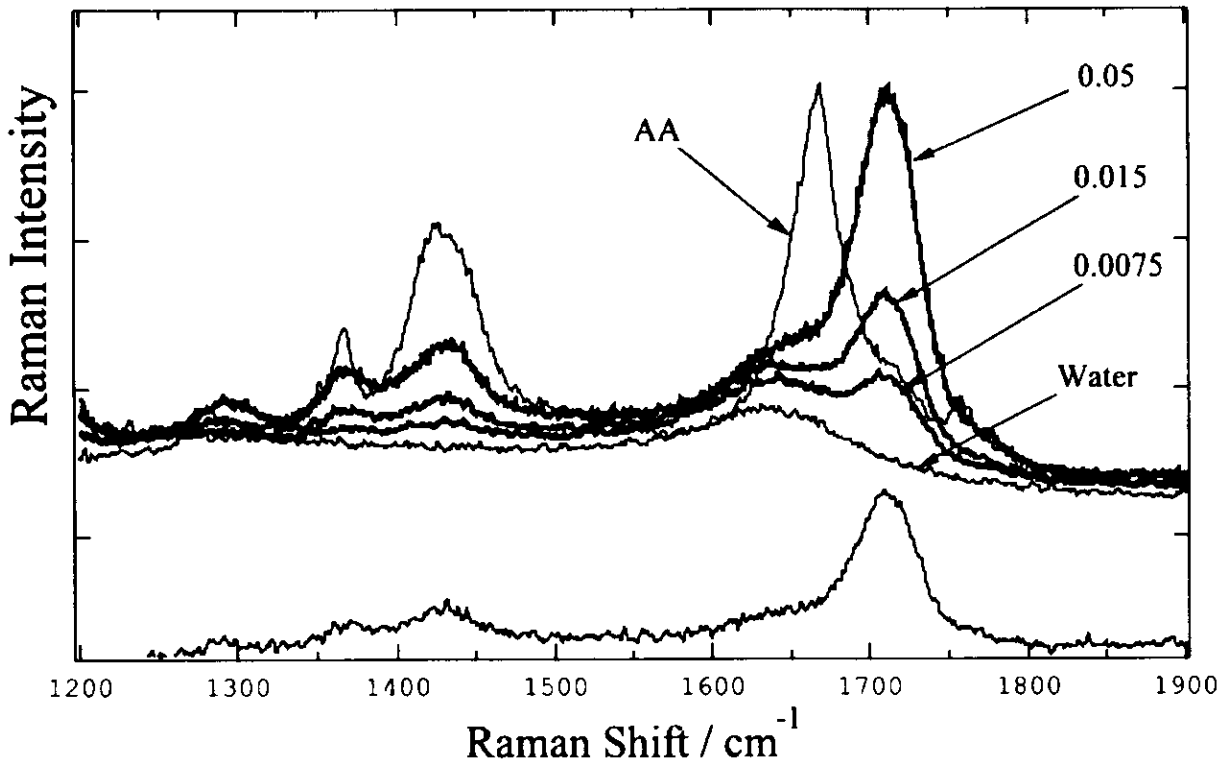

Figure III-2. Raman spectra of acetic acid aqueous solutions with χ_A = 0.0075, 0.015, and 0.05 in the region of 1200-1900 cm^{-1}. The spectra of water and crystalline acetic acid at 286 K (AA) are also shown for comparison. The intensity of AA is reduced to approximately 1/15. The bottom spectrum is obtained by subtracting the water spectrum from the spectrum of the aqueous solution at χ_A = 0.015.

III.D.2. Raman spectra in the O–H and C–H stretching vibrational region

The frequencies of the O–H stretching vibrations of water molecules reflect strengths of hydrogen bonds in neat liquid or aqueous solutions. Raman spectra of acetic acid aqueous solutions with $x_A = 0.10$ and 0.20 in the region of 2700–3700 cm^{-1} are shown in Figure III-3. The spectra of liquid acetic acid and water are also shown for comparison. In the spectra of pure acetic acid and acetic acid aqueous solutions, a strong band is located at 2945 cm^{-1}. As the concentration of acetic acid becomes higher, the intensity of the band becomes larger. The spectra of pure water and acetic acid aqueous solutions show broad bands in the region of 3000–3700 cm^{-1}. As the concentration of acetic acid becomes higher, the intensity of the broad band, especially the component under 3350 cm^{-1}, become weaker.

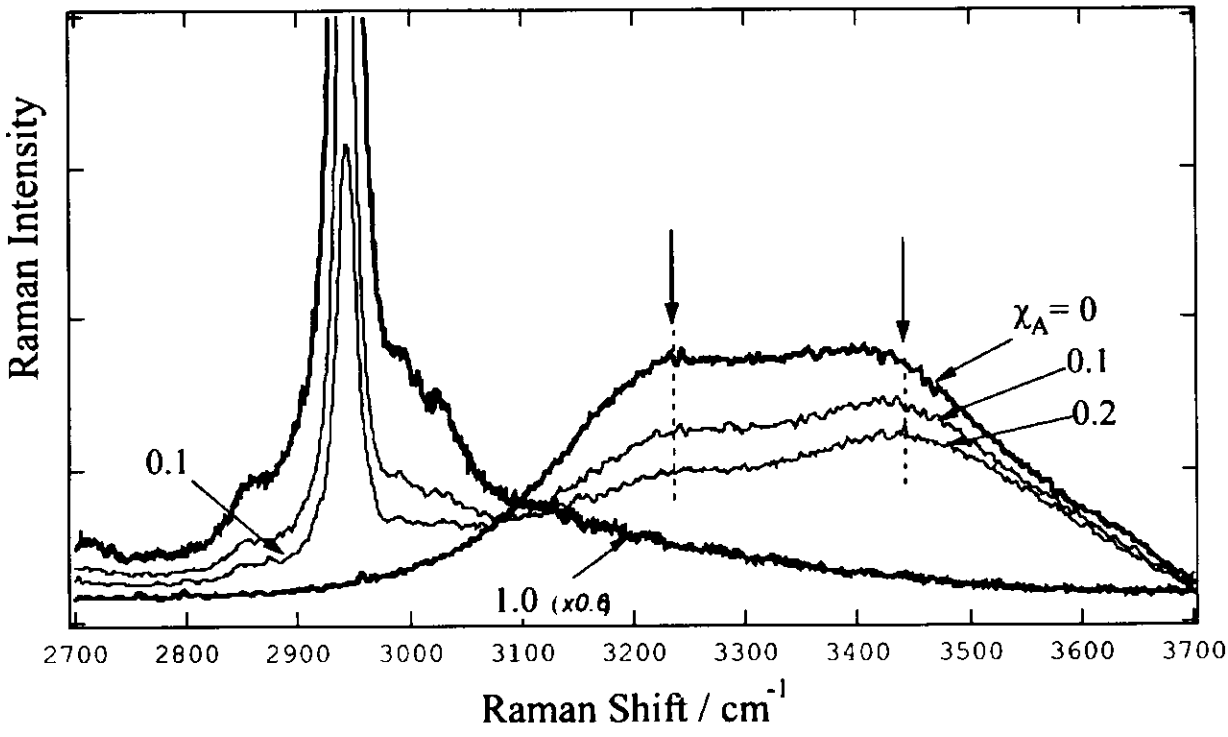

Figure III-3. Raman spectra of acetic acid aqueous solutions with χ_A = 0.10 and 0.20 in the region of 2700-3700 cm^{-1}. The spectra of liquid acetic acid and water are also shown for comparison.

III.D.3. Low-frequency Raman spectra

Low-frequency Raman spectra of binary solutions provide information on the intermolecular hydrogen-bonding in solute-solute, solute-solvent, and solvent-solvent complexes. Figure III-4 shows $R(\bar{\nu})$ spectra of acetic acid/water mixtures at x_A =0 (water), 0.1, 0.2, 0.3, 0.5, 0.8, 0.9, and 1.0 (liquid acetic acid). *ip*H and *ip*L stand for the isosbestic points in the high acetic acid region of $0.5 \leq x_A < 1.0$ and in the low acid region of $0.1 \leq x_A \leq 0.5$, respectively. $R(\bar{\nu})$ spectra of aqueous solutions of acetic acid with x_A =0.0075, 0.015, 0.05, and 0.07 are shown in Figure III-5. We also observe the Bose-Einstein corrected very low-frequency Raman spectra of water and acetic acid aqueous solutions with x_A = 0.0075 and 0.07 and these are shown in Figure III-6-A, III-6-B, and III-6-C, respectively.

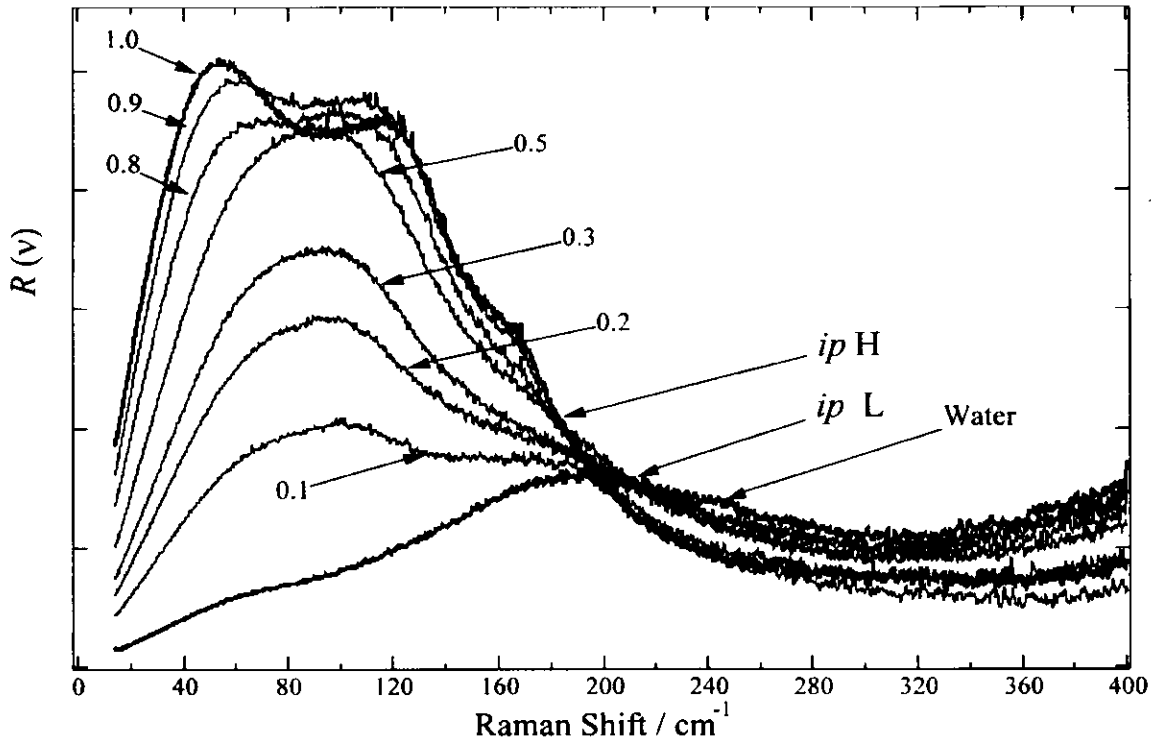

Figure III-4. $R(\tilde{\nu})$ spectra of acetic acid/water mixtures at $\chi_A = 0$ (water), 0.1, 0.2, 0.3, 0.5, 0.8, 0.9, and 1.0 (liquid acetic acid). *ip*H and *ip*L stand for the isosbestic points in the high acetic acid region of $0.5 \leq \chi_A \leq 1.0$ and in the low acetic acid region of $0.1 \leq \chi_A \leq 0.5$, respectively.

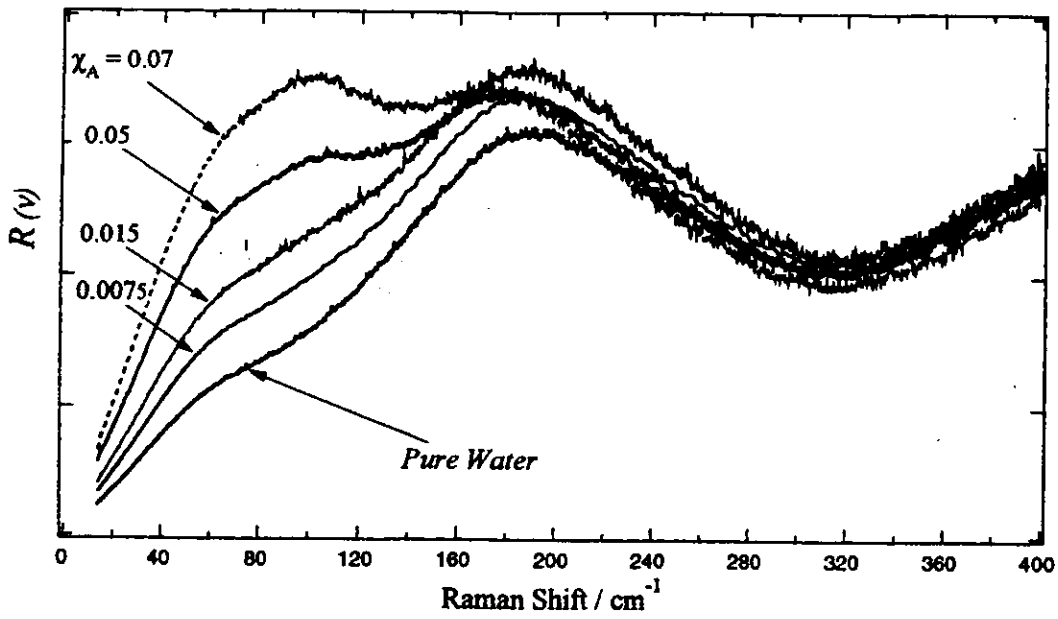

Figure III-5. $R(\tilde{\nu})$ spectrum of aqueous solutions of acetic acid with χ_A = 0.0075, 0.015, 0.05, and 0.07.

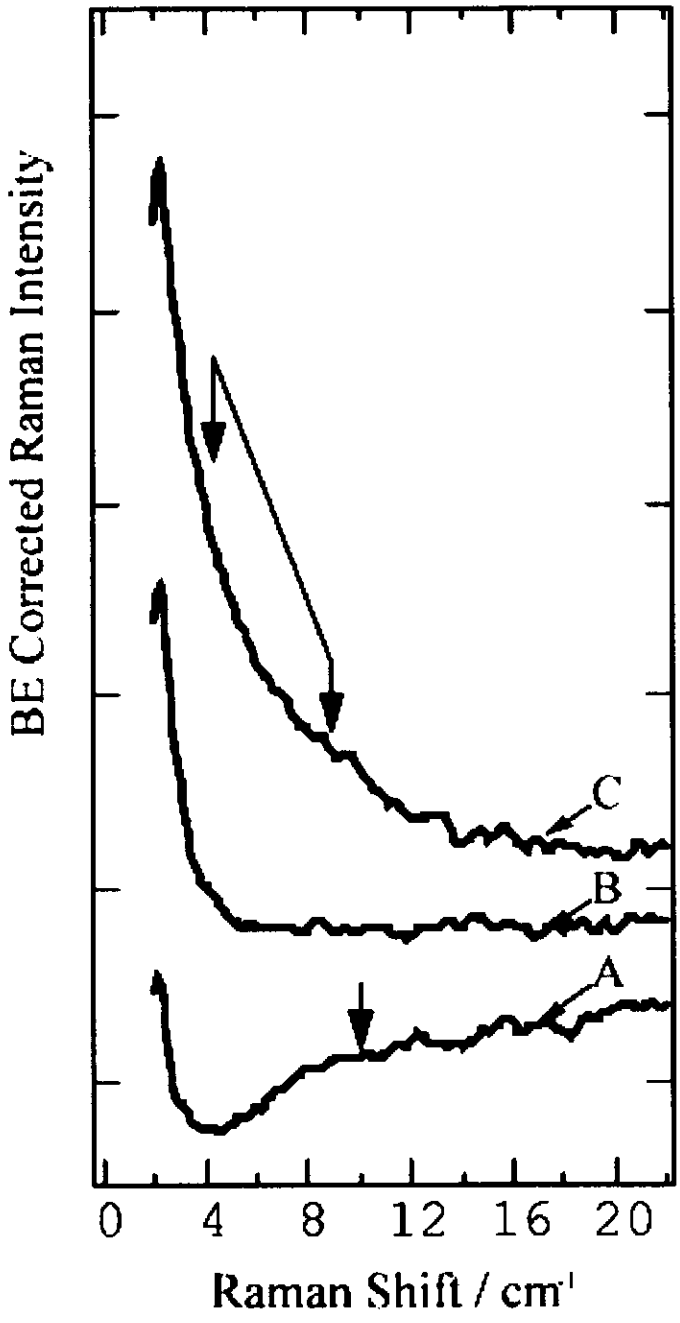

Figure III-6. Bose-Einstein (BE) corrected very low frequency Raman spectra of water (A) and acetic acid aqueous solutions with χ_A = 0.0075 (B) and 0.07 (C). Arrows indicate the peak positions or those of embedded components.

III.D.4. Ab initio molecular orbital calculations

The structures of the dimer species treated in this study are shown in Figure III-7. All of these dimer species contain two intermolecular hydrogen bonds. Two distinct structures of acetic acid-acetic acid dimer are taken into account for the calculation. One is the structure which contains one O–H···O=C hydrogen bond and one additional intermolecular hydrogen bond between the acidic hydrogen and the oxygen atom of the OH group. Hereafter, the dimer is called the side-on type dimer. The other structure is the cyclic dimer and contains two O–H···O=C hydrogen bonds and has C_{2h} symmetry. This dimer is dominant in the gas phase at temperatures below 150°C [10,11]. The optimized structure of the acetic acid-water hetero-dimer has C_s symmetry and contain one O–H···O=C and one O–H···O–H hydrogen bonds. The optimized structure of the acetic acid-methanol hetero-dimer also has C_s symmetry. This structure contain two hydrogen bonds: one O–H···O–H and one C–H···O=C hydrogen bonds.

The calculated binding energies of the dimer species are listed in Table III-I. The values for the side-on type dimer, the cyclic dimer, acetic acid-water dimer, and acetic acid-methanol dimer are –5.27, –12.31, –6.46, and –6.34 kcal/mol, respectively, at the HF/6-31++G(d,p) level. These values are corrected for the zero-point vibrational energies.

Table III-II shows the calculated dipole moments of the above four acetic acid homo- and heterodimers at the HF/6-31G++G(d,p). The side-on type dimer has the largest dipole moment among the four dimers. The value is

4.011 D. The value of dipole moment for the cyclic dimer is zero. The dipole moments of the acetic acid-water dimer and the acetic acid-methanol dimer are 1.106 and 2.220 D, respectively.

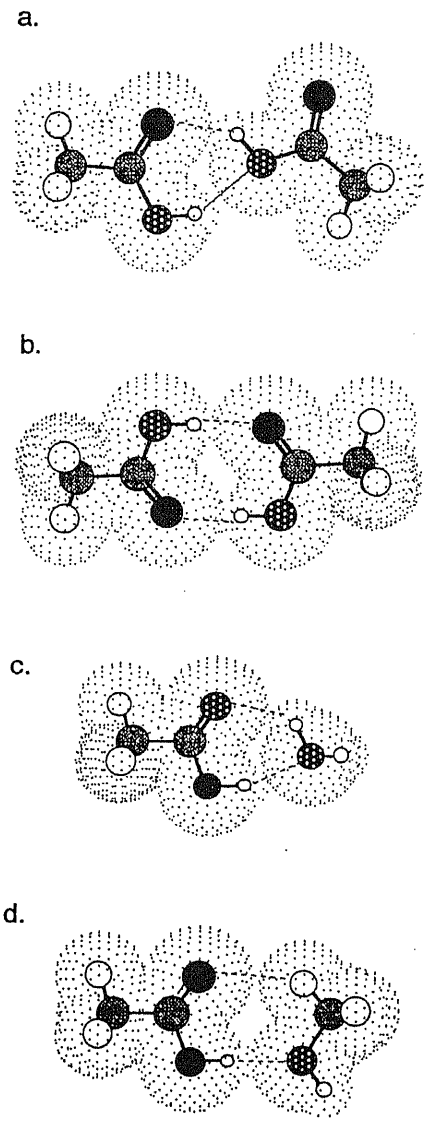

Figure III-7. Structures of acetic acid dimers; a side-on dimer (a), a cyclic dimer (b), an acetic acid-water heterodimer (c), and an acetic acid-methanol dimer (d) obtained by ab initio molecular orbital calculations at the HF/6-31++G(d,p) level. The binding energies of the respective dimers are given in Table III-I.

TABLE III-I. Calculated binding energies of acetic acid homo- and hetero-dimers at the HF/6-31++G(d,p) level after correction for ZPVE.

	binding energy / kcal mol^{-1}
side-on dimer	–5.27
cyclic dimer	–12.31
acetic acid–water	–6.46
acetic acid–methanol	–6.34

TABLE III-II. Calculated dipole moments of acetic acid homo- and hetero-dimers at the HF/6-31++G(d,p) level.

	dipoel moment / debye
side-on dimer	4.011
cyclic dimer	0.000
acetic acid–water	1.106
acetic acid–methanol	2.220

III.E. Discussion

III.E.1. Spectral shifts of Raman-active intramolecular vibrations

Frequency shifts of intramolecular vibrations provide qualitative information on the structural change related to solute-solvent and solute-solute interactions. In particular, hydrogen-bond formation of the C=O group of a carboxylic acid causes a clear spectral shift to a lower wavenumber dependent on the degree of its binding strength. [12,13] Bertie and Michaelian studied the Raman spectrum of the gas phase cyclic dimer. [14] They observed a C=O stretching vibration band of the cyclic dimer at 1681.5 cm^{-1} and a monomer band at 1789.6 cm^{-1}. Ng and Shurvell applied the factor analysis method to the Raman spectra of acetic acids in aqueous solution. [12] They assigned the major components in the spectrum of the mixture with x_A = 0.17 to monomer and cyclic dimer bands with the band positions at 1696 cm^{-1} and 1673 cm^{-1}, respectively, although they are overlapped forming a broad band. The difference is only 23 cm^{-1} in contrast to the large difference of 108 cm^{-1} in gas phase. The spectrum of the aqueous mixture with x_A = 0.10 is shown in Figure III-1 with a thin solid line. In the figure, the spectrum of an acetic acid/carbon tetrachloride mixture with x_A = 0.10 and that of crystalline acetic acid at 286 K are also shown with a dotted line and a thick solid line, respectively, for comparison. As clearly seen, the peak of the broad band is located at 1710 cm^{-1} shifted by 50 cm^{-1} to the higher wavenumber from the crystalline band position and 42

cm^{-1} from the peak of the carbon tetrachloride mixture band. At 343 K, the spectrum of the acetic acid and carbon tetrachloride mixture with $x_A = 0.10$ shows intensity increment of the bands at 1760 cm^{-1}, and the strong low wavenumber bands at 1668 cm^{-1} shows eminent intensity decrease. The band at 1760 cm^{-1} is assigned to acetic acid monomer species and that at 1668 cm^{-1} to the C=O group linearly hydrogen-bonded with the OH group of another acid. The temperature increase may induce the dissociation of the linear hydrogen bond. The dissociation energies are estimated to be 10 ($\pm$2) kcal/mol from the temperature dependence. Crystalline acetic acid has a network structure composed of strong linear hydrogen bonds. [15,16] In carbon tetrachloride, acetic acid molecules are expected to form a cyclic dimer structure or an aggregate structure similar to crystalline acetic acids. The spectral shift from the C=O stretching band of the free species amounts to approximately 100 cm^{-1}. This is in good coincidence with the shift in gas phase. [14] The peak position of the C=O stretching band of the aqueous solution is located just between the wavenumber for the free C=O and that of the strongly hydrogen-bonded one. As the factor analysis by Ng and Shurvell showed, the broad band at 1710 cm^{-1} is analyzed as a composite of two components. [14] Both of them cannot be attributed to the C=O group either with a linear hydrogen bond or free from any hydrogen bond. A bent-type hydrogen bond can explain this shift to the intermediate position. Figure III-2 shows the concentration dependence of the C=O stretching band in a low acid concentration region. The spectra obtained after the subtraction of the water spectrum (mostly ν_2 vibration) show essentially no

concentration dependence of the spectral shape in the region of $0.2 \geq x_A \geq 0.0075$. The subtracted spectrum of the mixture at $x_A = 0.015$ is shown in the lower part of Figure III-2 where one can see an asymmetric band shape of the C=O stretching band at 1710 cm^{-1}. This is attributed due to the presence of overlapping two bands at 1695 and 1715 cm^{-1}.

The O-H stretching vibrations of acetic acid and water are expected to exhibit large spectral shifts on hydrogen-bond formation. Figure III-3 shows the Raman spectra of aqueous solutions with x_A =0.1 and 0.2 in the region from 2700 cm^{-1} to 3700 cm^{-1}. The spectra of liquid acetic acid and water are also displayed for comparison. The strongest band at 2945 cm^{-1} is the C-H stretching band of acetic acid. The water spectrum shows the two peaks at 3230 cm^{-1} and 3420 cm^{-1}. The band contour of the water spectrum is reproduced by assuming 4 Gaussian components with the band centers at 3610, 3410, 3220, and 3100 cm^{-1}. The result of the Gaussian analysis of the water spectrum is shown at the top of Figure III-8, where the four components are designated as components 1, 2, 3, and 4, respectively. On the basis of the degree of wavenumber shift, component 1 at 3610 cm^{-1} is assigned to the ν_1 mode of a water molecule of which two hydrogen atoms are both free from hydrogen-bonding and corresponds to the 3657.1 cm^{-1} band in the gas phase [17]. Component 2 at 3410 cm^{-1} is to the ν_1 mode of a weakly associated water molecule of which one hydrogen is bonded to a neighbor water molecule but the other one is not bonded. In principle this kind of water molecule should show two O-H stretching bands. The very broad feature of this band could be attributed to the overlapping two

components of the weakly associated water molecule. Another possibility is due to a water dimer with non-linear hydrogen bonds such as bifurcated species. It is very difficult to assign this broad component to any specific structure of weakly associated dimers. Component 3 at 3220 cm^{-1} is to the ν_1 mode of a water molecule of which two hydrogen atoms are bonded to neighbor molecules. This strongly bonded water must be in different situation from that of the icy water with tetrahedral coordination that appears as component 4 at 3100 cm^{-1} in Figure III-8. Hare and Sorensen [18] observed a strong Raman band of ice at 3100 cm^{-1}. Here we call the molecules responsible to component 2 as weakly associated water molecules and the molecules with the two hydrogen atoms bonded (responsible to components 3 and 4) as strongly bonded water molecules.

The lower two spectra are obtained by subtracting the scaled liquid acetic acid spectrum from the spectra of the acetic acid/water mixtures with x_A =0.1(middle) and 0.2 (bottom). The subtraction is performed in order to eliminate the C-H stretching band of acetic acid. However, because of a little spectral shift of this band, the subtraction provides a negative and a positive spikes with equivalent intensity. With increasing acid concentration, decrease in the strongly bonded components becomes much eminent suggesting the break of the water structure. The ratios of the strongly bonded components to the weakly associated component at various molar fractions of acetic acid are plotted and fit to a double exponential function in Figure III-9:

[Strongly bonded] / [Weakly associated] =

$$0.252 + 0.114 \exp(-1.186\, x_A) + 0.220 \exp(-13.5\, x_A). \quad (1)$$

At a concentration of x_A =0.05, the second component becomes equivalent to the third component that is the main term in the high x_A region. This concentration of x_A =0.05 appears to have an important meaning in a later section.

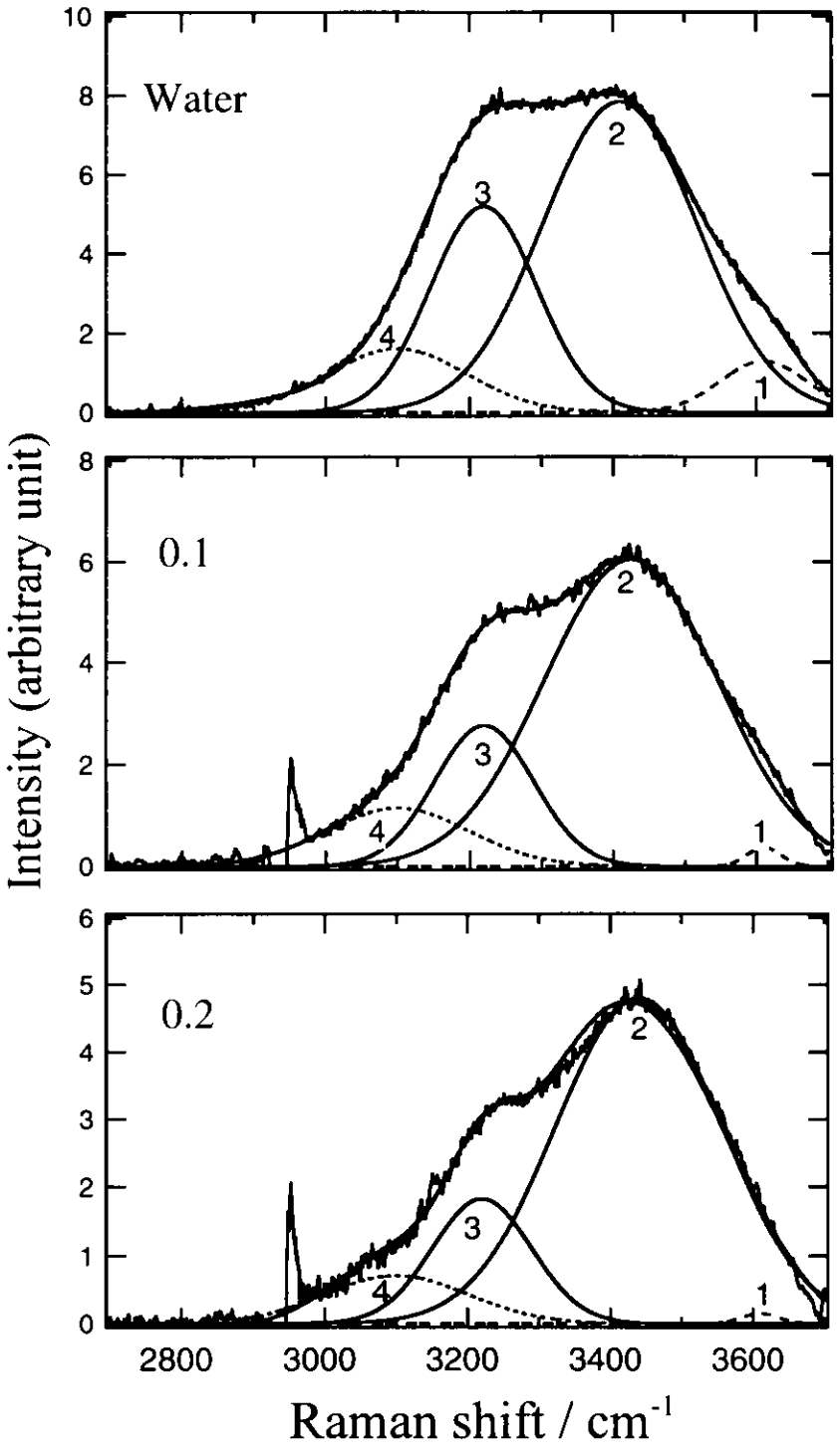

Figure III-8. Relative intensity change of the Gaussian components in the water spectra. The water spectra of the aqueous solution of acetic acid were obtained by subtracting the scaled spectrum of liquid acetic acid from the original spectra shown in Figure III-3. The scaling factor was obtained so as to extinguish the sharp C-H band of acetic acid at 2940 cm^{-1}. The assignment of components 1-4 is given in the text.

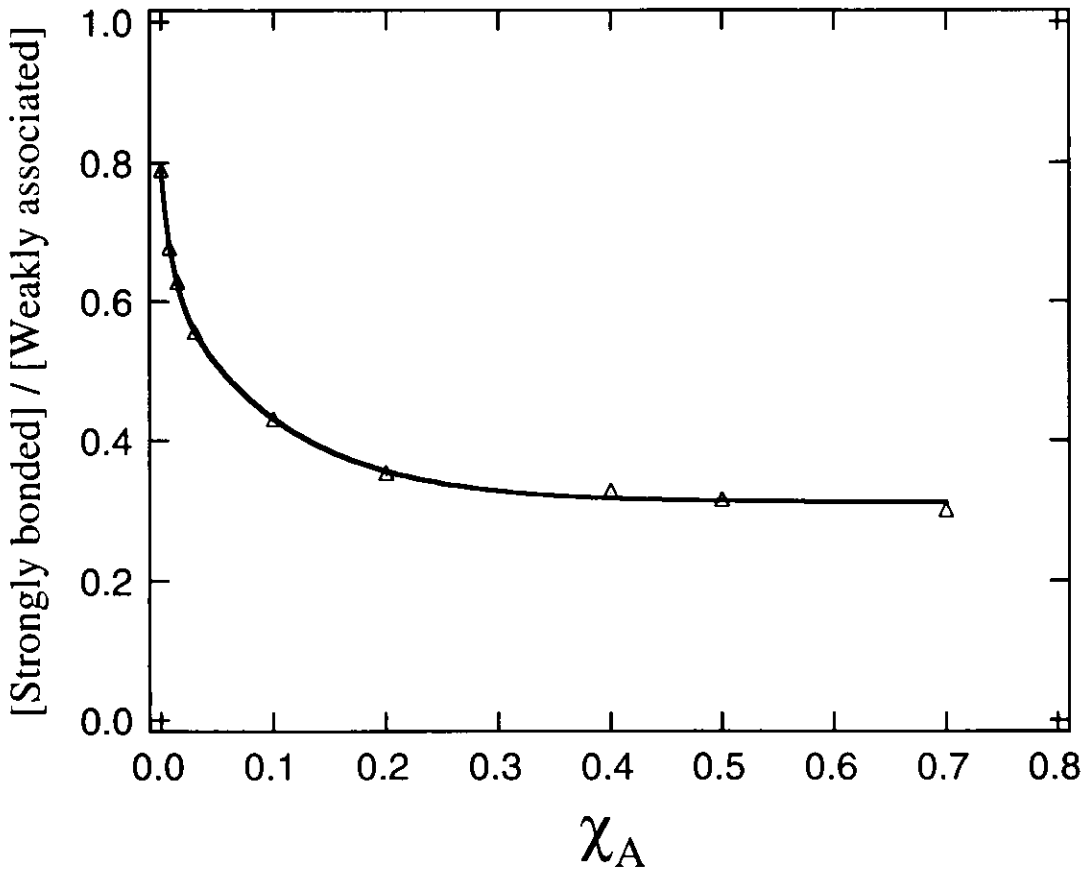

Figure III-9. Intensity ratio of the strongly bonded O-H components to the weakly associated components as a function of χ_A (acetic acid mole fraction).
The solid curve is a double-exponential function expressed by eq 1.

III.E.2. Low-frequency Raman spectra

The Rayleigh wing spectra have been presented in a function of the so-called $R(\bar{\nu})$ [4-8,19]:

$$R(\bar{\nu}) = I(\bar{\nu})(\bar{\nu_0} - \bar{\nu})^{-4}\,\bar{\nu}\,[1 - \exp(-hc\bar{\nu}/kT)] \quad , \qquad (2)$$

where $\bar{\nu_0}$ is the frequency of the exciting laser line (in cm^{-1}), and $I(\bar{\nu})$ is scattered light intensity of frequency $\bar{\nu}$. The $R(\bar{\nu})$ spectrum has the practical advantage of essentially removing the intensity of the exciting laser line and extracting from the measured Raman spectrum a quantity that is related to the vibrational density of states. Figure III-4 shows the $R(\bar{\nu})$ spectra of acetic acid/water mixtures at x_A =0 (water), 0.1, 0.2, 0.3, 0.5, 0.8, 0.9, and 1.0 (liquid acetic acid). With increasing acetic acid from x_A =0.1 to 0.5, an evolving spectral component is seen in the region from 50 to 120 cm^{-1}. This component has the same spectral feature with the spectrum at x_A =0.5. From x_A =0.5 to 1.0, the change is very much different from that in the low concentration region: the intensity change is not so large but the structural change is drastic. The spectrum at x_A =0.5 is completely different from that of liquid acetic acid (x_A = 1.0). The presence of the isosbestic points at 210 cm^{-1} in the low concentration region and 180 cm^{-1} in the high concentration region may suggest the three states of associates: pure water cluster state, 1:1 mixture state, and pure acetic acid state. Thus we have attributed the 1:1 mixture state to the acetic acid-water cluster state in reference 20. However, we are in face of a difficult situation for this assignment with new

experimental and theoretical results.

In Figure III-10-a, the low frequency Raman spectra of the acetic acid/water mixtures at x_A =0.5 (thick line) and 0.3 (thin line) are compared with that of acetic acid/methanol mixture at x_A =0.3 (thin broken line). The intensity scale is normalized for the peak intensities of the respective spectra. Although the spectra at x_A =0.3 contain some contribution from either the water clusters or the methanol clusters seen in the respective pure liquids, the main feature of the spectral pattern is similar to each other. The same molecular cluster(s) must be responsible to the low frequency spectra of the acetic acid/water and the acid/methanol mixtures. Vibrational wavenumbers of molecular complexes of acetic acid with methanol are expected to show large difference from those of acetic acid-water complexes because of the mass difference between the partners. Thus the two hetero-dimers are expected to show spectral features different from each other. In fact, the ab initio calculation (Fig. III-10-d) of an acetic acid-water and acetic acid-methanol dimers at the HF/6-31++G(d,p) level provides Raman active vibrations at higher wavenumbers in the region of 150-400 cm^{-1}. The geometries of the optimized dimers are shown in Figures III-7-c and III-7-d, respectively. We also examined the Raman activity spectra of various acetic acid homo-dimers. [21] The side-on type acetic acid dimer shown in Figure III-7-a provides a Raman structure in Figure III-10-b that well reproduces the spectral feature of the three spectra in Figure III-10-a. The cyclic dimer with the structure shown in Figure III-7-b also provides the four bands in the region of 50-160 cm^{-1}. The integrated Raman intensity of the

intermolecular bands of the side-on dimer is stronger than that of the cyclic dimer. The calculated spectral pattern of the side-on dimer shows a better fitting to the observed spectrum rather than that of the cyclic dimer. However, it is not so conclusive for the assignment of the observed low frequency spectra because of the broad feature of the observed spectra. From the calculated spectra, one can only say that the main origin of the low frequency spectra must be acetic acid dimer units. As shown in a previous section, however, the spectral position of the intramolecular C=O stretching vibration indicates that the C=O group is not so strongly hydrogen-bonded. Any dimer structure with a linear hydrogen-bond is not able to explain this point but the side-on dimer with the bent-type hydrogen-bonds accounts for all of the observed results. A problem is how the side-on dimer unit can be well stabilized in aqueous environment in spite of its small binding energy in gas phase compared with that of the cyclic dimer.

The calculated binding energies for the acid-water dimer, the acid-methanol dimer, the side-on type homo-dimer, and the cyclic homo-dimer are –6.46, -6.34, –5.27, and –12.31 kcal/mol, respectively, at the HF/6-31++G** level. These values are corrected for the zero-point vibrational energies. So, the gas phase dimerization energy of the side-on type dimer is not favorable to the hetero-dimers, although the differences from the values of the two hetero-dimers are approximately 1 kcal/mol. Apparently the binding energy of the cyclic dimer is more than twice as large as that of the side-on type dimer in gas phase. Thus in gas phase we have little possibility of observing the side-on dimer. Aqueous solution is an polar

environment where polar solute species are well stabilized by the surroundings.

Table III-II shows the calculated dipole moments of the above four acetic acid homo- and hetero-dimers. The side-on type dimer exhibits the largest dipole moment (4.011 D) among them in contrast to the null dipole moment of the cyclic dimer. In the concentration region studied here, dipole-dipole interaction between the dimer pairs can be also important for generating higher clusters. The energy of dimer-dimer interaction between the cyclic dimers is of the order of van der Waals interaction energies, while that between the anti-parallel pairs of two side-on dimers is expected to be sufficiently large. Recently, Nakabayashi et al. have performed a calculation of the binding energy change in aqueous environment of the two dimers by the RISM-SCF method, that predicts a little difference between the stabilization energies of the two dimer species in water. [22] The calculation suggests that the dimer-dimer interaction energy of the two side-on dimers fairly exceeds over that of the two cyclic dimers.

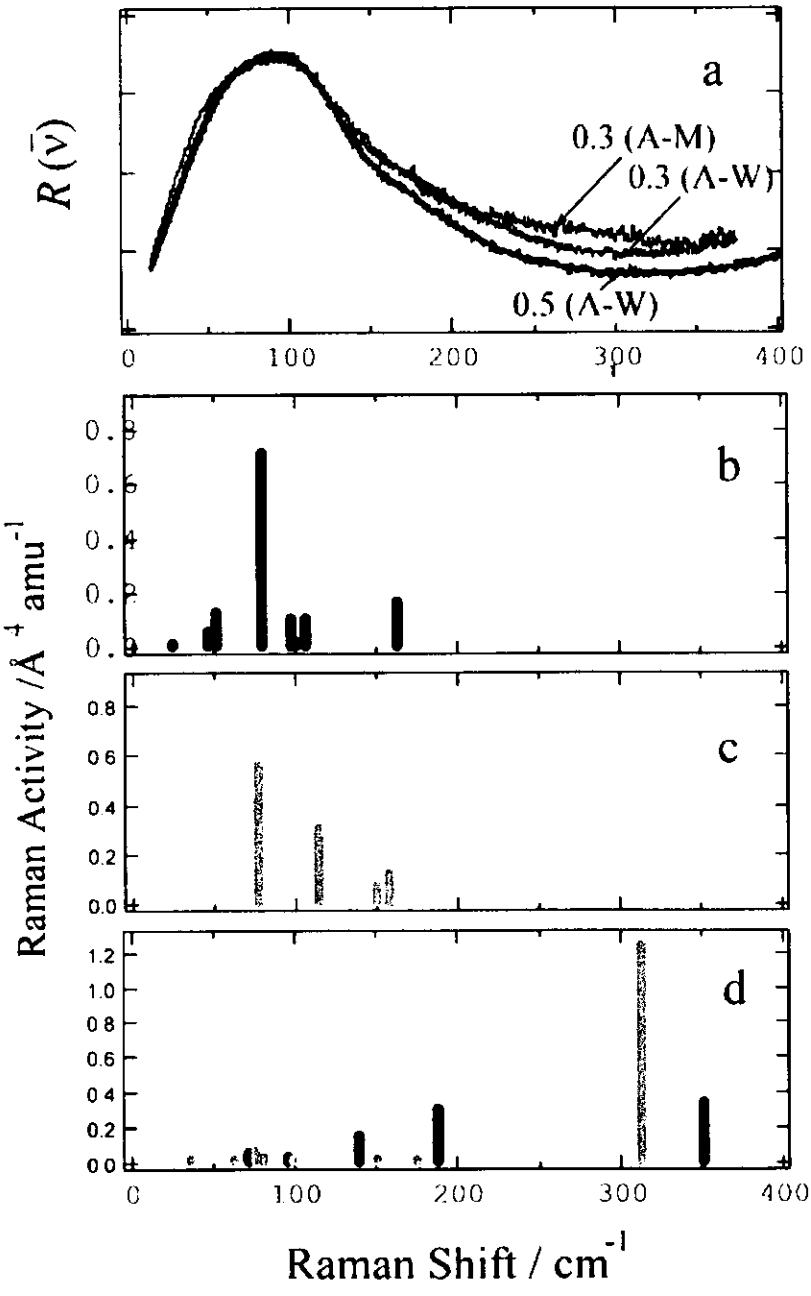

Figure III-10. (a) Low-frequency Raman spectra of the acetic acid/water mixtures at χ_A = 0.5 (thick line), at χ_A = 0.3 (thin line), and the spectrum of acetic acid-methanol mixture at χ_A = 0.3 (thin broken line). The intensity scale is normalized for the peak intensities of the respective spectra. (b) HF/6-31++G(d,p) level calculation of Raman activities of bimolecular vibrations of a side-on dimer. (c) The same level calculation of a cyclic dimer. (d) Calculated Raman activities of acetic acid-water (black bars) and acetic acid-methanol (gray bars) heterodimers.

III.E.3. Analysis of low-frequency spectra

The presence of the isosbestic points at 210 cm^{-1} in the low concentration region in Figure III-4 may suggest the presence of the two states: the pure water cluster state and the acetic acid cluster state with the side-on type (and less probably cyclic) dimer unit(s). The latter state dominates the spectrum of the mixture with x_A =0.5. As we saw in the case of ethanol/water mixtures [1], the $R(\bar{\nu})$ spectra can be explained without the contribution from any pair of water and acetic acid, or could be as the sum of the $R(\bar{\nu})$ spectrum of pure water and that of the mixture with x_A =0.5. Thus the $R(\bar{\nu})$ spectra of binary solutions are decomposed into linear combinations of the $R(\bar{\nu})$ spectra of pure water and the mixture with x_A =0.5:

$$R(\bar{\nu}; x_A) = aR(\bar{\nu}; x_A = 0) + bR(\bar{\nu}; x_A = 0.5), \qquad (3)$$

where $R(\bar{\nu}; x_A)$ is the $R(\bar{\nu})$ spectrum of an acetic acid/water binary solution with an acetic acid mole fraction of x_A, $R(\bar{\nu}; x_A = 0)$ is that of pure water, $R(\bar{\nu}; x_A = 0.5)$ is that of the 1:1 mixture, and *a* and *b* are the coefficients which should be calculated from the best fit procedure. Decomposition of the $R(\bar{\nu}; x_A)$ spectra was carried out with a conventional least squares fitting method. The all $R(\bar{\nu}; x_A)$ spectra were decomposed successfully into simple linear combinations and Figure III-11 shows some examples of the analysis for the spectra of the three mixtures with x_A = 0.015, 0.10, and 0.30. The coefficients *a* and *b* are plotted as a function of acetic acid mole fraction x_A in Figure III-12. The fact that the mixture spectra are reproduced with

linear combinations of the two basic spectra indicates that the mixtures are composed of the microscopic fragments of the two basic solutions. The dimer and small cluster units of water that characterize the low frequency spectra of water exist in the mixtures as fragments of liquid water. And such a unit in the 1:1 mixture must also exist in the intermediate region. This result is in accord with the microphase model of the aqueous mixtures proposed on the basis of ultrasonic absorption measurement. [23]

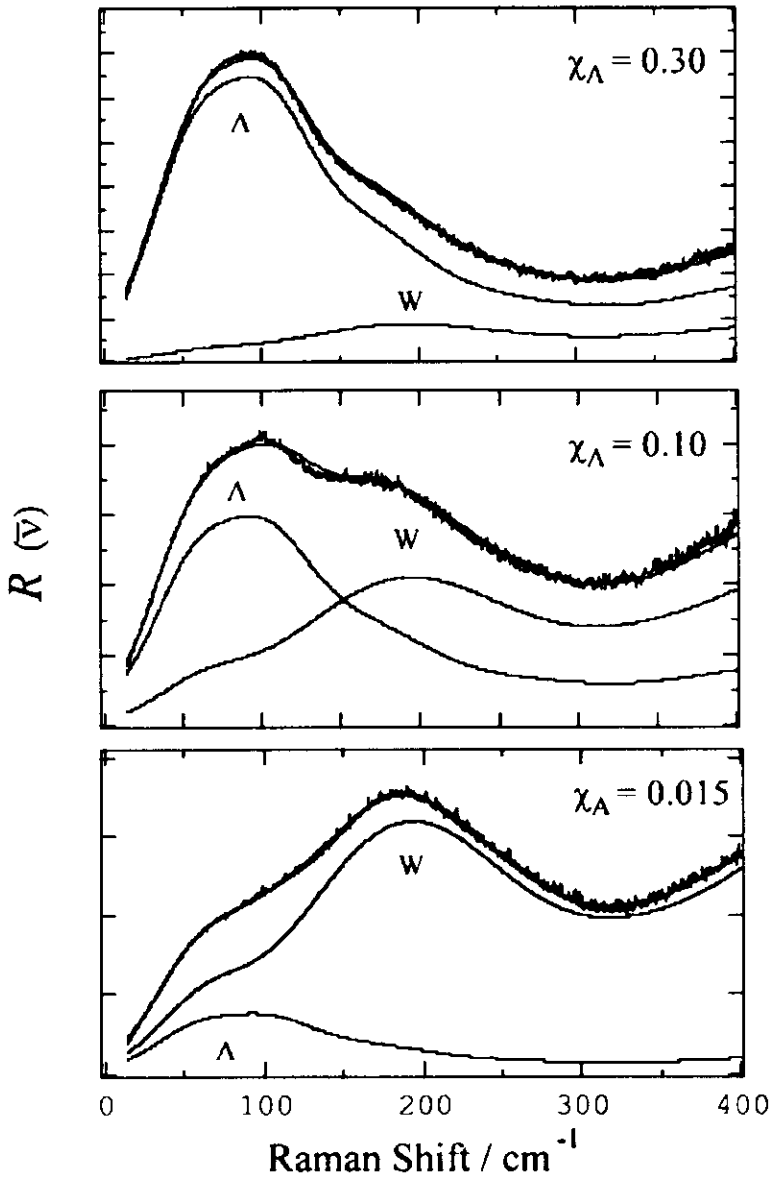

Figure III-11. Decomposition of the observed $R(\tilde{\nu})$ spectra of the binary solutions with χ_A = 0.015, 0.10, and 0.30 into linear combinations of the $R(\tilde{\nu})$ spectra of pure water and the mixture with χ_A = 0.5. The sum spectra calculated by a least-squares fitting method are shown with solid lines.

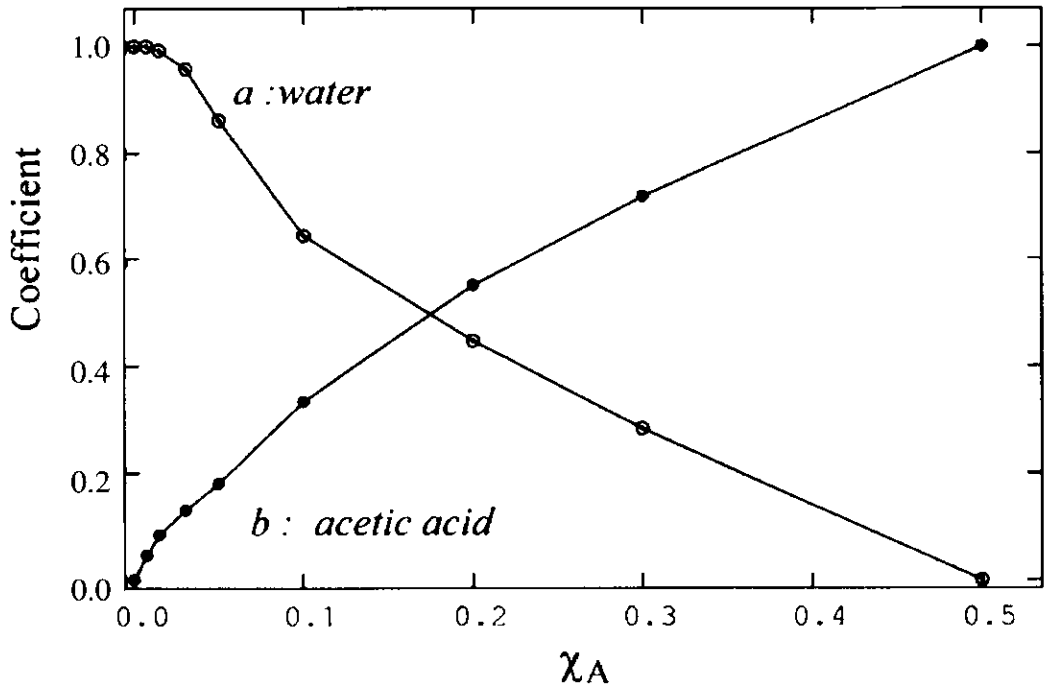

Figure III-12. Concentration dependence of the coefficients of the water component (a) and the acetic acid cluster component (b) that are the $R(\tilde{\nu})$ spectrum of the 1:1 mixture ($\chi_A = 0.5$).

III.E.4. Hydrophobic hydration

In this study, we measured the spectra with a mole fraction interval of 0.1 and observed the isosbestic point at 210 cm^{-1} in the low mole fraction region. In addition to this, we also measured the low-frequency Raman spectra of acetic acid aqueous solutions in the very low mole fraction region. Figure III-5 shows the $R(\bar{\nu})$ spectra of the aqueous solutions with x_A = 0.0075, 0.015, 0.05, and 0.07. The $R(\bar{\nu})$ spectra in Figure III-4 are for the solutions with $x_A \geq 0.10$. We can find intensity anomaly in the lower concentrations. The $R(\bar{\nu})$ spectra of the diluted solutions from x_A = 0.05 to 0.0075 exhibit surprising changes: 1) at x_A = 0.0075 the intensity of the water component increases more than that of pure water, and 2) drastic intensity drop of the water component is seen at $x_A \geq 0.03$ (Figure III-12). The intensity enhancement of the water component is synchronized with the drastic increase of the 1:1 mixture component. This means that the dimerization of acetic acid molecules becomes prominent at x_A = 0.0075. The anomaly 1) results in the deviation of the intensity from the isosbestic point at 210 cm^{-1}. One cannot see the isosbestic point in this lower concentration region. This is just because of the intensity enhancement of the water component around x_A = 0.015 as clearly seen in Figure III-5. Figure III-12 also indicates that the increase in the water component is accompanied with the intensity enhancement of acetic acid component at these low concentrations. Thus we attribute the increase of the water component to " hydrophobic hydration" coupled with the generation of larger hydrophobic area due to

the acetic acid clustering. This is what we saw in the mass spectrometric analysis of carboxylic acids in diluted aqueous solutions. [24] Apparently this phenomenon is enhanced for the systems with larger alkyl chains. However, hydrophobic hydration requires numbers of water molecules sufficient for the construction of a hydrophobic shell covering the hydrophobic area. At concentrations higher than $x_A = 0.05$, the average number of water molecules for the shell formation around one solute molecule is smaller than 20 and any stable shell is not formed with the lower water numbers. This must be related to the result that the spectral change of the intramolecular OH stretching vibration of water molecules shown in Figure III-9: the intensity of the O-H band of hydrogen-bonded O-H group decreases eminently with increasing acid concentration at $x_A \geq 0.05$. Hydrophobic hydration can be seen at the diluted solute concentrations.

III.E.5. Three-state model and density change

All the observed low frequency spectra of the mixtures are reproduced simply by the linear combination of the pure water spectrum and that of the 1:1 mixture in the low concentration region of $0 < x_A < 0.5$, and also by the combination of the spectrum of liquid acetic acid and that of the 1:1 mixture in the high concentration region, $0.5 < x_A < 1.0$. In addition to this fact, the observation of the two independent isosbestic points in the respective regions strongly suggests that there are three microscopic states of clusters (or aggregates). State 1: water cluster state in which intermolecular vibrations of water clusters are responsible for the low frequency Raman spectrum of water; state 2: acetic acid cluster state with side-on type dimer units associated with dipole-dipole interaction, the Raman spectrum of the 1:1 mixture reflects the structure of this state; and state 3: acetic acid cluster state with structures characteristic of liquid acetic acid. The densities of the mixtures [25] plotted as a function of acetic acid mole factions are shown in Figure III-13. The density of the 1:1 mixture shows a maximum at $x_A = 0.5$ that indicates the presence of the closest packing of the molecules at this mixing ratio. The density change in Figure III-13 clearly show the change of structures described by the three state model.

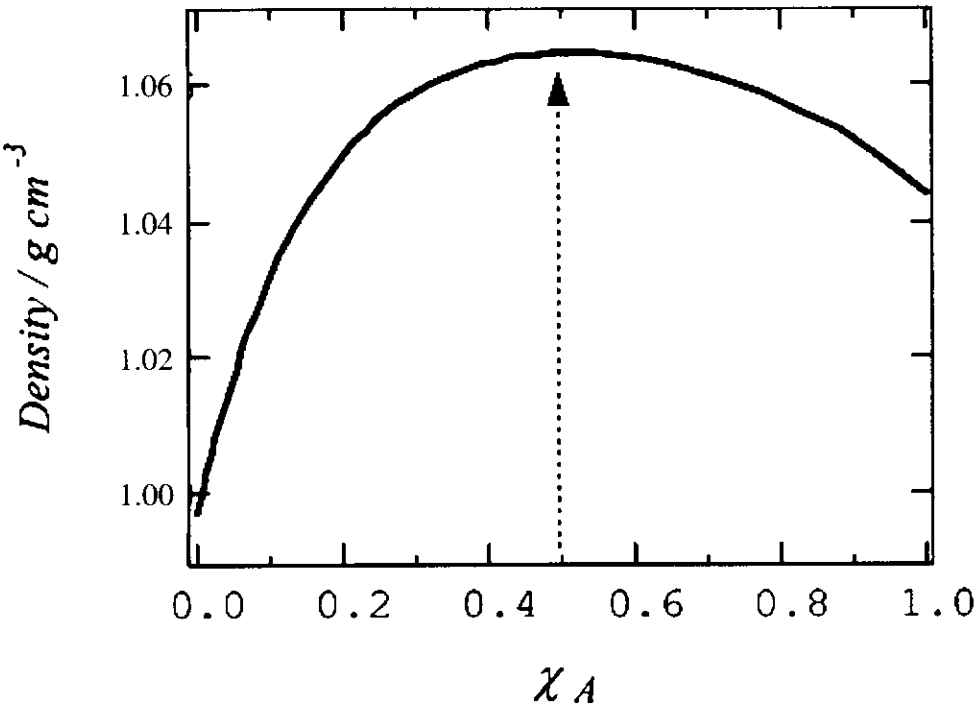

Figure III-13. Density change of aqueous mixtures of acetic acid against mole fractions of acetic acid; data are taken from ref. 25.

III.E.6. Rayleigh wing spectra and microphase formation

Kaatze et al. presented a microphase model for carboxylic acid/water mixtures [23] and alcohol/water mixtures [26] on the basis of dielectric studies. Information on the presence of microphases composed of solute and/or solvent molecules can be also obtained from very low frequency Raman spectra in the region $\bar{\nu} < 20\ cm^{-1}$. Figure III-6 shows Bose-Einstein (BE) corrected [27-29] very low frequency Raman spectra of water (spectrum A), aqueous mixtures with $x_A = 0.0075$ (spectrum B) and 0.07 (spectrum C). As reported by Rousset et al., [28] the water spectrum at 298 K exhibits a hump at 10 cm^{-1}. This signal is temperature dependent in intensity and the position. The frequency increases with increasing temperature and falls to zero at -30° C. Addition of a small amount of acetic acid in water enhances the wing intensity drastically, particularly in the region from 4 to 8 cm^{-1}.

Interpretation of the low frequency Raman component of water became very realistic after the simulation study by Madden and Impey. [4] They succeeded to explain the observed Raman band of water at 50 cm^{-1} with the motion of the molecular center of mass through the polarizability induced by dipole-dipole interaction between water molecules. Dipole-dipole interaction between the acetic acid clusters with large dipole moments is expected to induce strong Raman signals in the very low frequency region. On the basis of the Raman studies of nuclei in glasses and silica particles in aerogels, Rousset et al. assumed that the low frequency temperature-

dependent Raman scattering comes from oscillations of transient water aggregates with a somewhat ordered structure. Ohmine [30] showed that the orientational relaxation coupled with long range dipole-dipole interaction is responsible to the Raman spectrum of water at the low frequency of 5–20 cm^{-1}. The 10 cm^{-1} component in the water spectrum in Figure III-6 must be related to this orientational relaxation of large water clusters. From this signal, Rousset et al. estimated the average size of the clusters at room temperature to be 11 Å. Because of longer sizes and larger dipole moments of the side-on type dimer and higher clusters with the dimer unit, orientational relaxation of the clusters is expected to take much longer time than that of water. These factors may also result in the enhancement of the Raman intensity due to larger dipole-dipole interactions in the process of the orientational relaxation. The clusterization of acetic acid molecules with large dipole-dipole interaction thus provides us a reasonable elucidation for the enhanced activity of the very low frequency Raman component as compared with that of water. The microphase model is in accord with the present observation of the enhancement in the very low frequency component of the Raman spectra of the mixtures. As expected from the crystal structure of acetic acid, dipole-dipole interaction could be dominated in the acetic acid clusters elongating the lifetimes of the clusters in aqueous solutions.

On the basis of the measurement of excess partial molar enthalpies of small alcohols in aqueous solutions, Koga and his coworkers reported the importance of solute-solute association in the concentrations as low as a

solute mole fraction of 0.01. [31,32] In the mass spectrum of the ethanol/water mixture solution with an ethanol mole fraction of 0.01, dominant ethanol-ethanol association were also observed. [33] Generation of micro phases in aqueous solution must be a general trend seen for the most of solute species, although their sizes may vary dependent on concentration, temperature, and particularly interaction energies. Islaelachvili presented some unifying concepts in intermolecular and interparticle forces. [34] On the basis of a theoretical consideration on a simple model, he showed that the associated state of like molecules is energetically preferred to the randomly dispersed state of a binary molecular mixture and there is always an effective attraction between like molecules. Water network formation is one of the strongest interactions in neutral molecular systems. Water-water association therefore induces solute-solute association in a binary mixture. In the case of acetic acid/water mixtures, acid-acid interaction itself also has a large energy and can generate a large dipole moment stabilized with aqueous polar environment. Microphase formation in the binary mixtures is not so surprising in this sense. In Figure III-14, we show a model structure of an acetic acid microphase on the basis of all the spectroscopic data shown in this study and the data by Kaatze et al. [23,26] The side-on dimer structure is an elementary unit in this model. Along the direction shown by an arrow acetic acids stack up with alternating the orientation of the methyl group to the carboxyl group. A very dense stacking of molecules can be seen for a structure with the side-on dimer unit. The model cluster is built up by considering the dipole-dipole

interaction between acetic acid molecules and between the dimers, hydrophobic interaction between methyl groups, and electrostatic interaction (weak hydrogen bonding) between the carbonyl oxygen atom and the in-plane hydrogen atom of the methyl group. At this stage, this is just a model as a working hypothesis that must be subject from further critical theoretical and experimental examination.

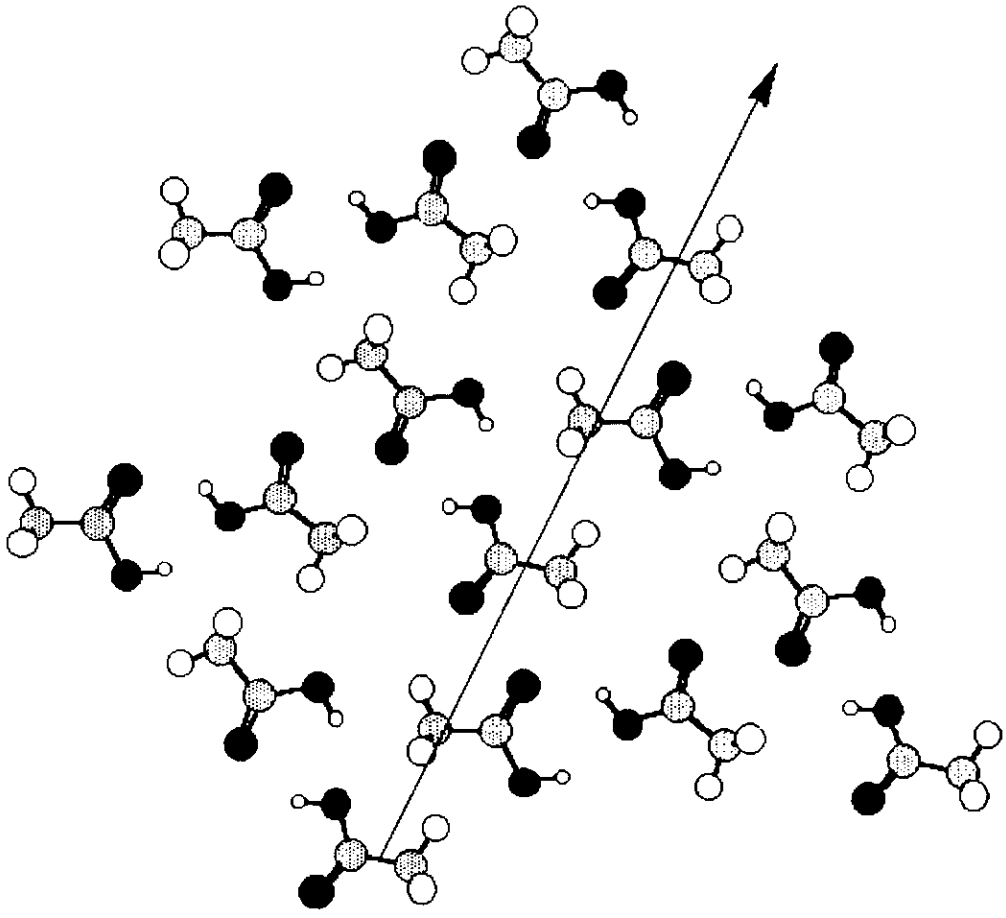

Figure III-14. Model of an acetic acid microphase proposed based on the spectroscopic data.

III.F. Conclusion

With the addition of water into liquid acetic acid, the C=O stretching vibration band of acetic acid shows high frequency shift from 1665 cm^{-1} to 1715 cm^{-1}. This means that the hydrogen-bond of the C=O group of acetic acid is not so strong as those seen in liquid acetic acid or in CCl_4 solution (in which the band appears at 1668 cm^{-1}). A bent type hydrogen-bond is accountable for this observation. On the other hand, the increase of acetic acid in water drastically decreases the intensity of the hydrogen-bonded O-H stretching Raman band of water at 3200 cm^{-1}. This suggests that acetic acid breaks the hydrogen-bond networks of water. Low frequency $R(\bar{\nu})$ spectra of acetic acid/water binary solutions are examined with new experimental data and ab initio molecular orbital analysis of intermolecular vibrational modes. The $R(\bar{\nu})$ spectrum of the aqueous mixture at $x_A = 0.5$ bears a very close resemblance to that of the acetic acid/methanol mixture with $x_A = 0.5$, indicating that the molecular complexes responsible to the Raman spectra are acetic acid clusters. The calculated low-frequency Raman feature of a side-on type dimer with bent-type hydrogen-bonds based on ab initio molecular orbital theory reproduces the observed Raman pattern nicely. Any evidence of the formation of stable acid-water pairs is not found in the low frequency Raman spectra. Furthermore, an isosbestic point is seen in the region of $0.1 \leq x_A$ (mole fraction of acetic acid) ≤ 0.5, and another one is also observed in $0.5 \leq x_A \leq 1.0$. The observed spectra in the region of $0 < x_A < 0.5$ are reproduced simply by linear combinations of the pure water spectrum

and the spectrum at x_A =0.5. These results strongly suggest the presence of the two microphases with homogeneously associated molecules: a water cluster phase and an acetic acid cluster phase. The spectral change in 0.5 < x_A < 1.0 is attributed to the coexistence of the acetic acid cluster phase in aqueous environment and the acid associated phase characteristic of liquid acetic acid.

References for chapter III

[1] K. Egashira and N. Nishi, J. Phys. Chem. B, **102**, 4054 (1998).

[2] K. Kosugi and N. Nishi, unpublished results.

[3] P. Waldstein and L. A. Blatz, J. Phys. Chem. **71**, 2271 (1967).

[4] P. A. Madden and R. W. Impey, Chem. Phys. Lett. **123**, 502 (1986).

[5] R. W. Impey, P. A. Madden, and I. R. McDonald, Mol. Phys. **46**, 513 (1982).

[6] S. Sastry, H. E. Stanley, and F. Sciortino, J. Chem. Phys. **100**, 5361 (1994).

[7] P. –A. Lund, O. F. Nielsen, and E. Praestgaard, Chem. Phys. Lett. **28**, 167 (1978).

[8] W. F. Murphy, M. H. Brooker, O. F. Nielsen, E. Praestgaard, and J. E. Bertie, J. Raman Spectrosc. 20, 695 (1989).

[9] M.J. Frisch, G.W. Trucks, H.B. Schlegel, P.M.W. Gill, B.G.. Johnson, M.A. Robb, J.R. Cheeseman, T. Keith, G.A. Petersson, J.A. Montgomery, K. Raghavachari, M.A. Al-Laham, V.G. Zakrzewski, J.V. Ortiz, J.B. Foresman, J. Cioslowski, B.B. Stefanov, A. Nanayakkara, M. Challacombe, C.Y. Peng, P.Y. Ayala, W. Chen, M.W. Wong, J.L. Andres, E.S. Replogle, R. Gomperts, R.L. Martin, D.J. Fox, J.S. Binskey, D.J. Defrees, J. Baker, J.P. Stewart, M. Head-Gordon, C. Gonzalez, and J.A. Pople, *GAUSSIAN 94*, Revision C.3, Gaussian Inc., Pittsburgh, PA, 1995.

[10] J. Karle, L. O. Brockway, J. Am. Chem. Soc. **66**, 574 (1944).

[11] J. L. Derissen, J. Mol. Struct. **7**, 67 (1971).

[12] J. B. Ng, H. F. Shurvell, J. Phys. Chem., **91**, 496 (1987).

[13] J. B. Ng, B. Petelenz, H. F. Shurvell, Can. J. Chem., **66**, 1912 (1988).

[14] J. E. Bertie and K. H. Michalian, J. Chem. Phys., 77, 5267 (1982).

[15] I. Nahringbauer, Acta Chim. Scand., **24**, 453 (1970).

[16] J. L. Derissen, J. Mol. Struct., 7, 67 (1971).

[17] G. Herzberg, Molecular Spectra and Molecular Structure II, Infrared and Raman Spectra of Polyatomic Molecules, Krieger Publishing Co., Malabar, Florida, p. 281 (1991).

[18] D. E. Hare and C. M. Sorensen, J. Chem. Phys., **96**, 13 (1992).

[19] S. Krishnamurthy, R. Bansil, and J. Wiafe-Akenten, J. Chem. Phys., **79**, 5863 (1983).

[20] K. Kosugi, T. Nakabayashi, and N. Nishi, Chem. Phys. Lett., **78**, 652 (1983).

[21] T. Nakabayashi, K. Kosugi, and N. Nishi, J. Phys. Chem. A, **103**, 8595 (1999).

[22] T. Nakabayashi, H. Sato, F. Hirata, and N. Nishi, in press

[23] U. Kaatze, K. Menzel, and R. Pottel, J. Phys. Chem., **95**, 324 (1991).

[24] K. Yamamoto and N. Nishi, J. Am. Chem. Soc., **112**, 549 (1990).

[25] E. W. Washburn, Editor-in-chief, National Research Council of U.S.A. International Critical Tables, vol. III, McGraw-Hill: New York, 123-124 (1928).

[26] M. Brai and U. Kaatze, J. Phys. Chem., 96, 8946 (1992).

[27] G. E. Walrafen, J. Phys. Chem., **94**, 2237 (1990).

[28] J. L. Rousset, E. Duval, A. Boukenter, J. Chem. Phys., **92**, 2150

(1990).

[29] K. Mizoguchi, Y. Hori, and Y. Tominaga, J. Chem. Phys., **97**, 1961 (1992).

[30] I. Ohmine, J. Phys. Chem., **99**, 6767 (1995).

[31] Y. Koga and P. Westh, Bull. Chem. Soc. Jpn., **69**, 1505 (1996).

[32] S. H. Tanaka, H. I. Yoshihara, A. H. Ho, F. W. Lau, P. Westh, Y. Koga, Can. J. Chem., **74**, 713 (1996).

[33] N. Nishi, S. Takahashi, M. Matsumoto, A. Tanaka, K. Muraya, T. Takamuku, and T. Yamaguchi, J. Phys. Chem., **99**, 462 (1995).

[34] J. N. Islaelachvili, Intermolecular and Surface Forces; Academic Press: Orlando, chapter 9 (1985).

CHAPTER IV

Charge transfer interaction in acetic acid-benzene cation complex

This chapter is based on J. Chem. Phys. 114, 4805 (2001).

IV.A. Introduction

IV.A.1. Photodissociation spectroscopy

Various conventional spectroscopic techniques such as direct absorption spectroscopy, laser-induced fluorescence (LIF) spectroscopy, and electron-impact fluorescence spectroscopy have been used to investigate the electronic and vibrational structures, geometrical structures, and the excited state dynamics of molecular ions in both the condensed phase and the gas phase [1–5]. A number of electronic absorption spectra of cluster ions have been measured in the low temperature matrices. The solvent effect sometimes changes the spectrum drastically in the matrices. Although no solvent effect exists in the gas phase, it is very difficult to apply conventional experimental techniques to cluster ions due to very low number densities. Only a few reports have been published on cluster ions in the gas phase with the use of the conventional techniques. The LIF spectra of the $C_6F_5H^+$–Ar_n [6] and $C_6F_6^+$–X_n systems (X = He, Ne, or Ar) [7, 8] have been measured. However, it is very difficult to identify the species responsible for the photoprocesses by using conventional spectroscopic techniques.

Photodissociation spectroscopy is one of the most powerful techniques to examine the ion species. Since the photodissociation spectroscopy monitors not photons but ion particles, high detection sensitivity can be easily obtained. Therefore, it is possible to apply photodissociation spectroscopy to minor species whose number density is very low in the sample. In addition,

it can be used for non-emissive species. When photodissociation spectroscopy is combined with mass spectrometry, the ambiguity of identifying the species responsible for the photoabsorption can be removed except for isomers. Because of these advantages, the photodissociation spectroscopy becomes one of the most popular techniques to examine the ion species.

A number of electronic spectra of monomer ions have been measured by using the photodissociation spectroscopy. Dunbar and co-workers measured the electronic spectra of substituted benzene ions in the visible and ultraviolet (UV) regions by ion cyclotron resonance technique [9-12]. They assigned the electronic spectra on the basis of the photoelectron spectra of these molecules. Schlag and co-workers observed the resonance-enhanced multiphoton dissociation spectra of the $D_1 \leftarrow D_0$ ($^2E_{2g} \leftarrow {}^2E_{1g}$) transition of benzene cation, $C_6H_6^+$ [13]. In their experiment, photodissociation occurs via one-photon resonant multiphoton absorption. The $C_6H_6^+$ ion photodissociates into $C_6H_5^+$ and H, and the yield of the fragment $C_6H_5^+$ was monitored as a function of the photon energy. Fujii and co-workers reported the electronic spectra of fluorobenzene cations by using mass-selected ion dip spectroscopy [14]. They used a qudrupole mass spectrometer, and monitored the depletion of the parent ion as a function of the photon energy. In this case, dissociation occurs through two-photon process. Nishi and co-workers showed a laser photodissociation spectrum of $C_7H_7^+$ in the 265-530 nm region [15]. The parent $C_7H_7^+$ was created through UV multiphoton ionization of *p*-chlorotoluene. They observed the photodissociation

spectrum of $C_7H_7^+$ by monitoring the yields of a fragment $C_5H_5^+$ as a funcion of the photon energy. In the spectrum, two broad bands emerged at 4.4 and 3.1 eV. These bands were attributed to the tropylium and benzyl isomers of $C_7H_7^+$, respectively. Sasaki and Mikami reported the trapped ion photodissociation spectra of *p*-dichlorobenzene cation, *p*-$C_6H_4Cl^+$ [16]. Although the former case of the dissociation occurs through a two-photon process, the latter one is induced through an one-photon process. A number of studies on the laser photodissociation of methyl iodide cation, CH_3I^+, have been carried out by using electron-impact ionization [17, 18] and multiphoton ionization [19–22].

Photodissociation spectroscopy has been frequently utilized also for various kinds of cluster ion. Although it is impossible to mention all of the reprts of the photodissociation of cluster ions, several important studies on benzene cluster ions that are ones of the most repeatedly investigated species by the photodissociation spectroscopy will be described in later section.

IV.A.2. Benzene monomer ion

The electronic structure of benzene monomer ion has been investigated by conventional photoelectron spectroscopy [23, 24]. Molecular orbitals of π (e_{1g}), σ (e_{2g}), and π (a_{2u}) were observed in the energy region of 9-14 eV. Kimura and co-workers investigated the resonant multiphoton ionization photoelectron spectrum of benzene [25]. In their experiment, benzene is ionized by four photons through various two-photon allowed vibronic levels of the $^1B_{2u}$ (S_1) excited state. They concluded that fast intramolecular vibrational relaxation occurs at the third-photon states within the $^1E_{1u}$ (π, π^*) state and subsequent ionization takes place from vibrationally relaxed levels. In the last decade, high-resolution zero kinetic energy photoelectron (ZEKE) spectroscopy has been applied to benzene. Müller-Dethlefs and co-workers reported rotationally-resolved ZEKE spectra of benzene, and they discussed the dynamic Jahn-Teller effect and the structure of benzene ion [26-29]. Neusser et al. measured a high resolution mass-selective pulsed-field threshold ionization (MATI) spectrum of benzene [30, 31].

Another powerful spectroscopic technique for studying benzene monomer ion is photodissociation spectroscopy. Freser and Beauchamp measured the photodissociation spectrum of benzenemonomer cation by using a mercury-xenon arc lamp and a monochrometor [32]. The absorption band exhibits its onset at 300 ± 10 nm (4.1 eV) and a maximum at 255 ± 10 nm (4.9 eV). Two possibilities were proposed for the assignment of the band. One is dipole-allowed $^2E_{1u} \leftarrow {}^2E_{1g}$ transition (in D_{6h} symmetry) from a similarity

with the photoelectron spectrum of benzene. The other is the π-π^* ($^2E_{2u} \leftarrow {}^2E_{1g}$) transition, which is also allowed even in D_{6h} symmetry. Fujii and co-workers reported the photodissociation spectrum of benzene ion in the 19000-24000 cm^{-1} region [14]. The spectrum gradually increases its intensity towards the higher frequency until 24000 cm^{-1}. They assigned this band to dipole-allowed $D_2 \leftarrow D_0$ ($^2A_{2u} \leftarrow {}^2E_{1g}$) transition. Schlag and co-workers investigated the resonance-enhanced multiphoton dissociation spectra of benzene ion in 17300-20200 cm^{-1} region [13]. The spectra show well resolved vibronic structure, and are assigned to dipole-forbidden $D_1 \leftarrow D_0$ ($^2E_{2g} \leftarrow {}^2E_{1g}$) transition of benzene ion.

Only one paper on the fluorescence spectrum of the benzene cation was reported by Miller and Andrews [33], although it is well known that the benzene cation is non-emissive in the gas phase and in low temperature matrices. They observed the fluorescence spectrum of the benzene cation in solid argon at 12 K. Laser excitation at 421 nm produces weak emission with vibronic bands at 19770, 19140, and 18290 cm^{-1}. These bands are assigned to the $D_2 \rightarrow D_0$ ($^2A_{2u} \rightarrow {}^2E_{1g}$) transition of the benzene cation.

Finally, Johnson and co-workers recently reported a new spectroscopic technique to investigate the electronic spectra of molecular ions [34]. They measured the vibrationally resolved spectra of dipole-forbidden $D_1 \leftarrow D_0$ ($^2E_{2g} \leftarrow {}^2E_{1g}$) transition of benzene monomer ion by using photoinduced Rydberg ionization (PIRI) spectroscopy. Two step processes are involved in PIRI. First step is the preparation of the molecule in a high-*n* Rydberg state converging upon a specific vibrational state using either a single or

multiphoton excitation. The second step is the optical excitaion of the ion core of Rydberg molecule. The resonant transitions within the ion core are then detected through either the fast electronic autoionization of the core-excited Rydberg molecule or the fragments generated by the absorption of further photons into a dissociative state. From the PIRI spectra, pseudo-Jahn-Teller activity was discussed in the benzene ion D_1 ($^2E_{2g}$) state.

IV.A.3. Charge transfer cation complexes of aromatic molecules

Generation of charge transfer complexes in supersonic jet is favorable for the studies of charge transfer interaction in a molecule pair, since these are cooled and isolated from solvation. In the electronic spectra of the charge transfer complexes, new bands appear due to intermolecular charge transfer interaction. These bands are called charge transfer (CT) bands. An electronic ground state of a charge transfer ion complex composed of molecules A and B is described by the wave function: $\Psi_G = a\psi(A)\psi(B^+) + b\psi(A^+)\psi(B)$, where $a^2+b^2=1$. In the case where the ionization potential of A is higher than that of B, $|a| >> |b|$. The electronic transition from the ground state to an excited state described by the wave function: $\Psi_E = c\psi(A)\psi(B^+) + d\psi(A^+)\psi(B)$, where $c^2+d^2=1$ and $|d| >> |b|$, accompanies the change in intermolecular charge distribution. CT bands arise from this kind of the transitions. The transition probability of the CT band depends on the degree of intermolecular charge transfer which significantly depends on the geometrical structure of the complex. The CT bands of the cation complexes with two aromatic molecules have been measured by photodissociation spectroscopy [35-37]. For example, a CT band of the benzene-naphthalene hetero-dimer cation is observed at 10870 cm^{-1} [35]. In the spectrum of the benzene-toluene hetero-dimer ion, three CT bands are detected at 8510, 10870 and 14925 cm^{-1} [36]. Ohashi et al. measured vibrational and electronic spectra of the benzene-benzyl alcohol hetero-dimer ion by photodissociation spectroscopy and observed the CT band at 10525

cm^{-1} [37]. From the observation of the hydroxyl group stretching vibration free from intermolecular perturbations at 3662 cm^{-1}, the geometrical structure of the cation complex is attributed to a sandwich-like structure suitable for the charge transfer interaction. The geometrical structures of these cation complexes that show the CT bands are characterized with overlapping of the π-electron systems of the respective aromatic rings. This situation is similar to the benzene dimer cation that shows intermolecular charge resonance (CR) bands in the near-infrared region [38-40]. In contrast, the CT band is not observed in the spectra of the cation complexes with strong hydrogen-bonding interactions. The electronic spectrum of the benzene-phenol hetero-dimer cation shows the lack of the CT band [41]. Fujii et al. observed the vibrational spectrum of the benzene-phenol hetero-dimer ion [42]. They found an extremely large red-shift and a substantial broadening of the O-H stretching vibrational band. The result indicates that the cation complex has a structure with a hydrogen bond between the O-H bond of phenol and the π-electrons of benzene. Ohashi et al. reported that no CT band can be seen in the electronic spectrum of the aniline-benzene hetero-dimer ion [43]. Aniline-benzene hetero-dimer ions are also reported to have hydrogen-bonded structures, where aniline is bound to benzene through a π-type hydrogen bond [44]. In these dimer ions, the hydrogen-bonding interaction overwhelms the charge transfer interaction.

IV.A.4. Aims of the present study

In the present study, we report the intermolecular interactions between the carboxyl group and the cationic benzene ring in the acetic acid-benzene hetero-dimer cation. The ionization potentials of acetic acid and benzene are 10.87 [45] and 9.24 eV [46], respectively. The positive charge is expected to be localized at the benzene ring in the ground state, because of the large difference in the ionization potentials [34]. Thus we abbreviate the acetic acid-benzene hetero-dimer cation as $(CH_3COOH)\cdot(C_6H_6)^+$ hereafter. Since the carboxyl group exists in a large number of biologically important molecules, understanding of its interaction with ionic molecules is very important. Molecules with the carboxyl groups are expected to show specific hydrogen-bonding interaction with other hydrogen-donating or –accepting molecules [47-51]. Non-bonding orbitals of the carboxyl group may interact with the positively charged π-electron system. We investigate the geometrical structures and electronic states of $(CH_3COOH)\cdot(C_6H_6)^+$, experimentally and theoretically. In order to obtain information on the geometrical structures, the vibrational spectrum of $(CH_3COOH)\cdot(C_6H_6)^+$ was measured in the 3000-3680 cm^{-1} region by using the photodissociation spectroscopy. We also performed ab initio molecular orbital calculations and obtained optimized geometries, binding energies, and vibrational frequencies. The calculated frequencies of the optimized geometries are compared with the experimental spectrum to clarify the structures of $(CH_3COOH)\cdot(C_6H_6)^+$. On the basis of the optimized geometrical structures,

we carried out the calculations of the electronic transition energies to assign the bands in electronic spectrum that is also observed by using the photodissociation spectroscopy.

IV.B. Experimental

Figure IV-1 shows a schematic diagram of the ion trap system used for the IR photodissociation spectroscopy of cluster ions. The mixture of acetic acid and benzene was prepared by flowing the carrier Ar gas over liquid benzene and liquid acetic acid situated separately in the respective sample folders. The former was located 2 m away and the latter was 5 cm to a pulsed nozzle (General Valve P/N 9-279-900). The mixture of the sample and the carrier gas was then introduced and expanded into the vacuum chamber through the pulsed nozzle. The total stagnation pressure was 1.1 X 10^5 Pa. Neutral clusters were ionized by electron-impact with an electron energy of 350 eV near the exit hole of the pulsed nozzle. The ions, $(CH_3COOH)\cdot(C_6H_6)^+$, of interest were selected by a quadrupole mass filter. Then the ion beam was deflected 90 degree by a quadrupole ion bender and introduced into a quadrupole ion guide. IR or visible laser beam propagated coaxially along the quadrupole and irradiated the trapped ions. The excited cluster ions with sufficient energy for the dissociation can produce benzene monomer cations as a fragment species. The fragment cations were deflected 90 degree by another quadrupole ion bender and mass-analyzed with the third quadrupole mass filter connected to a secondary electron multiplier. Photodissociation spectra were obtained by recording the yields of the fragments against the excitation energies. The tunable light source for the IR region was a optical parametric oscillator (OPO) system (Continuum Mirage 3000) pumped with an injection-seeded Nd:YAG laser

(Continuum Powerlite 9000). The resolution of the OPO laser was less than 0.02 cm^{-1}. This laser system was also used in the 12020-13405 cm^{-1} (746-832 nm) region. A dye laser (Lambda Physik LPD3000) pumped with an excimer laser (Lambda Physik LPX100) was used in the 14925-29410 cm^{-1} (340-670 nm) region. Spectroscopy grade acetic acid and benzene were purchased from Wako Pure Chemical Company and used without further purification.

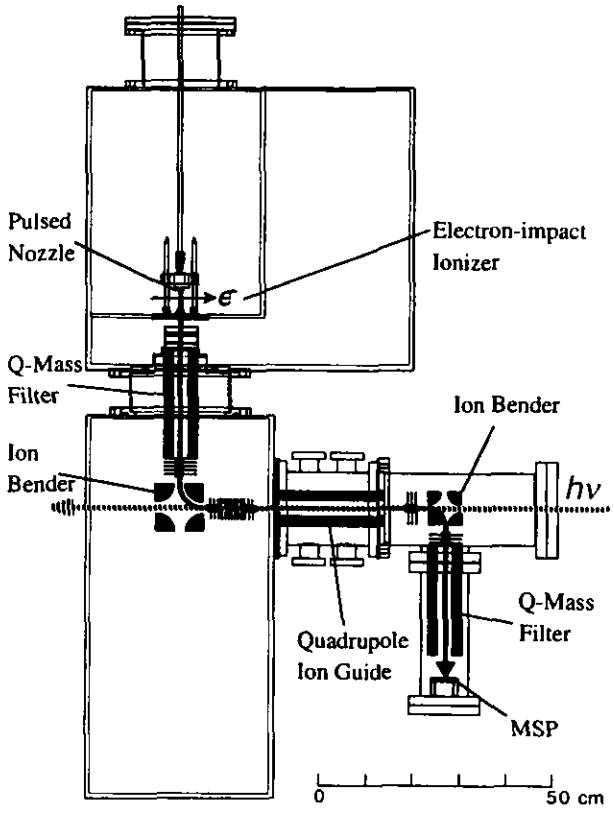

FIG. IV-1. Schemaitc diagram of the ion-trap mass spectrometer for photodissociation spectroscopy

IV.C. Computational details

Ab initio molecular orbital calculations were performed using the Gaussian 98W program package [52] and the PC GAMESS version [53] of the GAMESS (US) QC package [54] on commercial computers. The Pople's 6-31G(d,p) basis set was employed for all the calculations. The ground state optimized geometries and their vibrational frequencies were determined by the CASSCF calculations. Seven π electrons were treated as active electrons and distributed among seven active orbitals. The active orbitals of benzene cation consist of two bonding π and two anti-bonding π^* orbitals, and those of acetic acid are a bonding π, an anti-bonding π^* and one of non-bonding orbitals. Geometry optimizations and vibrational frequency evaluation were also carried out by the calculations based on the density functional theory (DFT) in which Becke's three-parameter hybrid functional [55] are combined with the Lee-Yang-Parr (LYP) correlation functional [56, 57] (B3LYP).

The ground and excited state energies of the complexes with the geometries optimized at the CASSCF(7,7) level were calculated by the state-averaged CASSCF method and the second-order multiconfiguration quasi-degenerate perturbation theory (MCQDPT) [58]. For these calculations, we extended the active space by adding four electrons and three orbitals (bonding σ, π, and anti-bonding π^* orbitals) to the active space mentioned above: the state-averaged CASSCF(11,10) and MCQDPT(11,10) calculations. In order to know the electron distribution between component molecules in

the ground and excited states of isomer complexes, Mulliken population analysis [59-62] was carried out for the respective electronic states. Radiative transition dipole moments and oscillator strengths between the ground and excited states were also calculated at the state-averaged CASSCF(11,10) level. Molecular orbitals shown in this paper were pictured by using MacMolPlt. [63]

IV.D. Results

IV.D.1. Observed vibrational spectrum

Figure IV-2 exhibits an IR photodissociation spectrum of $(CH_3COOH)\cdot(C_6H_6)^+$ in the region of 3000-3680 cm^{-1}. Three bands are observed in this region. In the O-H stretching vibrational region, a weak band is seen on the high frequency side of the strongest band. They are located closely and overlap with each other. The doublet spectrum is decomposed into two bands by fitting two Lorentzians (dotted curves) to the observed data as shown in Figure IV-3. The decomposition reveals that the positions of the intensive band and the weak one are located at 3577 and 3617 cm^{-1}, respectively. Another weak band is also observed in the C-H stretching vibrational region. The frequency of the band is 3080 cm^{-1}.

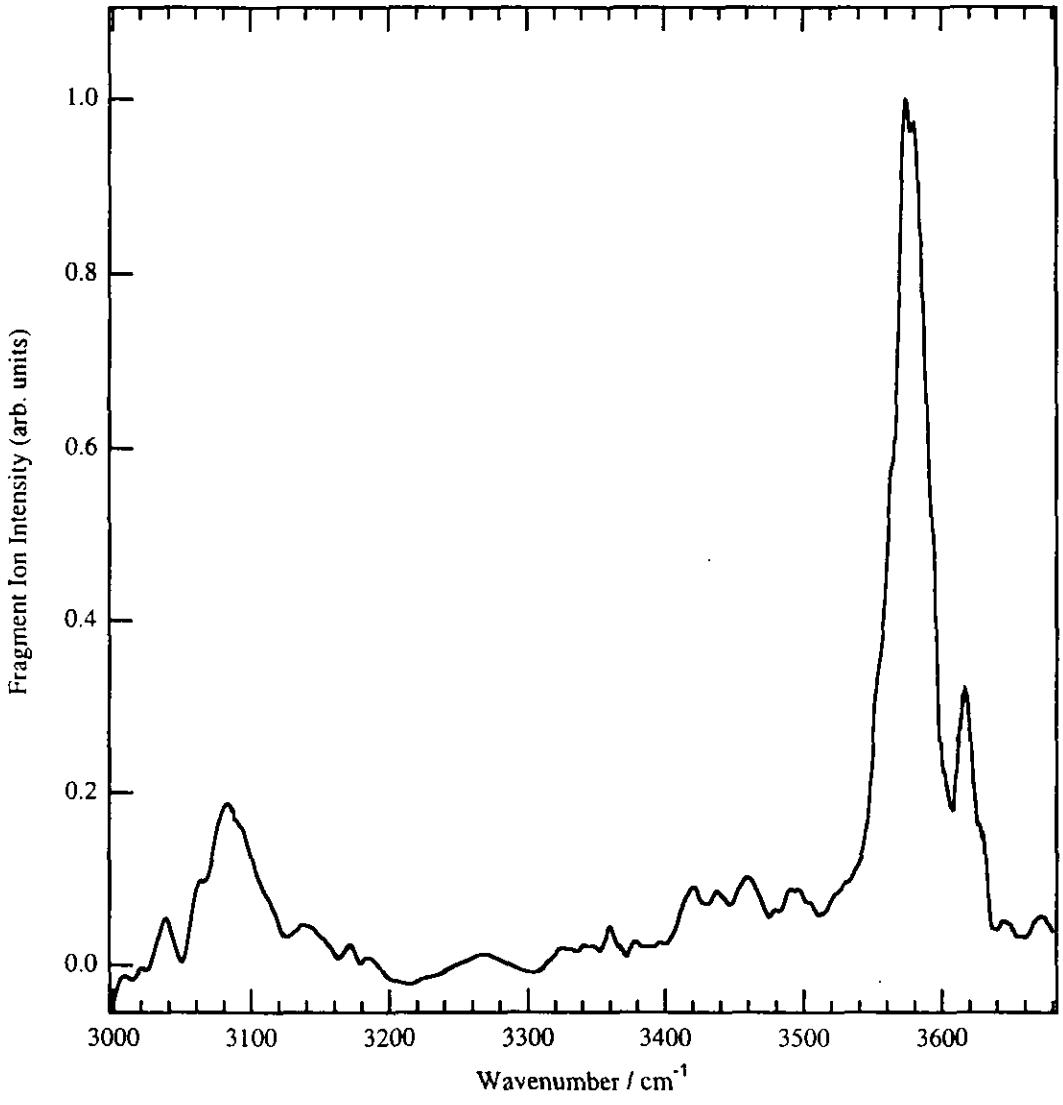

FIG. IV-2. Vibrational spectrum of acetic acid-benzene cation complex.

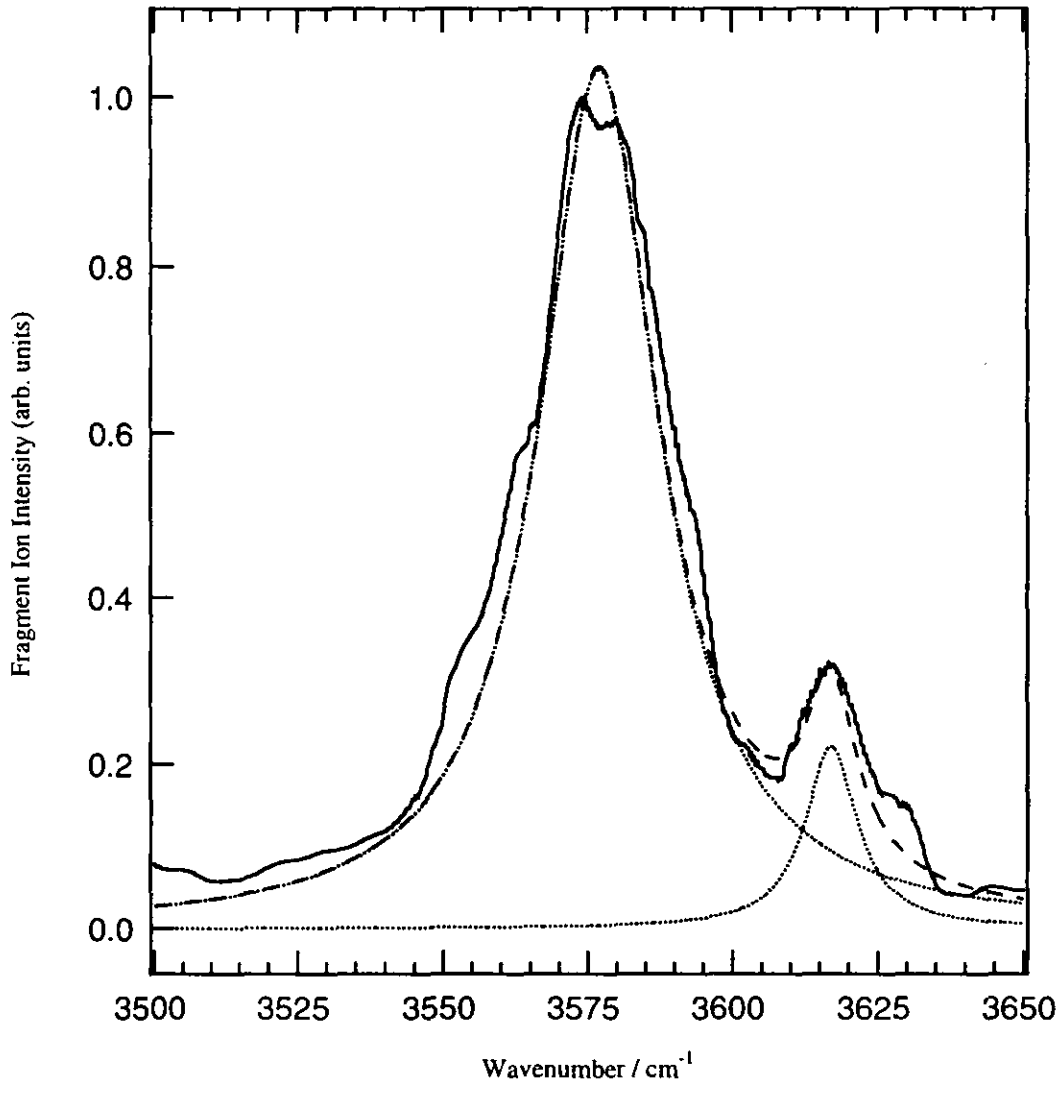

FIG. IV-3. Vibrational spectrum in the O-H stretching region.

IV.D.2. Calculated structures and binding energies at the CASSCF(7,7)/6-31G(d,p) level

There are two isomers for the acetic acid monomer as shown in Figure IV-4: the hydroxyl hydrogen and the carbonyl oxygen located on the same side of the C-O single bond (*cis*-isomer) and on the opposite side (*trans*-isomer). Geometry optimizations of $(CH_3COOH)\cdot(C_6H_6)^+$ were carried out with various initial structures of C_s symmetry or C_1 symmetry which include one of the two isomers of acetic acid. In consequence, three stationary points were found at the CASSCF(7,7)/6-31G(d,p) level. All the optimized structures at these minima have a C_s plane on which the acetic acid molecule is sitting except for two methyl hydrogens located symmetrically above and under the plane. These structures displayed in Figure IV-5 are classified into the two types distinguished by the relative position of the carboxyl group to the benzene ring. One is a horizontal complex in which an acetic acid molecule and a benzene cation are situated on the same plane forming hydrogen bonds between the carboxyl oxygen and the two hydrogen atoms of the benzene ring. The other is a vertical complex where the carboxyl plane is at a right angle with the benzene plane and the carboxyl oxygen directly interacts with the π-electron system of the benzene cation. For each type of the complexes, two isomers containing a *cis*-isomer or a *trans*-isomer of acetic acid are expected. In the case of the horizontal complex, both of the isomers are found to have their own optimized geometries. "Horizontal *cis*-isomer" designates the one containing the *cis*-isomer and the other with the

trans-isomer is called "horizontal *trans*-isomer". On the other hand, the *trans*-isomer is the only structure at a minimum of the vertical complex: the vertical *trans*-isomer. The vertical *cis*-isomer structure exhibits a saddle point with imaginary frequencies.

The calculated total energies of the optimized structures of $(CH_3COOH)\cdot(C_6H_6)^+$ and the energies relative to the most stable species at the CASSCF(7,7)/6-31G(d,p) level are shown in Table IV-I. We corrected those for zero-point vibrational energies (ZPVE) and the corrected energies are also displayed in Table IV-I. The most stable complex species is the vertical *trans*-isomer. The horizontal *cis*-isomer is the second stable species and 2459 and 2621 cm^{-1} less stable than the vertical *trans*-isomer before and after ZPVE correction, respectively. The least stable species is the horizontal *trans*-isomer that is 2936 and 3053 cm^{-1} less stable than the vertical *trans*-isomer before and after ZPVE correction, respectively.

We also carried out the geometry optimization on the two isomers of acetic acid and a benzene cation. The total energies of these monomer species before and after ZPVE correction are listed in Table IV-II. As shown in Table IV-III, the energy gap between the *cis*- and *trans*-isomers of acetic acid is 2210 cm^{-1} (6.32 kcal/mol) and 2116 cm^{-1} (6.05 kcal/mol) at the CASSCF(7,7)/6-31G(d,p) level before and after ZPVE correction, respectively.

For $(CH_3COOH)\cdot(C_6H_6)^+$, the energy gap between the horizontal *cis*-isomer and the horizontal *trans*-isomer is also shown in Table IV-III. The values are 477 cm^{-1} (1.36 kcal/mol) and 432 cm^{-1} (1.24 kcal/mol) at the CASSCF(7,7)/6-31G(d,p) level before and after ZPVE correction, respectively.

Table IV-IV shows the binding energies of the geometry optimized complexes of $(CH_3COOH)\cdot(C_6H_6)^+$ at the CASSCF(7,7)/6-31G(d,p) level. The binding energy is defined as the difference of the total energy of $(CH_3COOH)\cdot(C_6H_6)^+$ from the sum of the component monomer energies. Corrected energies for ZPVE are also shown in Table IV-IV. The binding energy of the horizontal *cis*-isomer is 6315 cm^{-1} (18.06 kcal/mol, 0.78 eV) and 6093 cm^{-1} (17.42 kcal/mol, 0.75 eV) before and after ZPVE correction, respectively. On the other hand that of the horizontal *trans*-isomer is 8047 cm^{-1} (23.01 kcal/mol, 1.00 eV) and 7777 cm^{-1} (22.24 kcal/mol, 0.96 eV) before and after ZPVE correction, respectively. The binding energy of the vertical *trans*-isomer is 10984 cm^{-1} (31.40 kcal/mol, 1.36 eV) and 10830 cm^{-1} (30.96 kcal/mol, 1.34 eV) before and after ZPVE correction, respectively.

The optimized geometrical parameters of three isomers of $(CH_3COOH)\cdot(C_6H_6)^+$ and two isomers of acetic acid at the CASSCF(7,7)/6-31G(d,p) level are collected in Table IV-V.

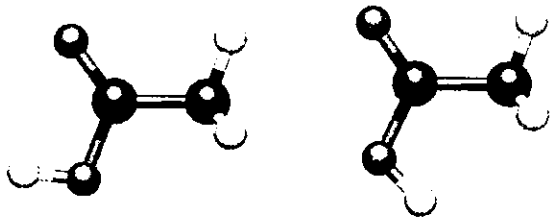

cis-isomer *trans*-isomer

FIG. IV-4. Two isomers of acetic acid. The cis-isomer (left) is stabilized by intramolecular hydrogen-bonding interaction between the carbonyl oxygen and the hydroxyl hydrogen; consequently, it is more stable than the trans-isomer (right). A black ball stands for a carbon atom, gray one is oxygen, and white one represents a hydrogen atom.

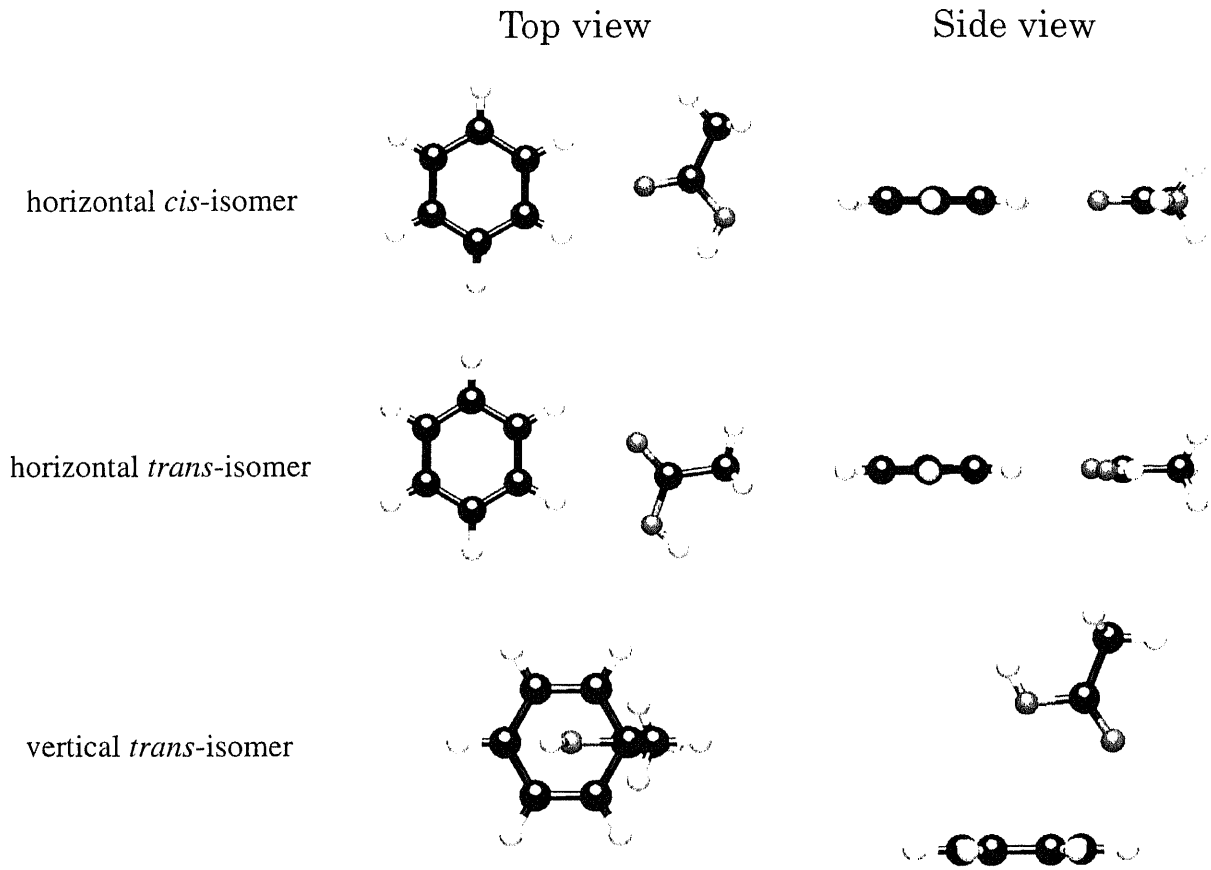

FIG. IV-5. Geometrical structures of $(CH_3COOH)(C_6H_6)^+$ optimized at the CASSCF(7,7)/6-31G(d,p) level. The three structures (the horizontal cis-isomer, the horizontal trans-isomer, and the vertical trans-isomer) are found to be at minima on the potential surface in agreement with those obtained at the B3LYP/6-31G(d,p) level. Each of these structures is viewed from the top and the side of the benzene ring.

TABLE IV-I. Total energies (hartree) and energy gaps relative to the most stable species (cm^{-1}) of $(CH_3COOH)^{\bullet}(C_6H_6)^{+}$ at the CASSCF(7,7)/6-31G(d,p) and B3LYP/6-31G(d,p) levels.

		horizontal *cis*	horizontal *trans*	vertical *trans*
CASSCF(7,7)/6-31G(d,p)				
without ZPVE correction	total energy	-458.319530	-458.317354	-458.330733
	energy gap	2459	2936	0
after ZPVE correction	total energy	-458.147229	-458.145260	-458.159172
	energy gap	2621	3053	0
B3LYP/6-31G(d,p)				
without ZPVE correction	total energy	-461.044106	-461.040888	-461.048177
	energy gap	894	1600	0
after ZPVE correction	total energy	-460.883041	-460.879404	-460.885483
	energy gap	536	1334	0

TABLE IV-II. Total energies (hartree) of benzene monomer cation and acetic acid monomers at the CASSCF(7,7)/6-31G(d,p) and B3LYP/6-31G(d,p) levels.

	benzene monomer cation	acetic acid	
		cis	*trans*
CASSCF(7,7)/6-31G(d,p)			
without ZPVE correction	-230.442057	-227.848701	-227.838632
after ZPVE correction	-230.337077	-227.782392	-227.772750
B3LYP/6-31G(d,p)			
without ZPVE correction	-231.932185	-229.091479	-229.081701
after ZPVE correction	-231.834320	-229.029469	-229.020016

TABLE IV-III. Energy gaps (cm^{-1}) between the *cis*- and trans-isomers at the CASSCF(7,7)/6-31G(d,p) and B3LYP/6-31G(d,p) levels.

	horizontal cluster	acetic acid monomer
CASSCF(7,7)/6-31G(d,p)		
without ZPVE corr.	477	2210
after ZPVE corr.	432	2116
B3LYP/6-31G(d,p)		
without ZPVE corr.	706	2146
after ZPVE corr.	798	2075

TABLE IV-IV. Binding energies (cm^{-1}) of $(CH_3COOH)^{\bullet}(C_6H_6)^{\bullet}$ at the CASSCF(7,7)/6-31G(d,p) and B3LYP/6-31G(d,p) levels.

	horizontal		vertical
	cis	*trans*	*trans*
CASSCF(7,7)/6-31G(d,p)			
without ZPVE corr.	6315	8047	10984
after ZPVE corr.	6093	7777	10830
B3LYP/6-31G(d,p)			
without ZPVE corr.	4487	5926	7526
after ZPVE corr.	4225	5502	6836

TABLE IV-V. Calculated geometrical parameters of cluster species and acetic acid monomers at the CASSCF(7,7)/6-31G(d,p) level.

	horizontal cluster		vertical cluster	acetic acid monomer	
	cis	*trans*	*trans*	*cis*	*trans*
R(C-H)[a]	1.0728	1.0728	1.0731		
R(C-H)[b]	1.0751	1.0751	1.0739		
R(C=O)	1.2043	1.1960	1.1980	1.1951	1.1902
R(C-O)	1.3231	1.3403	1.3376	1.3385	1.3441
R(O-H)	0.9472	0.9450	0.9450	0.9472	0.9429
R(C-C)[c]	1.4985	1.5031	1.5028	1.5010	1.5089
R(C-H)[d]	1.0800	1.0791	1.0789	1.0802	1.0796
R(C-H)[e]	1.0834	1.0852	1.0853	1.0840	1.0859
α(O-C=O)	122.2394	118.3665	118.6151	122.2051	119.9548
α(C-C=O)	125.3561	124.7704	124.5056	125.6422	124.2604
α(C-O-H)	110.5537	112.9698	112.5781	108.5520	112.0483
R(C-H···O=C)[f]	2.3862	2.3218	2.5457		
R(C-H···O=C)[g]	2.4508	2.5962	3.4300		
R(C···O=C)[h]	3.1164	3.1073	2.6170		
R(C-H···O-C)[i]	4.1951	2.5692	4.1248		
R(C···O-C)[j]	5.1169	3.6232	3.6158		
R(C-H···H-O)[k]	3.7452	3.4351	4.7506		

[a] The shortest bond in the benzene ring. [b] The longest bond in the benzene ring.

[c] The C-C bond of acetic acid. [d] The C-H bond of acetic acid in the plane of the carboxyl group.

[e] C-H bonds of acetic acid out of the plane of the carboxyl group.

[f] Intermolecular H···O distance between the carbonyl oxygen and the nearest hydrogen atom of the benzene ring. [g] Intermolecular H···O distance between the carbonyl oxygen and the second nearest hydrogen atom of the benzene ring. [h] Intermolecular C···O distance between the carbonyl oxygen and the nearest carbon atom of the benzene ring. [i] Intermolecular H···O distance between the hydroxyl oxygen and the nearest hydrogen atom of the benzene ring. [j] Intermolecular C···O distance between the hydroxyl oxygen and the nearest carbon atom of the benzene ring.

[k] Intermolecular H···H distance between the hydroxyl hydrogen and the nearest hydrogen atom of the benzene ring.

IV.D.3. Calculated structures and binding energies at the B3LYP/6-31G(d,p) level

Geometry optimizations were also performed at the B3LYP/6-31G(d,p) level. Three optimized geometries are obtained in agreement with the CASSCF calculations. The total energies of these isomers of $(CH_3COOH)\cdot(C_6H_6)^+$ are listed in Table IV-I. Those of acetic acid monomers and the benzene monomer cation are shown in Table IV-II. Energy gaps between the *cis*- and *trans*-isomers at the B3LYP/6-31G(d,p) level are listed in Table IV-III. The binding energies of $(CH_3COOH)\cdot(C_6H_6)^+$ at the B3LYP/6-31G(d,p) level are shown in Table IV-IV. The optimized geometrical parameters at the B3LYP/6-31G(d,p) level are collected in Table IV-VI.

TABLE IV-VI. Calculated geometrical parameters of cluster species and acetic acid monomers at the B3LYP/6-31G(d,p) level.

	horizontal cluster		vertical cluster	acetic acid monomer	
	cis	*trans*	*trans*	*cis*	*trans*
R(C-H)[a]	1.0841	1.0841	1.0828		
R(C-H)[b]	1.0864	1.0871	1.0861		
R(C=O)	1.2238	1.2155	1.2270	1.2104	1.2035
R(C-O)	1.3387	1.3493	1.3338	1.3575	1.3633
R(O-H)	0.9722	0.9693	0.9705	0.9724	0.9677
R(C-C)[c]	1.5020	1.5090	1.5066	1.5073	1.5190
R(C-H)[d]	1.0888	1.0887	1.0886	1.0891	1.0891
R(C-H)[e]	1.0938	1.0953	1.0955	1.0940	1.0957
α(O-C=O)	122.3148	118.4551	119.3970	122.4909	120.0143
α(C-C=O)	125.6639	124.6081	122.0039	126.0892	124.7190
α(C-O-H)	108.3232	111.4904	111.3016	105.8073	110.2626
R(C-H···O=C)[f]	2.2557	2.2519	2.3513		
R(C-H···O=C)[g]	2.3276	2.3208			
R(C···O=C)[h]	2.9897	2.9837	2.3754		
R(C-H···O-C)[i]	4.0674	3.0668	3.9918		
R(C···O-C)[j]	5.0099	4.1381	3.3983		
R(C-H···H-O)[k]	3.5703	4.0295	4.8404		

[a-k] See the footnote of Table V.

IV.D.4. Calculated frequencies and IR intensities of the C-H and O-H stretching vibrations at the B3LYP/6-31G(d,p) level

Table IV-VII shows the calculated frequencies and IR intensities of the C-H and O-H stretching vibrations of the three $(CH_3COOH)^+(C_6H_6)$ isomers and the two acetic acid isomers at the B3LYP/6-31G(d,p) level. The frequencies were also calculated at the CASSCF(7,7)/6-31G(d,p) level and they are higher than those obtained at the B3LYP/6-31G(d,p) level for all the vibrational modes shown here. In general, the frequencies obtained by DFT are closer to the experimental values than those calculated by the CASSCF method.

TABLE IV-VII. Calculated vibrational frequencies (cm^{-1}) and IR intensities (km/mole) of cluster species and acetic acid isomers at the B3LYP/6-31G(d,p) level.

	horizontal cluster		vertical cluster	acetic acid monomer	
	cis	*trans*	*trans*	*cis*	*trans*
CH_3 sym. str.	3073	3058	3057	3067	3050
(acetic acid)	(0.505)	(0.557)	(3.335)	(1.851)	(4.319)
CH_3 asym. str.	3140	3123	3126	3133	3114
(acetic acid)	(0.143)	(1.439)	(0.006)	(5.242)	(9.431)
CH_3 sym. str.	3188	3188	3193	3185	3181
(acetic acid)	(4.808)	(0.936)	(0.528)	(5.612)	(3.927)
CH_3 sym. str.	3212	3209	3208		
(benzene cation)	(2.365)	(40.968)	(0.044)		
CH_3 asym. str.	3218	3213	3220		
(benzene cation)	(19.542)	(10.155)	(0.071)		
CH_3 sym. str.	3223	3222	3222		
(benzene cation)	(4.103)	(2.268)	(0.009)		
CH_3 saym. str.	3230	3231	3232		
(benzene cation)	(23.017)	(15.086)	(0.660)		
CH_3 sym. str.	3237	3237	3233		
(benzene cation)	(5.840)	(4.742)	(0.598)		
CH_3 sym. str.	3240	3241	3250		
(benzene cation)	(13.525)	(16.037)	(3.458)		
O-H str.	3758	3789	3780	3751	3802
(acetic acid)	(51.170)	(88.941)	(126.531)	(43.763)	(30.891)

IV.D.5. Observed electronic spectrum

The electronic spectrum of $(CH_3COOH)\cdot(C_6H_6)^+$ obtained by the photodissociation spectroscopy is shown in Figure IV-6. Two distinct maxima are seen in the spectrum. One has its intensity maximum around 24500 cm^{-1}. The other band begins at 12000 cm^{-1} and extends to the 24500 cm^{-1} band, with an intensity maximum around 17500 cm^{-1}. The band width of the 17500 cm^{-1} band is approximately 5000 cm^{-1} and that of the 24500 cm^{-1} band is 4000 cm^{-1}.

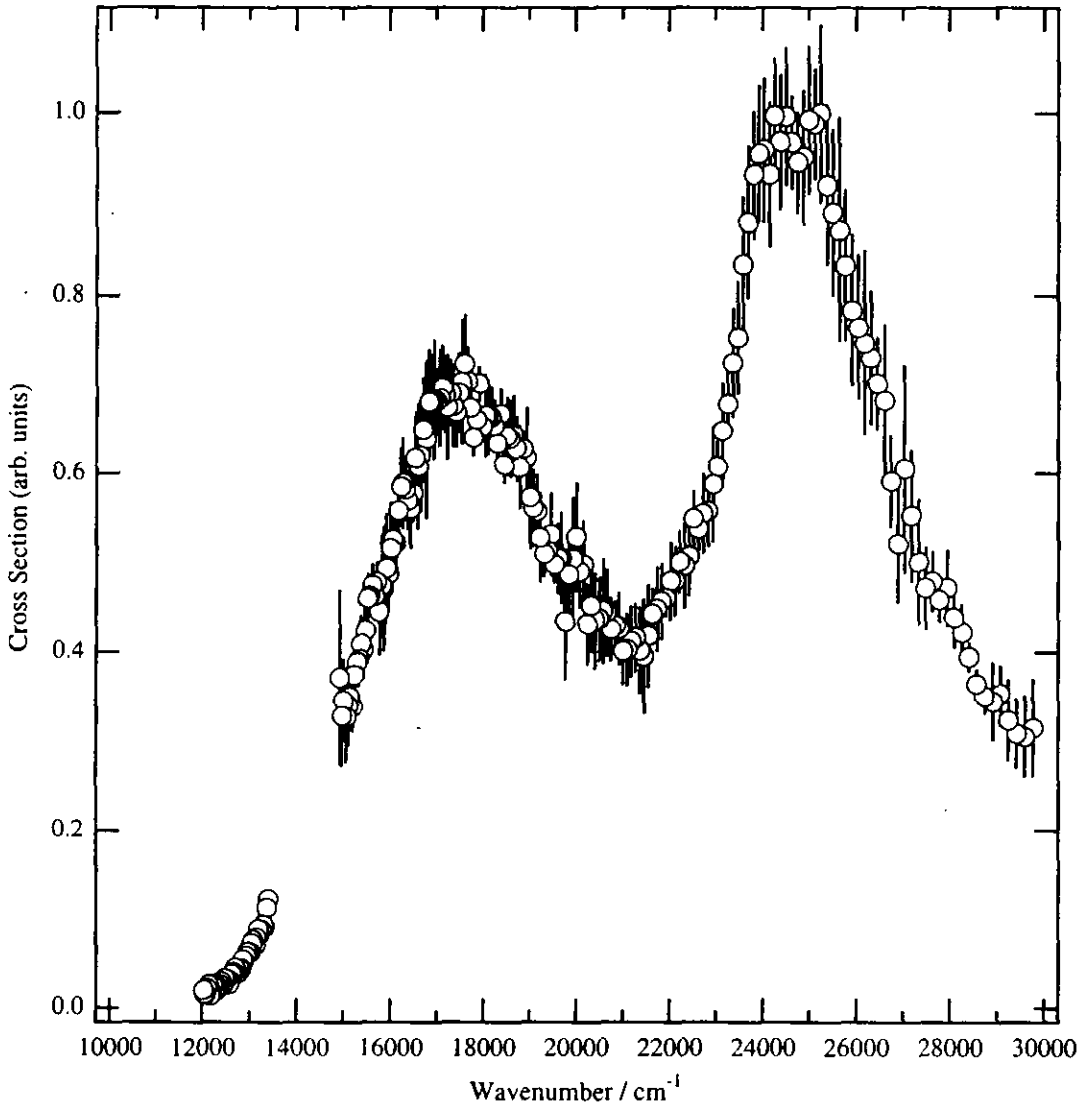

FIG. IV-6. Electronic spectrum of acetic acid-benzene cation complex

IV.D.6. Calculated electronic states

The presence of the two isomers (the horizontal *cis*-isomer and the vertical *trans*-isomer) of $(CH_3COOH)\cdot(C_6H_6)^+$ is revealed by the vibrational spectrum and ab initio molecular orbital calculations as discussed in the previous section. We investigate the electronic states of the two isomers using the multiconfiguration self-consistent field (MCSCF) calculations with the active space which consists of eleven electrons and ten orbitals.

The six valence π orbitals in the benzene cation are designated in the order of energy by π_1, π_2, π_3, π_4^*, π_5^*, and π_6^*, respectively. The first two are doubly occupied and the π_3 is the singly occupied molecular orbital (SOMO) in the ground state of the benzene cation. Table IV-VIII shows the CASSCF configurations for the ground and four excited states of the horizontal *cis*-isomer. Those of the vertical *trans*-isomer are listed in Table IV-IX. In those tables, molecular orbitals are designated by two characters such as Aπ. The first character (A or B) indicates the component molecule (acetic acid or benzene, respectively) and the second character designate the type of the molecular orbital (σ orbital, π orbital or non-bonding orbital); A*n* means the non-bonding orbital of acetic acid. (A*n*+Bπ_1) and (A*n*–Bπ_1) denote the intermolecular bonding and anti-bonding orbitals originated from one non-bonding orbital of acetic acid and the π_1 orbital of the benzene cation, respectively. Figure IV-7 shows these orbitals with the π_3 orbital of the vertical *trans*-isomer. (Aπ+Bπ_1) and (Aπ–Bπ_1) also means intermolecular bonding and anti-bonding orbitals derived from π orbitals of the respective

component molecules. The charge distributions between acetic acid and benzene in the respective states are obtained based on the Mulliken charges listed in Table IV-X. The calculated excitation energies from the ground state to the respective excited states and the oscillator strengths of the two isomers of $(CH_3COOH)\cdot(C_6H_6)^+$ are listed in Table IV-XI.

The ground state of the horizontal *cis*-isomer is 1 ^{2}A" and well described by the Hartree-Fock configuration where the Bπ_3 orbital is SOMO. Thus 97.8 % of the positive charge is localized in the benzene ring. On the other hand in the ground state of the vertical *trans*-isomer, 4.7 % of the positive charge is transferred to acetic acid.

The first excited state is 2 ^{2}A" and well represented by a single π-π excitation of B$\pi_2\rightarrow$Bπ_3. The charge distribution between the component molecules is similar to that of the ground state. The transition energy from the ground state to the 2 ^{2}A" state is estimated to be 4604 cm^{-1} at the CASSCF level and 3877 cm^{-1} at the MCQDPT level. The oscillator strength is computed to be 1.5 X 10^{-5}. Thus this transition is forbidden.

The 1 ^{2}A' state is well represented by a single configuration where the non-bonding orbital of acetic acid is SOMO. As expected from the configuration, the positive charge is almost localized on acetic acid in the 1 ^{2}A' state. The 1 ^{2}A' state is predicted to locate at 29172 cm^{-1} at the CASSCF level and 19211 cm^{-1} at the MCQDPT level. The calculated oscillator strength is 0 thus the transition is completely forbidden.

The 3 ^{2}A" state comes mainly from a single π-π excitation configuration of (Aπ+Bπ_1)$\rightarrow$Bπ_3. However, the state also contains a single π-π excitation of

$(A\pi\text{–}B\pi_1)\rightarrow B\pi_3$, two single π-π^* excitation of $B\pi_2\rightarrow B\pi_4^*$ and its conjugate $B\pi_3\rightarrow B\pi_5^*$, and a double excitation of $B\pi_2\rightarrow B\pi_3$ and $B\pi_2\rightarrow B\pi_5^*$. The coefficients of the $B\pi_2\rightarrow B\pi_4^*$ and the $B\pi_3\rightarrow B\pi_5^*$ excitation have different signs from each other. According to Mulliken charges, 95.0 % of the positive charge is located on the benzene ring. Therefore the 3 ^{2}A" state is the local excited state whose main character is π-π excitation configuration of the benzene cation. The excitation energy to the 3 ^{2}A" state is computed to be 24848 and 24221 cm^{-1} at the CASSCF and MCQDPT levels, respectively. The calculated oscillator strength of 2.7 X 10^{-2} shows this π-π transition is allowed. The result agrees with the fact that the π-π transitions are observed in the spectra of cation complexes with benzene cation.

The 2 ^{2}A' state is well described by the single σ-π excitation configuration of $B\sigma\rightarrow B\pi_3$. The charge distribution shows the 2 ^{2}A' state is a locally excited state. The excitation energy is computed to be 34168 cm^{-1} at the CASSCF level and 29542 cm^{-1} at the MCQDPT level. The calculated oscillator strength of 7.5 X 10^{-5} suggest the σ-π transition to the 2 ^{2}A' state is forbidden.

The ground state of the vertical *trans*-isomer is well represented by the Hartree-Fock configuration where SOMO is the $B\pi_3$ orbital. Mulliken charges show that 95.3 % of the positive charge is on the benzene ring in the ground state.

The first excited state is 1 ^{2}A" and well described by a single π-π excitation of $B\pi_2\rightarrow B\pi_3$. Thus this state corresponds to the 2 ^{2}A" state of the horizontal *cis*-isomer. The charge distribution shows the 1 ^{2}A" is a local excited state. The transition energy is computed to be 5597 cm^{-1} and 5322

cm^{-1} at the CASSCF and MCQDPT levels, respectively. The oscillator strength is calculated to be 7.1 X 10^{-5}. Thus the transition to the 1 ^{2}A" state is forbidden.

The 2 ^{2}A' state comes mainly from the two single excitation of (An–Bπ_1)→Bπ_3 with a coefficient of 0.784 and (An+Bπ_1)→Bπ_3 with a weight of 0.273. The two single π-π^* excitations of Bπ_3→Bπ_4^* and Bπ_2→Bπ_5^* also give rise to the 2 ^{2}A' state. The charge distribution shows that 30.0 % of the positive charge is on acetic acid. Thus the excitation from the ground state to the 2 ^{2}A' state accompanies the charge transfer from the benzene cation to acetic acid. The transition energy is estimated to be 11050 cm^{-1} at the MCQDPT level, while that obtained by the CASSCF method is 29172 cm^{-1}. The discrepancy in the transition energy shows that the recovery of dynamical correlation energy in MCSCF wavefunction is important for this state. The calculated oscillator strength is 5.5 X 10^{-2}. This indicates that the charge transfer transition to the 2 ^{2}A' state can be observed.

The 2 ^{2}A" state is well represented by the single σ-π excitation of Bσ→Bπ_3. As expected, the Mulliken charge shows that the 2 ^{2}A" state is a locally excited state. The calculated excitation energy is 36751 cm^{-1} at the CASSCF level and 29542 cm^{-1} at the MCQDPT level, respectively. The results suggest the recovery of the dynamical correlation energy is also important for this state. The oscillator strength is estimated to be 2 X 10^{-6}. This σ-π transition is forbidden.

The main configurations that give rise to the 3 2A' state are the same to those of the 2 ^{2}A' state. The principle configuration in the 3 ^{2}A' state is the

single excitation of (An+Bπ_1)→Bπ_3 with a coefficient of 0.759. The single excitation of (An–Bπ_1)→Bπ_3 with a weight of –0.404 is the second most efficient configuration. The charge distribution shows that the 3 ^{2}A' state also has the charge transfer character. The transition energy is computed to be 29905 cm^{-1} and 28061 cm^{-1} at the CASSCF and MCQDPT levels, respectively. The calculated oscillator strength of 6.1 X 10^{-2} suggests that the charge transfer transition to the 3 ^{2}A' state is allowed.

TABLE IV-VIII. Main configurations of the horizontal *cis*-isomer at the CASSCF(11,10)/6-31G(d,p) level.

State	Coefficients	$B\sigma$	$A\pi+B\pi_1$	$A\pi-B\pi_1$	An	$B\pi_2$	$B\pi_3$	$B\pi_4^*$	$B\pi_5^*$	$A\pi^*$	$B\pi_6^*$
$1\,^2A''$	0.933	2	2	2	2	2	1	0	0	0	0
$2\,^2A''$	0.924	2	2	2	2	1	2	0	0	0	0
$1\,^2A'$	0.912	2	2	2	1	2	2	0	0	0	0
$3\,^2A''$	0.725	2	1	2	2	2	2	0	0	0	0
	-0.330	2	2	2	2	1	1	1	0	0	0
	0.312	2	2	1	2	2	2	0	0	0	0
	0.267	2	2	2	2	2	0	0	1	0	0
	-0.202	2	2	2	2	0	2	0	1	0	0
$2\,^2A'$	0.912	1	2	2	2	2	2	0	0	0	0

TABLE IV-IX. Main configurations of the vertical *trans*-isomer at the CASSCF(11,10)/6-31G(d,p) level.

State	Coefficients	$B\sigma$	$A\pi$	$An+B\pi_1$	$An-B\pi_1$	$B\pi_2$	$B\pi_3$	$B\pi_4^*$	$B\pi_5^*$	$A\pi^*$	$B\pi_6^*$
$1\,^2A'$	0.931	2	2	2	2	2	1	0	0	0	0
$1\,^2A''$	0.916	2	2	2	2	1	2	0	0	0	0
$2\,^2A'$	0.784	2	2	2	1	2	2	0	0	0	0
	0.273	2	2	1	2	2	2	0	0	0	0
	0.257	2	2	2	2	1	1	0	1	0	0
	0.253	2	2	2	2	2	0	1	0	0	0
$2\,^2A''$	0.911	1	2	2	2	2	2	0	0	0	0
$3\,^2A'$	0.759	2	2	1	2	2	2	0	0	0	0
	-0.404	2	2	2	1	2	2	0	0	0	0
	0.227	2	2	2	2	2	0	1	0	0	0

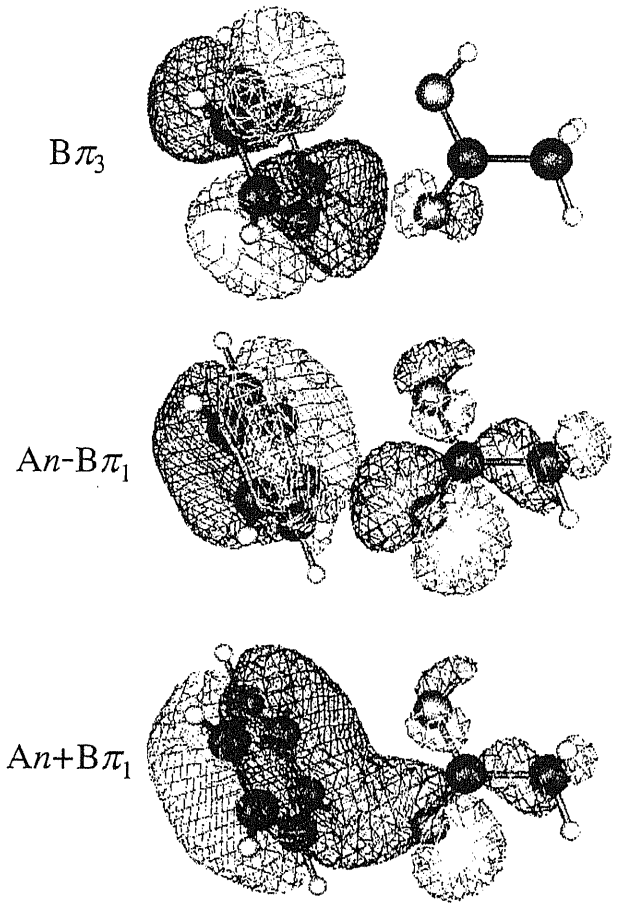

FIG. IV-7. Molecular orbitals of acetic acid-benzene caiton complex.

TABLE IV-X. Charge distributions based on Mulliken charges.

State	Acetic Acid	Benzene
Horizontal *cis*-isomer		
$1\ ^2A''$	+0.022	+0.978
$2\ ^2A''$	+0.022	+0.978
$1\ ^2A'$	+0.990	+0.010
$3\ ^2A''$	+0.050	+0.950
$2\ ^2A'$	+0.028	+0.972
Vertical *trans*-isomer		
$1\ ^2A'$	+0.047	+0.953
$1\ ^2A''$	+0.019	+0.981
$2\ ^2A'$	+0.300	+0.700
$2\ ^2A''$	+0.023	+0.977
$3\ ^2A'$	+0.697	+0.303

TABLE IV-XI. Calculated excitation energies (cm^{-1}) and oscillator strength of $(CH_3COOH)\cdot(C_6H_6)^+$.

State		Excitation Energy		Oscillator Strength
		MCQDPT	CASSCF	
Horizontal *cis*-isomer				
$2\ ^2A''$	(π-π)	3877	4604	1.5×10^{-5}
$1\ ^2A'$	CT	19211	29172	0
$3\ ^2A''$	(π-π)	24221	24848	2.7×10^{-2}
$2\ ^2A'$	(σ-π)	29542	34168	7.5×10^{-5}
Vertical *trans*-isomer				
$1\ ^2A''$	(π-π)	5322	5597	7.1×10^{-5}
$2\ ^2A'$	CT	11050	23413	5.5×10^{-2}
$2\ ^2A''$	(σ-π)	21397	36751	2×10^{-6}
$3\ ^2A'$	CT	28061	29905	6.1×10^{-2}

IV.E. Discussion

IV.E.1. Geometrical structures of $(CH_3COOH)\cdot(C_6H_6)^+$ isomers

IV.E.1.1. Assignment of vibrational spectrum in the C–H stretching region

The complex of $(CH_3COOH)\cdot(C_6H_6)^+$ has two types of the C-H bonds; one is that of benzene monomer cation and the other is that of acetic acid. In most cases, the frequencies of the C-H stretching vibrations of an aromatic ring are higher than that of a methyl group. It is difficult to observe acetic acid monomers in supersonic jet because of the high stability of the cyclic dimers in gas phase. Thus, IR spectra of acetic acid monomer species were observed at 150 and 175 °C. Weltner observed three C-H stretching vibrational bands at 2935, 2983, and 3027 cm^{-1} [64]. Haurie and Novak also observed the IR spectrum of gaseous acetic acid where the C-H stretching bands are located 2944, 2996, and 3051 cm^{-1} [65] in accord with the previously reported frequencies of 2961, 2997, and 3048 cm^{-1} [66], respectively. On the other hand, the C-H stretching vibrations of benzene were observed using supersonic jet technique. Using IR-UV double resonance spectroscopy, Lee and co-workers observed three bands at 3048, 3079, and 3101 cm^{-1} in the C-H stretching region of neutral benzene [67]. They explained the three bands in terms of the Fermi resonance among one IR-active C-H stretching vibration and two combination bands of the in-plane vibrations. Fujii et al. observed an IR spectrum of benzene monomer

cation using the messenger technique [68]. They observed only a single band at 3094 cm^{-1} in the C-H stretching region. According to these investigations, one can expect the C-H stretching vibrations of acetic acid in the region from 2935 to 3051 cm^{-1} and that of benzene at 3094 cm^{-1}. In the IR spectrum of $(CH_3COOH)\cdot(C_6H_6)^+$, the frequencies of some C-H stretching vibrations coupled with intermolecular binding can be red-shifted due to the cluster formation. The band at 3080 cm^{-1} observed in our spectrum is assigned to a C-H stretching vibration of the benzene molecule in $(CH_3COOH)\cdot(C_6H_6)^+$.

IV.E.1.2. Assignment of vibrational spectrum in the O–H stretching region

The O-H stretching vibration of a carboxyl group is only responsible for the strong band observed in the region over 3500 cm^{-1}. The appearance of the two bands at 3577 and 3617 cm^{-1} suggests the two possibilities of either the presence of two isomers or Fermi resonance intensity enhancement of a combination band. Here we disregard the latter possibility because acetic acid has little possibility showing any combination band at 3617 cm^{-1}. There is no combination of vibrational frequencies responsible for the Fermi resonance. In fact, no Fermi resonance band is reported in this region [65, 66]. Thus the doublet can be originated from two distinct geometries of $(CH_3COOH)\cdot(C_6H_6)^+$. The O-H stretching vibration of the acetic acid monomer was observed at 3577 cm^{-1} in gas phase by Wilmshurst [66]. Haurie and Novak observed the corresponding band at 3583 cm^{-1} [65]. The discrepancy in the frequencies is probably due to the broadness of the band with enhanced rotational envelopes at high temperatures. The frequency of the strong band (3577 cm^{-1}) is just the same as that of the acetic acid monomer and assigned to the free O-H stretching vibration of $(CH_3COOH)\cdot(C_6H_6)^+$. The frequency of the weak band (3617 cm^{-1}) is 40 cm^{-1} higher than that of the strong band. This suggests that the O-H bond of the isomer is stronger than that of the 3577 cm^{-1} band and can be completely free from hydrogen-bonding. The O-H bond of the carboxyl group is affected by weak intramolecular hydrogen-bonding interaction with the carbonyl oxygen. The isomer with a geometry where the intramolecular hydrogen bond is

weaker than that of the observed acetic acid monomer species can be responsible for the weak band at 3617 cm^{-1}.

The hydroxyl group of the *cis*-isomer of acetic acid is stabilized due to intramolecular hydrogen-bonding interaction with the carbonyl oxygen. In contrast to this, the hydroxyl group of *trans*-isomer is almost free, therefore the O-H stretching frequency of the *trans*-isomer is expected to be higher than that of the *cis*-isomer. Turi and Dannenberg studied these isomers by ab initio molecular orbital calculations [69]. They reported the frequency of the O-H stretching vibration of the *trans*-isomer is 59.6 cm^{-1} higher than that of the *cis*-isomer at the MP2/6-31G(d) level. Thus the weak band at 3617 cm^{-1} can be assigned to the O-H stretching vibration of the *trans*-isomer in the cation complex. However, only the *cis*-isomer is observed in the vibrational spectrum of the acetic acid monomer because the ground state energy of the *trans*-isomer is higher than that of the *cis*-isomer. The energy difference was calculated to be 6.1 kcal/mol at the MP2/6-31G(d,p) level [69]. In a complex of $(CH_3COOH)^+(C_6H_6)$, one can expect the intermolecular interaction of the *trans*-isomers with the benzene monomer cation at the oxygen atoms of the carbonyl and the hydroxyl groups, since the *trans*-isomer has the space faced by the two oxygen atoms for the complex formation. In this case, the total energy of the complex with the *trans*-isomer can be lowered much more than that of the *cis*-isomer. Our assignment should be reinforced with the ab initio molecular orbital calculations with sufficient reliability.

IV.E.1.3. Energetic and geometrical differences among cluster species

As shown in Table IV-III, the *trans*-isomer of acetic acid is less stable than the *cis*-isomer. The energy gap between the *cis*- and *trans*-isomers of acetic acid is 2116 cm^{-1} (6.05 kcal/mol) at the CASSCF(7,7)/6-31G(d,p) level after ZPVE correction. Our result is in good agreement with the value of 6.1 kcal/mol calculated by Turi and Dannenberg at the MP2/6-311++G(d,p) level without ZPVE correction [69]. The repulsive interaction between the hydroxyl hydrogen and the methyl group of *trans*-isomer also contributes to the instability of the *trans*-isomer. The large energy gap prevents the *trans*-isomer from being observed in gas and liquid phase.

The energy gap of the horizontal cluster is only 20 % of that of acetic acid monomer at the CASSCF(7,7)/6-31G(d,p) level after ZPVE correction. As we shall see later, the geometrical differences of the acetic acid isomers from those in the horizontal clusters are not large enough to explain the drastic change in the energy gap. Therefore, the large change in the stabilization energies is attributed to the intermolecular binding energies of the horizontal clusters.

The binding energy of the horizontal *trans*-isomer is 1684 cm^{-1} larger than that of the horizontal *cis*-isomer. This suggests that the conformational change of the carboxyl group produces large difference in the strength of the intermolecular interaction and the *trans*-isomer is much preferable for the in-plane intermolecular interaction between acetic acid and the benzene monomer cation.

On the other hand, the intermolecular bond in the vertical *trans*-isomer is about 1.4 times stronger than that of the horizontal *trans*-isomer. This means that the intermolecular interaction in the vertical complex has a nature different from the hydrogen-bonding interaction seen in the horizontal complexes.

The point is that the *trans*-isomer of acetic acid is preferable to the *cis*-isomer not only for the formation of the vertical complex but also for the horizontal complexes. The geometrical change of the component molecules upon the complex formation reflects the change of electron density. Geometrical parameters of intermolecular lengths give information on the character of the intermolecular bonding. Therefore, let us consider this point from the optimized geometrical parameters of the complex cations and acetic acid monomers.

To start with, we compare those of the horizontal *cis*-isomer with those of the horizontal *trans*-isomer. The C-H bond lengths of the methyl groups of both the horizontal complexes are almost equal to those of the acetic acid monomers. This result indicates that the intermolecular interaction does not affect the electron density of the methyl group. The intermolecular bond lengths between the carbonyl oxygen and the first and the second nearest hydrogen atoms of the benzene cation are 2.3862 and 2.4508 Å, respectively, for the horizontal *cis*-isomer. Those for the horizontal *trans*-isomer are 2.3218 and 2.5962 Å, respectively. These indicate that the carbonyl oxygens of both the horizontal complexes form double hydrogen bonds with two of the hydrogens of the benzene cations. Because of the

hydrogen bonds at the carbonyl group, the C=O bonds of the horizontal complexes are longer than those of the acetic acid monomers.

There are important differences between the horizontal *cis*- and *trans*-isomers in the intermolecular interaction of the hydroxyl group with the benzene ring. The C-O bond of the horizontal *cis*-isomer is 0.0154 Å shorter than that of the monomer, while that of the horizontal *trans*-isomer is shortened only by 0.0038 Å. In addition, the degree of the variation of the C-O-H angle by the complex formation is large in the horizontal *cis*-isomer. This is probably due to the repulsion between the hydroxyl group and the benzene ring. The hydroxyl hydrogen and the hydrogen atoms of benzene cation repel each other and the repulsion may shorten the C-O single bond and enlarge the C-O-H angle. In the horizontal *trans*-isomer, the hydroxyl hydrogen is on the opposite side to the benzene ring and the hydroxyl oxygen which is partially negatively charged is close to the hydrogen atoms of benzene cation. Therefore the repulsion mentioned above is weak in the horizontal *trans*-isomer. The intermolecular C-H···O-C bond length is 2.5692 Å in the horizontal *trans*-isomer, while that of the horizontal *cis*-isomer is 4.1951 Å. The O-C=O angle is also varied largely in the horizontal *trans*-isomer. This suggests that the hydroxyl oxygen interacts with the hydrogen atom of benzene cation and the additional hydrogen bond is formed between them in the horizontal *trans*-isomer. Thus the increment in the binding energy of the horizontal *trans*-isomer is attributed to this additional C-H···O-C hydrogen bond and the weakened hydrogen-hydrogen repulsion.

The intermolecular binding energy of the vertical complex is larger than

those of the horizontal complexes where the double or triple hydrogen bonds are formed, although only one hydrogen atom of the benzene cation locates near the hydroxyl oxygen in the vertical *trans*-isomer. In the vertical *trans*-isomer, the carbonyl oxygen interacts with the benzene ring from vertical direction at an intermolecular C···O=C distance as close as 2.6170 Å. This indicates that the carbonyl oxygen interacts strongly with the π-electron system of the benzene cation. The binding energy of the vertical *trans*-isomer cannot be explained only by electrostatic interaction like the horizontal complexes, since the overlap of non-bonding orbitals of the carbonyl group with π-orbitals of benzene cation can change the electronic structures. We shall try to give a more detailed discussion on this point in a later section.

IV.E.1.4. Comparison between the CASSCF and DFT calculations

Three optimized geometries are obtained at the B3LYP/6-31G(d,p) level in agreement with the CASSCF calculations. At the B3LYP/6-31G(d,p) level, the most and least stable species is the vertical *trans*-isomer and the horizontal *trans*-isomer, respectively. This result agrees with that obtained at the CASSCF(7,7)/6-31G(d,p) level. The value of energy gaps between the *cis*- and *trans*-isomers for the horizontal complex is 798 cm^{-1} after ZPVE correction. This is 366 cm^{-1} larger than that obtained at the CASSCF(7,7)/6-31G(d,p) level. In contrast, the energy gap between the *trans*- and the *cis*-isomers of acetic acid exhibits similar values at both the levels of the methods: 2075 cm^{-1} at the B3LYP/6-31G(d,p) level and 2116 cm^{-1} at the CASSCF(7,7)/6-31G(d,p) level after ZPVE correction.

The intermolecular interaction at the B3LYP/6-31G(d,p) level is estimated to be weaker than that at the CASSCF(7,7)/6-31G(d,p) level. However the relative tendency is in the consistent with the CASSCF calculations; the vertical complex has binding energy larger than those of the horizontal complexes and the *trans*-isomer can form stronger intermolecular binding than the *cis*-isomer.

Intramolecular bond lengths except that of the C-O bond of the vertical *trans*-isomer are estimated to be longer at the B3LYP/6-31G(d,p) level relative to those obtained by the CASSCF calculations. On the other hand, the intermolecular distances become short by approximately 0.1 and 0.2 Å in the horizontal *cis*- and vertical *trans*-isomers, respectively. In contrast, the

intermolecular distance between the benzene ring and the hydroxyl group of the horizontal *trans*-isomer at the B3LYP/6-31G(d,p) level is approximately 0.5 Å longer than that obtained at the CASSCF(7,7) level.

IV.E.1.5. Comparison between calculated and observed vibrational spectra

Since our main concern in the observed vibrational spectrum is the assignment of the weak band located on the high frequency side of the free O-H stretching vibration, we discuss the relative values of the O-H stretching frequencies at each level of the theories. The frequencies of the O-H stretching vibration of the *trans*-isomer of acetic acid are 53 and 51 cm^{-1} higher than those of the *cis*-isomer at the CASSCF(7,7)/6-31G(d,p) and B3LYP/6-31G(d,p) levels, respectively. These values are in good agreement with the value of 59.6 cm^{-1} calculated by Turi and Dannenberg at the MP2/6-31G(d) level [69]. As mentioned in previous section, the frequency of the strongest band in the vibrational spectrum of $(CH_3COOH)\cdot(C_6H_6)^+$ is 3577 cm^{-1} that is close to the frequency of the *cis*-isomer of acetic acid. The calculated O-H stretching frequency of the horizontal *cis*-isomer is also close to that of the *cis*-isomer of acetic acid at the both levels. Therefore the strongest band at 3577 cm^{-1} is assigned to the O-H stretching vibration of the horizontal *cis*-isomer. The calculated frequencies of the O-H stretching vibrations of the horizontal and vertical *trans*-isomer are 26 and 27 cm^{-1} higher than that of the horizontal *cis*-isomer at the CASSCF(7,7)/6-31G(d,p) level. At the B3LYP/6-31G(d,p) level, two *trans*-isomers also exhibit the O-H vibrational frequencies higher than the horizontal *cis*-isomer. These results suggest that the weak band at 3617 cm^{-1} can be attributed to the vertical and/or horizontal *trans*-isomers. As already mentioned, the vertical *trans*-isomer is the most stable species and the horizontal *trans*-isomer is

3053 cm^{-1} less stable than the vertical *trans*-isomer. Therefore we assign the band at 3617 cm^{-1} to the O-H stretching vibration of the vertical *trans*-isomer.

Now we have a problem on the intensities. The intensity ratio of the strongest band at 3577 cm^{-1} to that of the weak band at 3617 cm^{-1} cannot reflect the abundance of the horizontal *cis*-isomer to that of the vertical *trans*-isomer correctly. The observed IR spectrum is measured by the photodissociation spectroscopy that is related to the internal temperature of the complexes and the dissociation thresholds. The calculated binding energy of the vertical *trans*-isomer is 4737 and 2611 cm^{-1} larger than that of the horizontal *cis*-isomer at the CASSCF(7,7)/6-31G(d,p) and B3LYP/6-31G(d,p) levels, respectively. The binding energy larger than the photon energies is less preferable for the efficiency of photodissociation of the vertical *trans*-isomer. Only the species in highly vibrationally excited states can contribute to the photodissociation spectrum in this case.

IV.E.2. Electronic states of $(CH_3COOH)\cdot(C_6H_6)^+$ isomers

IV.E.2.1. Assignment of electronic spectrum

The excitation energy of the 24500 cm^{-1} band is close to that of an local excitation (LE) band of a benzene monomer cation observed in the photodissociation spectra of a series of charge resonance and charge transfer complexes with a benzene cation [35, 36, 38-40]. However, this assignment is dangerous for the vertical complex because the π-π excited states of the vertical complex can be different from that of the benzene monomer cation due to the interaction between π-electrons of the benzene cation and non-bonding electrons of acetic acid. The band width is approximately 2.5 times wider than those of the LE bands observed in the previous works [35, 36, 38-40, 70]. An LE band of the benzene cation in the horizontal complexes can be embedded under the 24500 cm^{-1} band. The other band at 17500 cm^{-1} cannot be assigned to an LE band of a component molecule, since neither this benzene cation nor acetic acid exhibits any LE band in this region. This suggests the presence of the cluster species where the electronic states are much different from those of the component molecules. The change in the electronic states can be due to the intermolecular charge transfer interaction in the cation complex. The spectral feature with a broad band width remind us a similar broadness of the CR band of a benzene dimer cation [38-40]. The nature of the charge transfer interaction is highly related to the geometry of the cation complex.

IV.E.2.2. Comparison between calculated and observed electronic spectra

On the basis of the comparison between the observed spectrum of $(CH_3COOH)\cdot(C_6H_6)^+$ and the spectra of the charge resonance and charge transfer complexes with a benzene cation, we have assigned in the previous section that the LE bands of the benzene cation in the horizontal complex is embedded under the 24500 cm^{-1} band. The 17500 cm^{-1} band can be attributed to a CT band. The calculated electronic spectra of the two isomers are obtained using the calculated transition energies and oscillator strengths mentioned in previous section. Figure IV-8 shows the calculated spectrum where populations of the two isomers are supposed to be equal. For comparison, the observed spectrum is also displayed in Figure IV-8. The computational results suggest that only three electronic transitions can be observed in this region. One is the π-π transition of the horizontal *cis*-isomer and the others are the two charge transfer transitions of the vertical *trans*-isomer. The excitation energy of the π-π transition of the horizontal *cis*-isomer is estimated to be 24221 cm^{-1} at the MCQDPT level and correspond to the observed band at 24500 cm^{-1}. By considering the analysis of the vibrational spectrum, we assign the 17500 cm^{-1} band to one of the charge transfer transition of the vertical *trans*-isomer. The other charge transfer transition is characterized by the excitation from an intermolecular bonding orbital, $(An+B\pi_1)$, to the $B\pi_3$ orbital that has intermolecular anti-bonding character, as already shown in Figure IV-7. This transition can be accompanied with large geometrical change along the intermolecular

coordinates. Therefore the CT band which arises from this transition can be broader than the band at 17500 cm^{-1}. On the basis of the present calculation and the broadness of the band, the 24500 cm^{-1} band can be assigned to the second CT band. However, the IR study also suggests the presence of the LE band of the horizontal *cis*-isomer in the same region.

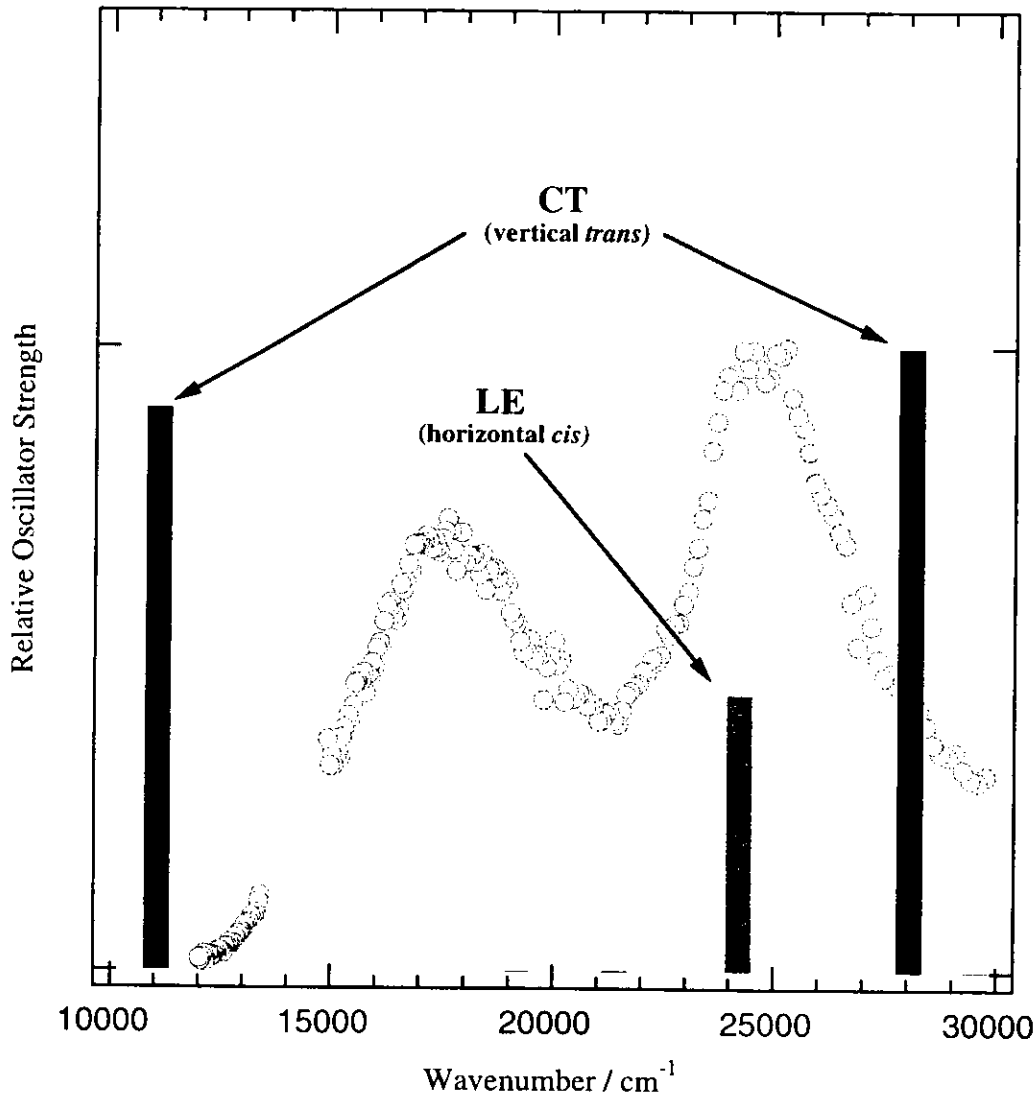

FIG. IV-8. Comparison between observed and calculated electronic spectra

IV.F. Conclusion

The geometrical structures and the electronic states of $(CH_3COOH)\cdot(C_6H_6)^+$ were studied experimentally and theoretically. Experimentally, the vibrational spectrum of $(CH_3COOH)\cdot(C_6H_6)^+$ in the supersonic jet was measured in the 3000-3680 cm^{-1} region using the photodissociation spectroscopy. The electronic spectrum was also observed in the 12000-13400 and 15000-29600 cm^{-1} regions. Theoretically, ab initio molecular orbital calculations were performed for geometry optimizations and calculations of vibrational frequency and electronic transition energy. The vibrational spectrum shows two distinct bands in the O-H stretching vibrational region. The frequency of the strong band (3577 cm^{-1}) is close to that of acetic acid and the weak one is located at 3617 cm^{-1}. On the basis of geometry optimizations and frequency calculations, the strong band is assigned to the O-H stretching vibration of the horizontal *cis*-isomer where the *cis*-isomer and the benzene cation are on the same plane and the hydrogen bonds are formed between the hydrogen atoms of the benzene cation and the carbonyl oxygen of acetic acid. The weak one is assigned to the vertical *trans*-isomer where the two oxygen atoms of the *trans*-isomer of acetic acid interact with the π-electron system of the benzene cation. The weakness of the high frequency band in the photodissociation spectrum is attributed to the binding energy larger than the photon energy injected. Only hot vertical *trans*-isomers can be dissociated by the IR excitation. The electronic spectrum exhibits two bands with intensity maxima at 17500 cm^{-1}

and 24500 cm^{-1}. The calculations of electronic excitation energies and oscillator strengths suggest the CT bands of the vertical *trans*-isomer can be observed in this region in addition to an LE band of the horizontal *cis*-isomer. The appearance of the band due to the vertical *trans*-isomer suggests that the interaction between the π orbitals of the benzene cation and the non-bonding orbital of acetic acid is as strong as the double hydrogen bonds in the horizontal complex.

References for chapter IV

[1] M. Allan and J. P. Maier, Chem. Phys. Lett. 34, 442 (1975).

[2] M. Allan, J. P. Maier, and O. Marthaler, Chem. Phys. 26, 131 (1977).

[3] J. P. Maier and O. Marthaler, Chem. Phys. 32, 419 (1978).

[4] V. E. Bondybey, J. H. English, and T. A. Miller, J. Mol. Spectrosc. 84, 124 (1980).

[5] J. Jelvajian, B. M. Dekovan, and A. P. Baronavski, Chem. Phys. 90, 175 (1984).

[6] M. Heaven, T. A. Miller, and V. E. Bondybey, J. Chem. Phys. 76, 3831 (1982).

[7] L. F. Dimauro, M. Heaven, and T. A. Miller, Chem. Phys. Lett. 104, 526 (1984).

[8] R. A. Kennedy and T. A. Miller, J. Chem. Phys. 85, 2326 (1986).

[9] R. C. Dunbar, J. Am. Chem. Soc. 95, 6191 (1973).

[10] P. P. Dymerski, E. Fu, and R. C. Dunbar, J. Am. Chem. Soc. 96, 4109 (1974).

[11] R. C. Dunbar, Chem. Phys. Lett. 32, 508 (1975).

[12] H. H. Teng and R. C. Dunbar, Chem. Phys. Lett. 32, 508 (1975).

[13] K. Walter, R. Weinkauf, U. Boesl, and E. W. Schlag, Chem. Phys. Lett. 155, 8 (1989).

[14] M. Fujii, Y. Tsuchiya, and M. Ito, J. Mol. Structure 249, 55 (1991).

[15] P. Lablanquie, K. Ohashi, and N. Nishi, J. Chem. Phys. 98, 399 (1993).

[16] T. Sasaki and N. Mikami, Chem. Phys. Lett. 209, 379 (1993).

[17] J. A. Syage, J. E. Pollard, and J. Steadman, Chem. Phys. Lett. 161, 103 (1989).

[18] C. Lingbing, H. Figger, and W. Quint, Z. Phys. D 13, 61 (1989).

[19] W. A. Chupka, S. D. Colson, M. S. Seaver, and A. M. Woodward, Chem. Phys. Lett. 95, 171 (1983).

[20] A. M. Woodward, S. D. Colson, W. A. Chupka, and M. G. White, J. Phys. Chem. 90, 274 (1986).

[21] R. Weinkauf, K. Walter, U. Boesl, and E. W. Schlag, Chem. Phys. Lett. 141, 267 (1987).

[22] K. Walter, R. Weinkauf, U. Boesl, and E. W. Schlag, J. Chem. Phys. 89, 1914 (1988).

[23] J. Momigny and J. C. Lorquet, Chem. Phys. Lett. 1, 505 (1968).

[24] L. Åsbrink, O. Edqvist, E. Lindholm, and L. E. Selin, Chem. Phys. Lett. 5, 192 (1970).

[25] Y. Achiba, K. Sato, K. Shobatake, and K. Kimura, J. Chem. Phys. 79, 5213 (1983).

[26] R. Lindner, H. Sekiya, B. Beyl, and K. Müller-Dethlefs, Angew. Chem. Int. Ed. Engl. 32, 603 (1993).

[27] R. Lindner, H. Sekiya, and K. Müller-Dethlefs, Angew. Chem. Int. Ed. Engl. 32, 1364 (1993).

[28] H. Sekiya, R. Lindner, and K. Müller-Dethlefs, Chem. Lett. 485 (1993).

[29] H-J. Dietrich, R. Lindner, and K. Müller-Dethlefs, J. Chem. Phys.

101, 3399 (1994).

[30] H. Krause and J. J. Neusser, J. Chem. Phys. 97, 5923 (1992).

[31] H. Krause and J. J. Neusser, J. Photochem. Photobiol. A: Chem. 80, 73 (1994).

[32] B. S. Freiser and J. L. Beauchamp, Chem. Phys. Lett. 35, 35 (1975).

[33] J. H. Miller and L. Andrews, Chem. Phys. Lett. 72, 90 (1980).

[34] J. G. Goode, J. D. Hofstein, and P. M. Johnson, J. Chem. Phys. 107, 1703 (1997).

[35] M. Matsumoto, Y. Inokuchi, K. Ohashi, and N. Nishi, J. Phys. Chem. A **101**, 4574 (1997).

[36] K. Ohashi, Y. Nakane, Y. Inokuchi, Y. Nakai, and N. Nishi, Chem. Phys. **239**, 429 (1998).

[37] K. Ohashi, H. Izutsu, Y. Inokuchi, K. Hino, N. Nishi, and H. Sekiya, Chem. Phys. Lett. **321**, 406 (2000).

[38] K. Ohashi and N. Nishi, J. Chem. Phys. **95**, 4002 (1991).

[39] K. Ohashi and N. Nishi, J. Phys. Chem. **96**, 2931 (1992).

[40] K. Ohashi, Y. Nakai, T. Shibata, and N. Nishi, Laser Chem. **14**, 3 (1994).

[41] K. Ohashi, Y. Inokuchi, and N. Nishi (unpublished).

[42] A. Fujii, A. Iwasaki, K. Yoshida, T. Ebata, and N. Mikami, J. Phys. Chem. A **101**, 1798 (1997).

[43] K. Ohashi, Y. Inokuchi, H. Izutsu, K. Hino, N. Yamamoto, N. Nishi, and H. Sekiya, Chem. Phys. Lett. **323**, 43 (2000).

[44] T. Nakanaga, P. K. Chowdhury, F. Ito, K. Sugawara, and H. Takeo, J.

Mol. Struct. **413/414**, 205 (1997).

[45] K. Kimura, S. Katsumata, T. Yamazaki, and H. Wakabayashi, J. Electron Spectrosc. **6**, 41 (1975).

[46] R. Neuhauser, K. Siglow, and H. J. Neusser, J. Chem. Phys. **106**, 896 (1997).

[47] K. Kosugi, T. Nakabayashi, and N. Nishi, Chem. Phys. Lett. **291**, 253 (1998).

[48] T. Nakabayashi, K. Kosugi, and N. Nishi, J. Phys. Chem. A **103**, 8595 (1999).

[49] N. Nishi, T. Nakabayashi, and K. Kosugi, J. Phys. Chem. A **103**, 10851 (1999).

[50] P. Imhof, W. Roth, C. Janzen, D. Spangenberg, and K. Kleinermanns, Chem. Phys. **242**, 141 (1999).

[51] P. Imhof, W. Roth, C. Janzen, D. Spangenberg, and K. Kleinermanns, Chem. Phys. **242**, 153 (1999).

[52] M. J. Frisch, G. W. Trucks, H. B. Schlegel, G. E. Scuseria, M. A. Robb, J. R. Cheeseman, V. G. Zakrzewski, J. A. Montgomery, Jr., R. E. Stratmann, J. C. Burant, S. Dapprich, J. M. Millam, A. D. Daniels, K. N. Kudin, M. C. Strain, O. Farkas, J. Tomasi, V. Barone, M. Cossi, R. Cammi, B. Mennucci, C. Pomelli, C. Adamo, S. Clifford, J. Ochterski, G. A. Petersson, P. Y. Ayala, Q. Cui, K. Morokuma, D. K. Malick, A. D. Rabuck, K. Raghavachari, J. B. Foresman, J. Cioslowski, J. V. Ortiz, A. G. Baboul, B. B. Stefanov, G. Liu, A. Liashenko, P. Piskorz, I. Komaromi, R. Gomperts, R. L. Martin, D. J. Fox, T. Keith, M. A. Al-Laham, C. Y. Peng, A. Nanayakkara, C. Gonzalez, M.

Challacombe, P. M. W. Gill, B. Johnson, W. Chen, M. W. Wong, J. L. Andres, C. Gonzalez, M. Head-Gordon, E. S. Replogle, and J. A. Pople, *GAUSSIAN 98*, revision A.7, Gaussian, Inc., Pittsburgh PA, 1999.

[53] Alex A. Granovsky, www http://classic.chem.msu.su/gran/gamess/index.html.

[54] M. W. Schmidt, K. K. Baldridge, J. A. Boatz, S. T. Elbert, M. S. Gordon, J. J. Jensen, S. Koseki, N. Matsunaga, K. A. Nguyen, S. Su, T. L. Windus, M. Dupuis, J. A. Montgomery, J. Comput. Chem. **14**, 1347 (1993).

[55] A. D. Becke, J. Chem. Phys. **98**, 5648 (1993).

[56] C. Lee, W. Yang, and R. G. Parr, Phys. Rev. B **37**, 785 (1988).

[57] B. Miehlich, A. Savin, H. Stoll, and H. Preuss, Chem. Phys. Lett. **157**, 200 (1989).

[58] H. Nakano, J. Chem. Phys. **99**, 7983 (1993).

[59] R. S. Mulliken, J. Chem. Phys. **23**,1833 (1955).

[60] R. S. Mulliken, J. Chem. Phys. **23**, 1841 (1955).

[61] R. S. Mulliken, J. Chem. Phys. **23**, 2338 (1955).

[62] R. S. Mulliken, J. Chem. Phys. **23**, 2343 (1955).

[63] B. M. Bode and M. S. Gordon, J. Mol. Graphics Mod. **16**, 133 (1998).

[64] W. Weltner, J. Am. Chem. Soc. **77**, 3941 (1955).

[65] M. Haurie and A. Novak, J. Chim. Phys. **62**, 137 (1965).

[66] J. K. Wilmshurst, J. Chem. Phys. **25**, 1171 (1956).

[67] R. H. Page, U. R. Shen, and U. T. Lee, J. Chem. Phys. **88**, 5362 (1988).

[68] A. Fujii, E. Fujimaki, T. Ebata, and N. Mikami, J. Chem. Phys. **112**, 6275 (2000).

[69] L. Turi and J. J. Dannenberg, J. Phys. Chem. **97**, 12197 (1993).

[70] Y. Inokuchi, K. Ohashi, M. Matsumoto, and N. Nishi, J. Phys. Chem. **99**, 3416 (1995).

CHAPTER V

Photodissociation spectroscopic study on $(CH_3COOH)\cdot(C_6H_6)_2^+$ and $(CH_3COOH)_2\cdot(C_6H_6)_2^+$ in the gas phase

V.A. Introduction

V.A.1. benzene cluster ions

Since 1960's, several spectroscopic studies of benzene cluster ions have been carried out in the condensed phase. Ishitani and Nagakura measured an electronic absorption spectrum and an ESR spectrum of paracyclophane anion in low-temperature solutions [1]. In the absorption spectrum, the paracyclophane anion shows a strong absorption band at 760 nm. An ESR pattern with hyperfine structures of 41 lines emerges in the ESR spectrum. From these results, it was concluded that there exists a charge resonance (CR) interaction between the π electron systems belonging to the two benzene rings of the paracyclophane anion. The electronic absorption spectra of benzene dimer ion were measured by several groups. Badger and Brocklehurst observed the electronic absorption spectrum of the benzene dimer ion in γ-irradiated solutions at 77 K [2]. The effects of concentration and slight warming were used to assign the absorption bands to monomeric or dimeric ions. The assignments were supported by the resemblance of the dimer bands to those of paracyclophane cation. Shida also measured the electronic absorption spectra of benzene dimer cation in γ-irradiated solutions with changing benzene concentrations [3]. However, an ambiguity exists in the identification of the cluster size of benzene.

In the last decade, the studies on the photodissociation dynamics of benzene cluster ions, $(C_6H_6)_n^+$, have been carried out extensively in the gas

phase by using mass-selected photodissociation spectroscopy [4-15]. Recently, the mass-selected photodepletion spectra of $(C_6H_6)_n^+$ in the range of 800-1100 nm were reported [14]. The most important findings is that the absorption bands of $(C_6H_6)_n^+$ with n = 3-6 exhibit essentially the same features with that of $(C_6H_6)_2^+$, indicating the presence of a dimer ion core in the cluster ions. The translational energies of neutral molecules ejected following photoexcitaion of $(C_6H_6)_n^+$ have been measured in the photon energy range of 0.5-3.0 eV [14]. The fraction of the translational energies of the products in the excess energies has been estimated to be ≈ 15 % for n = 3 and ≈ 25 % for n = 8, respectively.

The binding energies of benzene cluster ions have been determined by thermodynamic and spectroscopic techniques. Meot-Ner measured the dissociation energies of benzene dimer ion, $(C_6H_6)_2^+$, and protonated dimer ion, $(C_6H_6)_2H^+$ [16]. The values of 17.0 and 11.0 kcal/mol were reported for the binding energies of $(C_6H_6)_2^+$ and $(C_6H_6)_2H^+$, respectively. Neusser and co-workers investigated the dissociation kinetics of benzene cluster ions [17-21]. They determined the binding energies of benzene cluster ions by measuring the ionization potentials and the appearance potentials of the respective decay channels of each of the cluster ions. The binding energies of benzene dimer, trimer, tetramer, and pentamer ions were reported as 660 ± 20, 270 ± 40, 130 ± 40, and ≤ 110 meV, respectively. Neusser and co-workers also investigated unimolecular fragmentation kinetics through the measurement of the binding energies of mass selected benzene cluster ions [22]. They determined the binding energies of benzene cluster ions, , up to

n = 23 from the metastable decay ratios assuming an evaporative ensemble model and applying a restricted RRKM formalism.

Theoretical studies on the geometrical and electronic structures of benzene dimer ion have been investigated by several groups. Hiraoka and co-workers determined the structure of benzene dimer ion by spin-restricted open-shell Hartree-Fock (ROHF) molecular orbital calculations [23]. They suggested that two structures, T-shape and parallel, are located at the potential energy minima, and that the T-shape structure is 3.0 kcal/mol more stable than the parallel structure at the ROHF/6-31G(d,p)//ROHF/3-21G levels. Miyoshi and co-workers performed complete active space self-consistent field (CASSCF) and multireference singly and doubly excited configuration interaction (MRSDCI) calculations for benzene dimer ion [24]. The calculations show that the minimum of the ground state of benzene dimer ion is at parallel, distorted C_{2h} geometry, and that sandwich (D_{6h}) and T-shaped (C_{2v}) structures are higher in energy than the minimum by 0.4 and 3.7 kcal/mol, respectively.

V.A.2. Aims of the present study

One of the most important and fundamental issues in the studies of cluster ions is to determine their electronic and geometrical structures. As mentioned above, $(C_6H_6)_n^+$ with n = 3-6 are thought to have a dimer ion core structure where charge resonance interaction fastens two benzene rings each other on the basis of similarity in spectral feature between electronic spectrum of $(C_6H_6)_2^+$ and those of $(C_6H_6)_n^+$. On the other hand, strong charge transfer interaction governs the geometrical structure of acetic acid-benzene cation complex, $(CH_3COOH)\cdot(C_6H_6)^+$, as mentioned in chapter IV. Which of the two intermolecular interactions is dominant in the system where both interactions can have posssibilities ?

In order to answer this question, the geometrical and electronic structures of the acetic acid-benzene cluster cations, $(CH_3COOH)\cdot(C_6H_6)_2^+$ and $(CH_3COOH)_2\cdot(C_6H_6)_2^+$, are studied in this study. The electronic and vibrational spectra of the cluster cations are observed by photodissociation spectroscopy. In order to clear the origin of vibrational bands, the vibrational spectra of $(CD_3COOD)\cdot(C_6H_6)_2^+$ and $(CD_3COOD)_2\cdot(C_6H_6)_2^+$ are also measured.

V.B. Experimental

All the cluster cations investigated in this study are produced by electron-impact ionization of neutral clusters with electron energies of 250-350 eV. Electronic and vibrational spectra of cluster cations were observed by photodissociation spectroscopy using two types of mass spectrometers: an ion trap photodissociation spectrometer [25-27] and a linear type time-of-flight (TOF) mass spectrometer. The former is equipped with a quadrupole ion guide and two quadrupole mass filters. The parent ions of interest are selected through the first quadrupole mass filter. After the deflection by an ion bender, the ion beam of the parent ion is decelerated and introduced into the quadrupole ion guide. A laser beam merges with the ion beam in the ion guide. Vibrational and electronic excitation induces the dissociation of the parent ions. After the deflection by another ion bender, the masses of the resulting fragment ions are analyzed by the second quadrupole filter.

A schematic diagram of the latter is shown in Figure V-1. It is composed of a source chamber and a drift tube. The source chamber is pumped with a turbo molecular pump (TMP) (Mitsubishi, PT-1500, 1600 l/s) backed by a mechanical pump (Alcatel, T2033A, 10.6 l/s). The drift tube is evacuated with the two same type of turbo molecular pumps (Mitsubishi, PT-500, 550 l/s). One is located at the middle of the drift tube and the other is near a detector. These are forepumped by mechanical pumps (Alcatel, T2021I, 5.5 l/s).

In the region from atmospheric value to 10^{-2} Torr (1 Torr $\approx$ 1.33 X 10^{2} Pa), the degree of vacuum at the source chamber is monitored by a pirani gauge tube (ULVAC, WP-02) with a controller (ULVAC, GP-2ARY). In a higher vacuum region where the chambers are pumped with TMP, the degree of vacuum are monitored at both the source chamber and the drift tube by ionization gauge tubes (ANELVA, NG-2) with a controller (ANELVA, MIG-831). The pressures of the drift tube are 3 X 10^{-7} and 4 X 10^{-8} Torr when the sample jet is on and off, respectively, while those of the source chamber are 3 X 10^{-6} and 5 X 10^{-7} Torr.

The TOF mass spectrometer has two accelerators. One is a Wiley-McLaren type accelerator (hereafter called the first accelerator) situated 15 cm downstream from the nozzle, and the other is a simple accelerator composed by two plates (hereafter called the second accelerator) located 1 m downstream from the first accelerator. In order to control the ion path, two sets of deflector and three ion lenses are employed. A deflector type mass-gate is also equipped. The first accelerator sorts ions by mass and the mass-gate let only the parent ions of interest through. The photodissociation laser beam intersects the mass selected ion bunch at the point that is 2 cm upstream from the second accelerator. The second accelerator separates fragment ions from the parent ions. The fragment and parent ions are observed by the microsphere plate (MSP) in the order of mass number. Photodissociation spectra were obtained by recording the yields of the fragments against the excitation energies.

The tunable light source for the IR region was a optical parametric

oscillator (OPO) system (Continuum Mirage 3000) pumped with an injection-seeded Nd:YAG laser (Continuum Powerlite 9000). The resolution of the OPO laser was less than 0.02 cm^{-1}. Another OPO system (Spectra-Physics MOPO-730) pumped with a Nd:YAG laser (Spectra-Physics GCR-250) was used in the 5920-13690 cm^{-1} (730-1690 nm) and 14590-21720 cm^{-1} (460-685 nm) regions. The output of a dye laser (Lambda Physik LPD3000) pumped with an excimer laser (Lambda Physik LPX100) was used in the 21560-27050 cm^{-1} (370-464 nm) region. Spectroscopy grade acetic acid and benzene were purchased from Wako Pure Chemical Company and used without further purification.

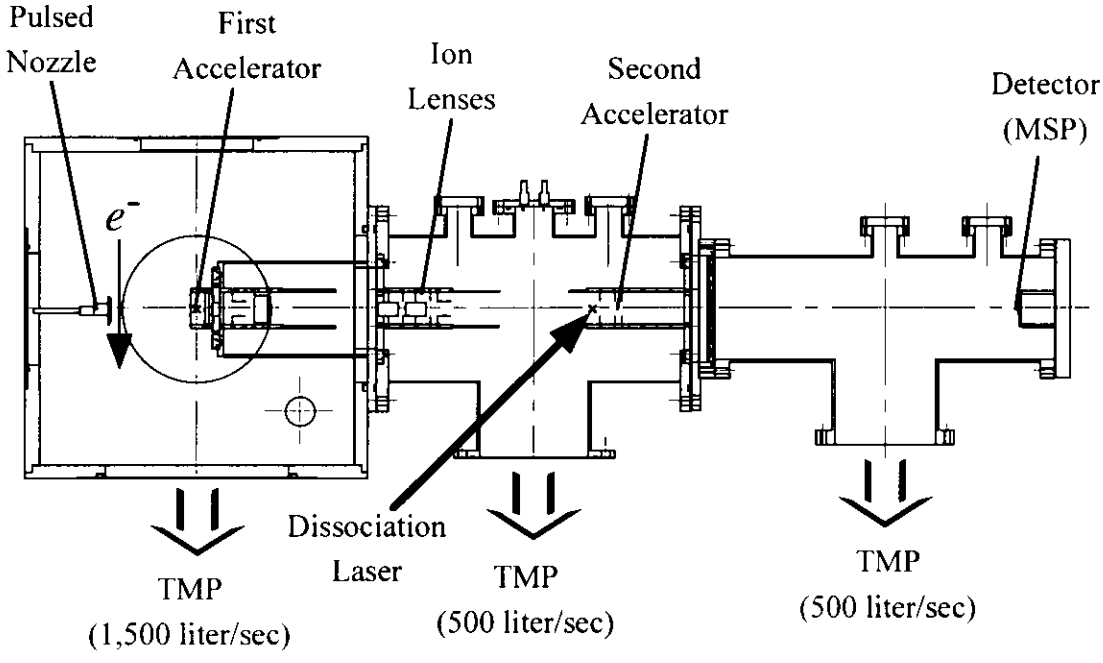

Figure V-1. Schematic diagram of the linear type time-of-flight mass spectrometer for the cluster ion photodissociation study.

V.C. Results

V.C.1. Electronic spectrum of $(CH_3COOH)\cdot(C_6H_6)_2^+$

Figure V-2 shows the electronic spectrum of $(CH_3COOH)\cdot(C_6H_6)_2^+$ in the region of 5920-24540 cm^{-1}. Two bands can be seen. A very strong band is observed in the near-IR region with its intensity maxima at 11000 cm^{-1}. The band is very broad. Its FWHM is 3300 cm^{-1}. On the other hand, a relatively weak band is located at 23500 cm^{-1}.

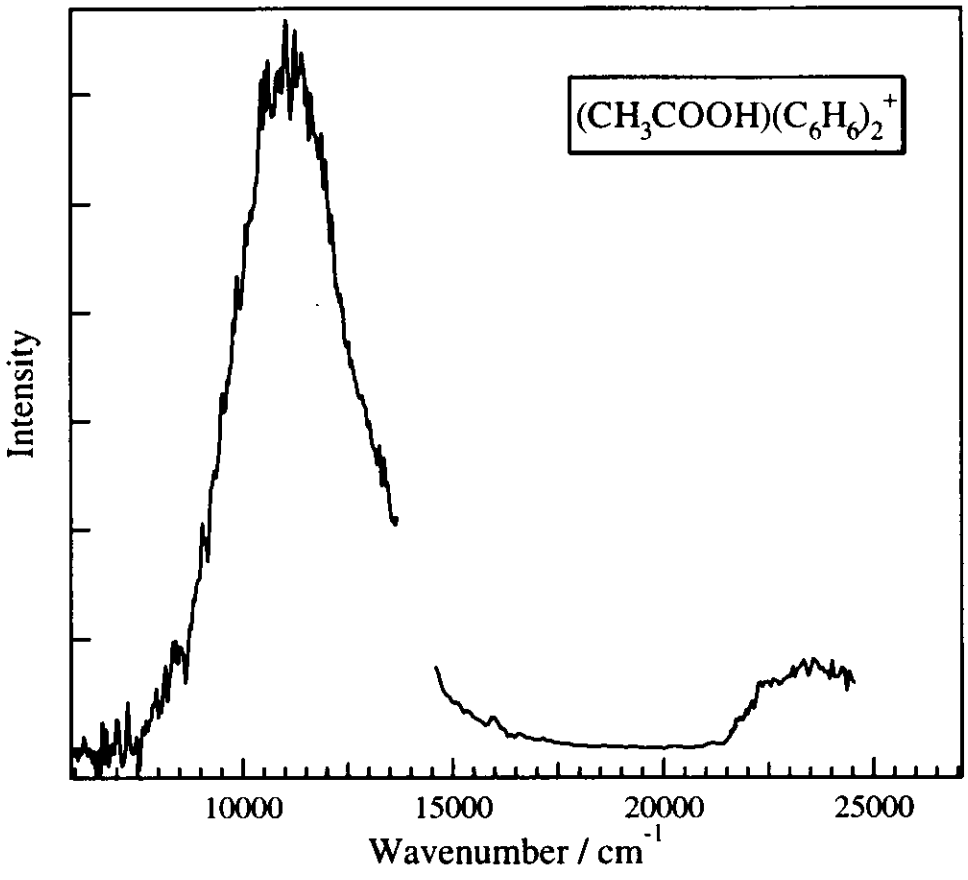

Figure V-2. Electronic spectrum of $(CH_3COOH)(C_6H_6)_2^+$.

V.C.2. Vibrational spectrum of $(CH_3COOH)\cdot(C_6H_6)_2^+$

Figure V-3 shows the vibrational spectrum of $(CH_3COOH)\cdot(C_6H_6)_2^+$ in the region of 2800-3700 cm^{-1}. Three bands are observed in this region. A strong band is located at 3084 cm^{-1}. The other two bands are seen in the O–H stretching region. The frequencies of the bands are 3585 and 3627 cm^{-1}. In order to clear the assignment of the vibrational bands, the vibrational spectrum of $(CD_3COOD)\cdot(C_6H_6)_2^+$ is also measured and is shown in Figure V-4. Only one band is observed at 3084 cm^{-1}.

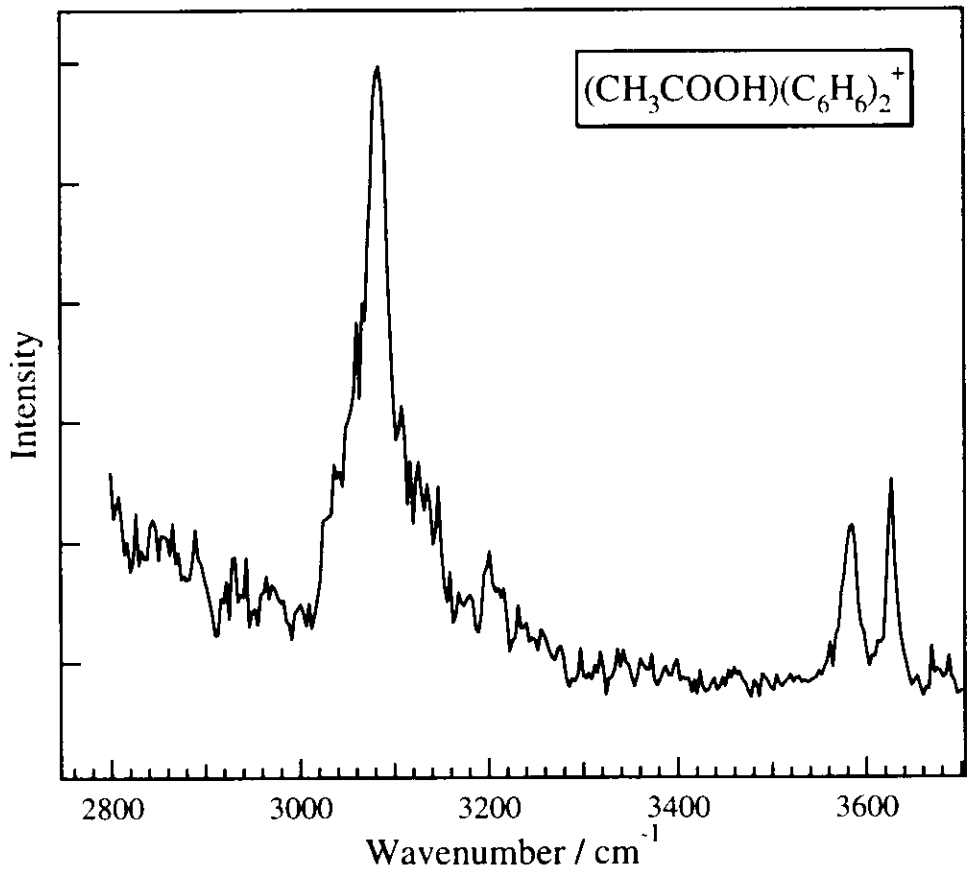

Figure V-3. Vibrational spectrum of $(CH_3COOH)(C_6H_6)_2^+$.

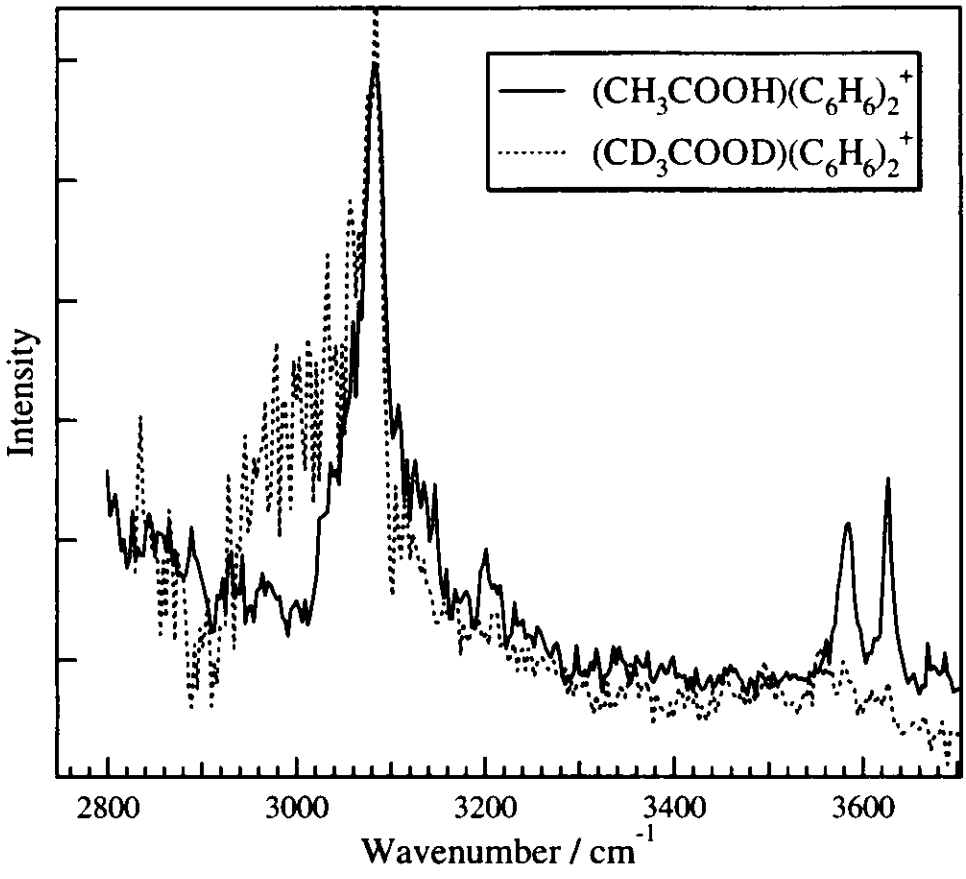

Figure V-4. Vibarational spectra of $(CH_3COOH)(C_6H_6)_2^+$ and $(CD_3COOD)(C_6H_6)_2^+$

V.C.3. Electronic spectrum of $(CH_3COOH)_2 \cdot (C_6H_6)_2^+$

Figure V-5 shows the electronic spectrum of $(CH_3COOH)_2 \cdot (C_6H_6)_2^+$ in the region of 5950-27000 cm^{-1}. Two bands can be seen. A very strong band is observed in the near-IR region with its intensity maxima at 10850 cm^{-1}. This band is very broad. Its FWHM is 3300 cm^{-1}. On the other hand, a relatively weak band is located at 23600 cm^{-1}. The feature of the electronic spectrum of $(CH_3COOH)_2 \cdot (C_6H_6)_2^+$ is similar to that of $(CH_3COOH) \cdot (C_6H_6)_2^+$.

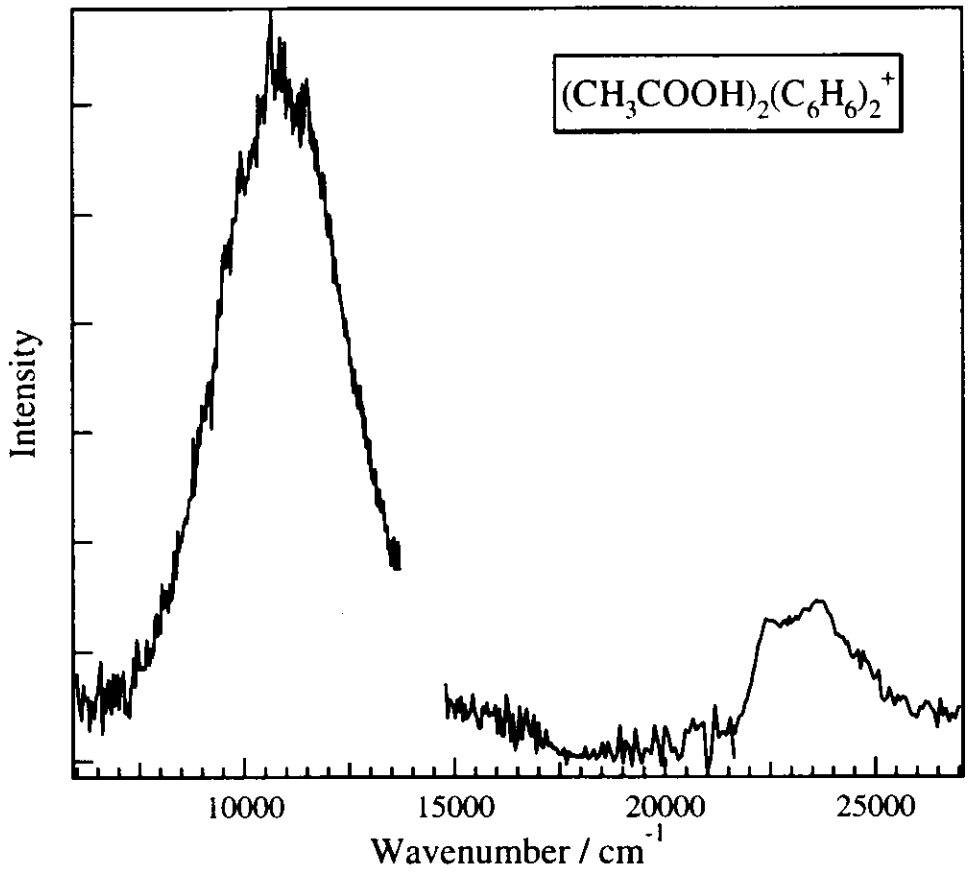

Figure V-5. Electronic spectrum of $(CH_3COOH)_2(C_6H_6)_2^+$.

V.C.4. Vibrational spectrum of $(CH_3COOH)_2 \cdot (C_6H_6)_2^+$

Figure V-6 shows the vibrational spectrum of $(CH_3COOH)_2 \cdot (C_6H_6)_2^+$ in the region of 2750-3700 cm^{-1}. The spectrum is very complicated. However, it is obvious that no band appears in the O–H stretching vibrational region and several bands are located in the region under 3100 cm^{-1} with overlapping each other. For assignment of the vibrational bands, the vibrational spectrum of $(CD_3COOD)_2 \cdot (C_6H_6)_2^+$ is measured and is shown in Figure V-7. Only one band is observed at 3042 cm^{-1}.

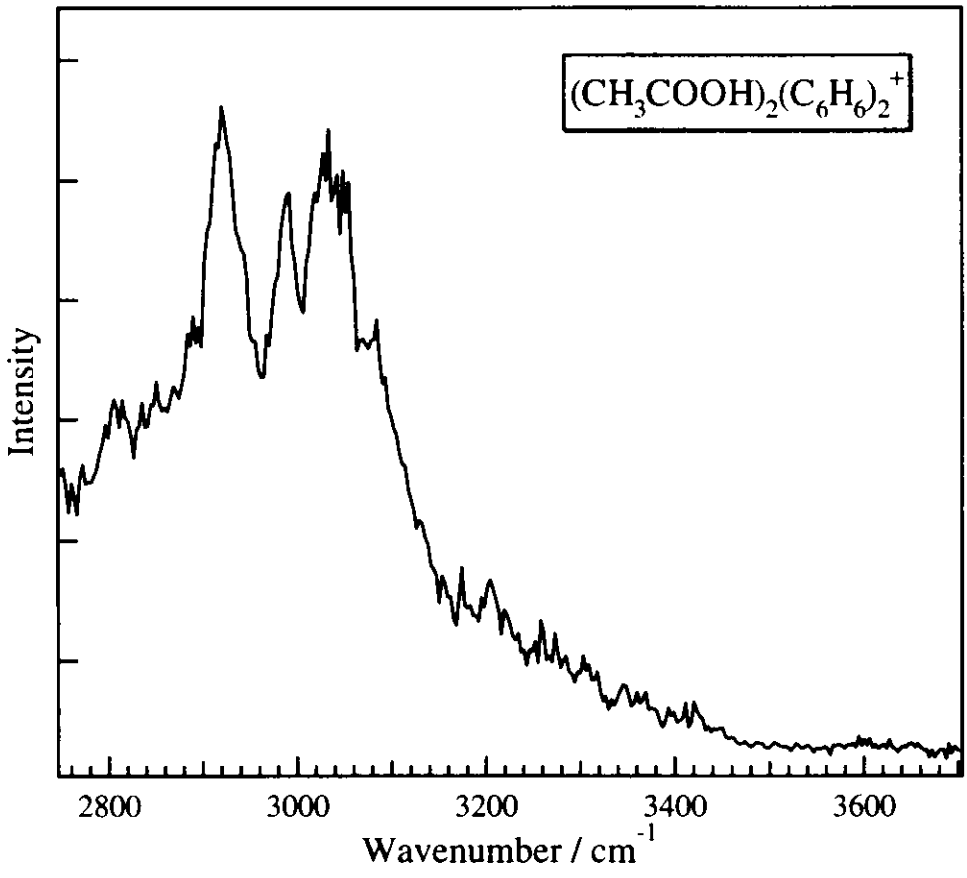

Figure V-6. Vibarational spectrum of $(CH_3COOH)_2(C_6H_6)_2^+$.

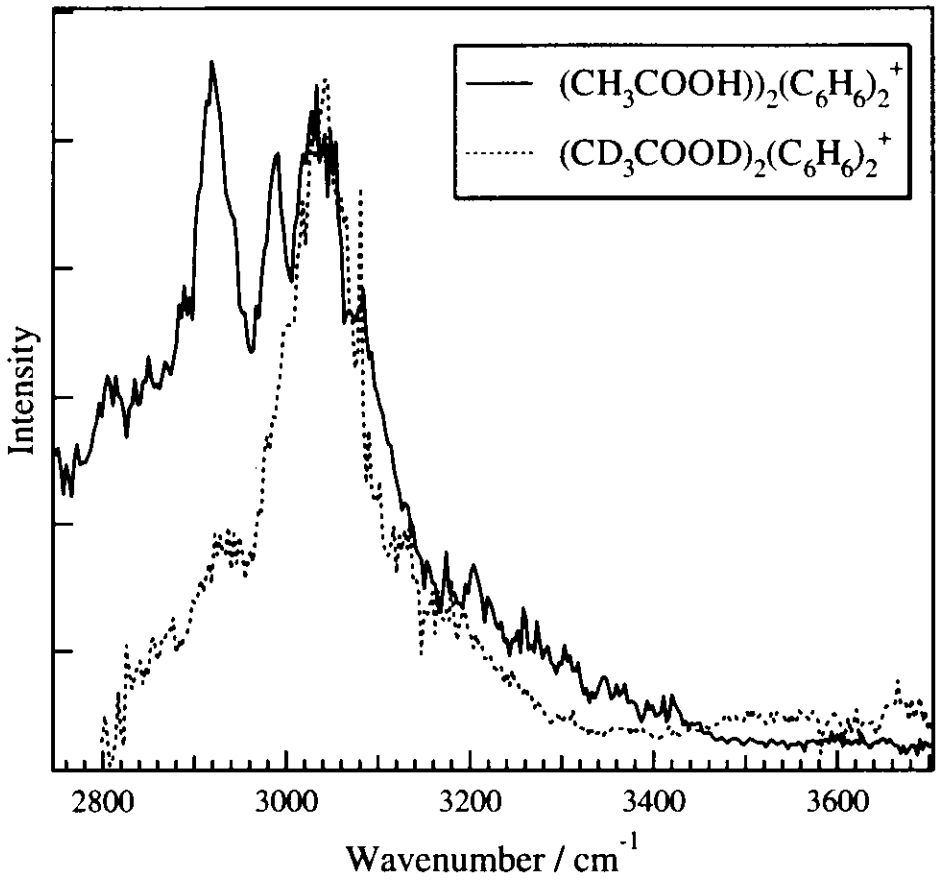

Figure V-7. Vibarational spectra of $(CH_3COOH)_2(C_6H_6)_2^+$ and $(CD_3COOD)_2(C_6H_6)_2^+$

V.D. Discussion

V.D.1. Structure of $(CH_3COOH)\cdot(C_6H_6)_2^+$

The electronic spectrum of $(CH_3COOH)\cdot(C_6H_6)_2^+$ has a very strong band in the near-IR region and a relatively weak band in the visible region as shown in Figure V-2. This feature is similar to that of benzene dimer cation, $(C_6H_6)_2^+$. In the electronic spectrum of benzene dimer cation, charge resonance (CR) bands are observed in the near-IR region with strong intensities and a local excitation (LE) band is located in the visible region with a relatively weak intensity. [5, 6, 10] In addition, one can not expect any band originated from acetic acid in this region. Therefore the strong band at 11000 cm^{-1} and relatively weak band at 23500 cm^{-1} are assigned to the CR and LE bands of benzene dimer cation in $(CH_3COOH)\cdot(C_6H_6)_2^+$, respectively. This suggests that the ion core of $(CH_3COOH)\cdot(C_6H_6)_2^+$ is benzene dimer cation. This is reasonable, since the ionization potential of benzene is 9.24 eV and is smaller than that of acetic acid (10.24 eV). The energies of the CR and LE bands of $(CH_3COOH)\cdot(C_6H_6)_2^+$ are close to those of benzene dimer cation and no band which is not observed in the electronic spectrum of benzene dimer cation appears. These facts indicate that the electronic structure of the ion core of $(CH_3COOH)\cdot(C_6H_6)_2^+$ is not disturbed by the acetic acid monomer as far as the observed species concerns. In other words, the intermolecular interaction between the ion core and the solvent molecule cannot be charge transfer interaction that is seen in

$(CH_3COOH)\cdot(C_6H_6)^+$ [27].

The band at 3084 cm^{-1} is solely observed in the vibrational spectrum of $(CD_3COOD)\cdot(C_6H_6)_2^+$, while the spectrum of $(CH_3COOH)\cdot(C_6H_6)_2^+$ shows other two bands in the O–H stretching region in addition to the same band. (Figure V-4) This indicates that the band at 3084 cm^{-1} originates from the benzene dimer cation and the other two bands observed in the O–H stretching region are vibrations of acetic acid. Inokuchi and Nishi measured the vibrational spectrum of benzene dimer cation and reported that the frequency of the C–H stretching vibration of benzene dimer cation is 3080 cm^{-1} [28]. Therefore the band at 3084 cm^{-1} is assigned to the C–H stretching vibration of benzene dimer cation in $(CH_3COOH)\cdot(C_6H_6)_2^+$.

The appearance of the two bands at 3585 and 3627 cm^{-1} suggests the two possibilities of either the presence of two isomers or Fermi resonance intensity enhancement of a combination band. The latter possibility can be poor, because no Fermi resonance band is reported in this region for the component molecules [29, 30]. Thus the two bands can be originated from two distinct geometries of $(CH_3COOH)\cdot(C_6H_6)_2^+$. The O–H stretching vibration of an acetic acid monomer in the gas phase is observed at 3583 cm^{-1} by Haurie and Novak [29]. Therefore the band at 3585 cm^{-1} is assigned to the free O–H stretching vibration of acetic acid in $(CH_3COOH)\cdot(C_6H_6)_2^+$.

The frequency of the other O–H stretching vibration is 42 cm^{-1} higher than that of the band assigned above. This indicates that there is an isomer whose O–H bond has a larger force constant than that of acetic acid observed in the gas phase. There are two isomers for the acetic acid monomer: the

hydroxyl hydrogen and the carbonyl oxygen located on the same side of the C–O single bond (*cis*-isomer) and on the opposite side (*trans*-isomer). The hydroxyl group of the *cis*-isomer is stabilized due to intramolecular hydrogen-bonding interaction with the carbonyl oxygen. In contrast to this, the hydroxyl group of *trans*-isomer is almost free, therefore the O–H stretching frequency of the *trans*-isomer is expected to be higher than that of the *cis*-isomer. Turi and Dannenberg studied these isomers by ab initio molecular orbital calculations [31]. They reported the frequency of the O–H stretching vibration of the *trans*-isomer is 59.6 cm^{-1} higher than that of the *cis*-isomer at the MP2/6-31G(d) level. Thus the band at 3627 cm^{-1} can be assigned to the O–H stretching vibration of the *trans*-isomer in the cation complex. However, only the *cis*-isomer is observed in the vibrational spectrum of the acetic acid monomer because the ground state energy of the *trans*-isomer is higher than that of the *cis*-isomer. The energy difference was calculated to be 6.1 kcal/mol at the MP2/6-31G(d,p) level [31]. In the complex of $(CH_3COOH)\cdot(C_6H_6)_2^+$, one can expect the intermolecular interaction of the *trans*-isomers with the benzene dimer cation at the oxygen atoms of the carbonyl and the hydroxyl groups, since the *trans*-isomer has the space faced by the two oxygen atoms for the complex formation. In this case, the total energy of the cluster with the *trans*-isomer can be lowered much more than that with the *cis*-isomer. In an isomer of $(CH_3COOH)\cdot(C_6H_6)^+$, the *trans*-isomer of acetic acid and benzene cation are bound each other by charge transfer interaction [27]. In $(CH_3COOH)\cdot(C_6H_6)_2^+$, however, the possibility of the charge transfer complex

is denied by the discussion mentioned above. Although there is not any further evidence, the geometry where two oxygen atoms of *trans*-acetic acid interact with the respective benzene rings of benzene dimer cation can be responsible for the 3627 cm^{-1} band.

V.D.2. Structure of $(CH_3COOH)_2 \cdot (C_6H_6)_2^+$

Electronic spectrum of $(CH_3COOH)_2 \cdot (C_6H_6)_2^+$ also shows a strong band in the near-IR region and a relatively weak band in the visible region and is similar to those of $(CH_3COOH) \cdot (C_6H_6)_2^+$ and benzene dimer cation. [5, 6, 10] This suggest the ion core of $(CH_3COOH)_2 \cdot (C_6H_6)_2^+$ is benzene dimer cation and the electronic structure of the ion core is not affected by solvent acetic acid molecules. The strong band at 10850 cm^{-1} is assigned to the CR band of benzene dimer cation in $(CH_3COOH)_2 \cdot (C_6H_6)_2^+$. The relatively weak band at 23600 cm^{-1} is assigned to the LE band of benzene dimer cation in $(CH_3COOH)_2 \cdot (C_6H_6)_2^+$.

In the vibrational spectrum of $(CH_3COOH)_2 \cdot (C_6H_6)_2^+$, no band is observed in the O–H stretching vibrational region and several bands appear with overlapping each other in the region around 3000 cm^{-1}. The vibrational spectrum of $(CD_3COOD)_2 \cdot (C_6H_6)_2^+$ shows only one band at 3042 cm^{-1}. This reveals that the band at 3042 cm^{-1} is a vibration of benzene dimer cation and the other bands originate from solvent acetic acid molecules. The band at 3042 cm^{-1} is assigned to the C–H stretching vibration of benzene dimer cation in $(CH_3COOH)_2 \cdot (C_6H_6)_2^+$. Although the spectral pattern of solvent acetic acid molecules is very complicated, it is clear that the free O–H stretching vibration is not observed. Therefore both two hydroxyl groups of $(CH_3COOH)_2 \cdot (C_6H_6)_2^+$ participate in intermolecular hydrogen-bonds as proton donors. There are two possibilities for hydrogen bond formation. One is the hydrogen-bonding between acetic acid molecules and benzene

dimer cation. The other is acetic acid dimer formation. However, the benzene dimer is the positively charged ion core of $(CH_3COOH)_2 \cdot (C_6H_6)_2^+$. Thus it is unlikely that the benzene ring participates intermolecular hydrogen-bonding as a proton acceptor. We can be fairly certain that the dimerization of acetic acid occurs in $(CH_3COOH)_2 \cdot (C_6H_6)_2^+$.

There are several geometrical structures for acetic acid dimer. We carried out ab initio molecular orbital calculations on four dimer species, all of which contain two intermolecular hydrogen bonds [32]. The structures of the dimer species are shown in Figure V-8. The most stable dimer species are the cyclic dimer where two O–H···O=C hydrogen bond are formed. The hydrogen-bonding energy of the cyclic dimer is –12.31 kcal/mol after correction for zero-point vibrational energy. The stability of the cyclic dimer is outstanding among the four dimer species. The result is consistent with a large number of references which report that the gaseous acetic acid undergoes a dimerization reaction to form cyclic structures containing two equivalent O–H···O=C hydrogen bonds [33-36]. Therefore the cyclic dimer can be formed and weakly interact with the benzene dimer cation in $(CH_3COOH)_2 \cdot (C_6H_6)_2^+$.

The vibrational spectra of acetic acid have been observed in the region over room temperature [29, 30, 37, 38]. Vibrational bands attributed to the O–H stretching vibration are observed in the region around 3000 cm^{-1}. However, the vibrational bands are so broad because of high temperatures that the spectral features are ambiguous. To the best of our knowledge, any vibrational spectrum of acetic acid in supersonic jet have not been reported

yet. Halupka and Sander observed the vibrational spectrum of acetic acid in argon matrix at 7 K [39]. Because this is the vibrational spectrum of the cyclic dimer of acetic acid observed at the lowest temperature and the effect of the argon matrix on the frequencies of the O–H stretching vibration of the cyclic dimer can be small, we compare this spectrum with that of $(CH_3COOH)_2{\cdot}(C_6H_6)_2^+$. Figure V-9 shows the vibrational spectrum by the matrix isolation (dotted line) with those of $(CH_3COOH)_2{\cdot}(C_6H_6)_2^+$ (solid line) and $(CD_3COOD)_2{\cdot}(C_6H_6)_2^+$ (dashed line). Although there are small gaps in vibrational frequency, one can interpret the vibrational spectrum of $(CH_3COOH)_2{\cdot}(C_6H_6)_2^+$ as a superposition of that of acetic acid cyclic dimer and the C–H stretching band of benzene dimer cation. This indicates that the benzene dimer cation and the cyclic dimer of acetic acid co-exist and weakly interact each other in $(CH_3COOH)_2{\cdot}(C_6H_6)_2^+$.

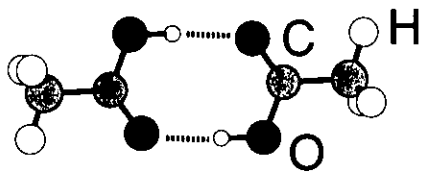

Dimer 1(cyclic dimer)

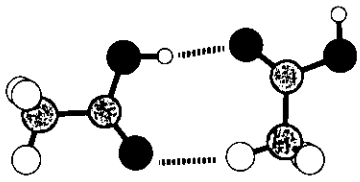

Dimer 2 (crystal-like dimer)

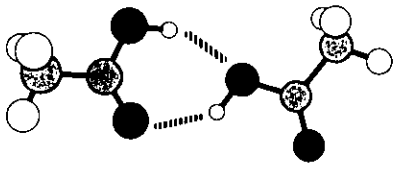

Dimer 3

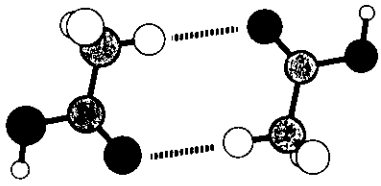

Dimer 4

Figure V-8. Four dimer species of acetic acid.

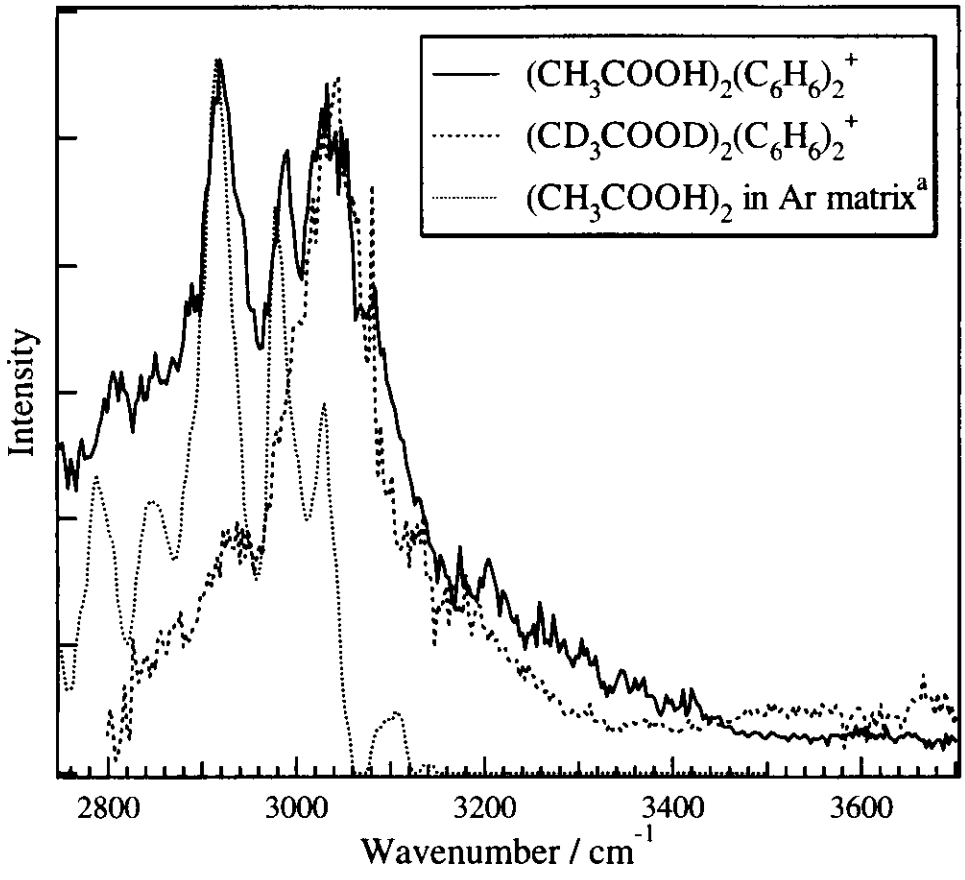

Figure V-9. Vibarational spectra of $(CH_3COOH)_2(C_6H_6)_2^+$ and $(CD_3COOD)_2(C_6H_6)_2^+$ with that of $(CH_3COOH)_2$ in argon matrix

[a] M. Halupka and W. Sander, Spectrochim. Acta Part A **54**, 495 (1998)

V.E. Conclusion

The geometrical and electronic structures of the acetic acid-benzene cluster cations, $(CH_3COOH)\cdot(C_6H_6)_2^+$ and $(CH_3COOH)_2\cdot(C_6H_6)_2^+$, were studied. The electronic and vibrational spectra of the cluster cations were observed by photodissociation spectroscopy. In order to make the origin of vibrational bands clear, the vibrational spectra of $(CD_3COOD)\cdot(C_6H_6)_2^+$ and $(CD_3COOD)_2\cdot(C_6H_6)_2^+$ were also measured. The electronic spectrum of $(CH_3COOH)\cdot(C_6H_6)_2^+$ in the region of 5920-24540 cm^{-1} shows two bands; the charge resonance band in the near-IR region and the local excitation band in the visible region. The spectral feature is similar to that of the benzene dimer cation. The vibrational spectrum of $(CH_3COOH)\cdot(C_6H_6)_2^+$ in the region of 2800-3700 cm^{-1} was also observed. Two O–H stretching bands that appear in the spectrum are assigned to the *cis*- and *trans*-isomers of acetic acid in the cluster cation. These results suggest that $(CH_3COOH)\cdot(C_6H_6)_2^+$ has two isomers where the *cis*- or *trans*-isomer of acetic acid interacts with the benzene dimer cation. The electronic spectrum of $(CH_3COOH)_2\cdot(C_6H_6)_2^+$ in the region of 5950-27000 cm^{-1} also shows the charge resonance and local excitation bands and resembles that of the benzene dimer cation. The vibrational spectrum of $(CH_3COOH)_2\cdot(C_6H_6)_2^+$ in the region of 2750-3700 cm^{-1} is interpreted as a superposition of that of the acetic acid cyclic dimer and the C–H stretching band of the benzene dimer cation. This indicates that the benzene dimer cation and the cyclic dimer of acetic acid weakly interact each other in $(CH_3COOH)_2\cdot(C_6H_6)_2^+$.

References for chapter V

[1] A. Ishitani and S. Nagakura, Mol. Phys. **12**, 526 (1967).

[2] B. Badger and B. Brockhurst, Trans. Faraday Soc. **65**, 2582 (1969).

[3] T. Shida, Electronic absorption spectra of radical ions, Elsevier, Amsterdam, p. 12 (1988).

[4] J. T. Snodgrass, R. C. Dunbar, and M. T. Bowers, J. Phys. Chem. **94**, 3648 (1990).

[5] K. Ohashi and N. Nishi, J. Chem. Phys. **95**, 4002 (1991).

[6] K. Ohashi and N. Nishi, J. Phys. Chem. **96**, 2931 (1992).

[7] Y. Nakai, K. Ohashi and N. Nishi, J. Phys. Chem. **96**, 7873 (1992).

[8] S. M. Beck and J. H. Hecht, J. Chem. Phys. **96**, 1975 (1992).

[9] K. Ohashi and N. Nishi, J. Chem. Phys. **98**, 390 (1993).

[10] K. Ohashi, Y. Nakai, T. Shibata, and N. Nishi, Laser Chem. **14**, 3 (1993).

[11] T. Shibata, K. Ohsshi, Y. Nakai, and N. Nishi, Chem. Phys. Lett. **229**, 604 (1994).

[12] K. Ohashi, Y. Nakai, and N. Nishi, Laser Chem. **15**, 93 (1995).

[13] K. Ohashi, Y. Inokuchi, and N. Nishi, Chem. Phys. Lett. **263**, 167 (1996).

[14] Y. Nakai, K. Ohashi, and N. Nishi, J. Phys. Chem. **101**, 472 (1997).

[15] Y. Nakai, K. Ohashi, and N. Nishi, Chem. Phys. Lett. **233**, 36 (1995).

[16] B. Meot-Ner (Mautner), J. Phys. Chem. **84**, 2724 (1980).

[17] A. Kiermeier, B. Ernstberger, H. J. Neusser, and E. W. Schlag, J.

Phys. Chem. **92**, 3785 (1988).

[18] B. Ernstberger, H. Krause, A. Kiermeier, and H. J. Neusser, J. Chem. Phys. **92**, 5285 (1985).

[19] H. Krause, B. Ernstberger, and H. J. Neusser, Chem. Phys. Lett. **184**, 411 (1991).

[20] B. Ernstberger, H. Krause, and H. J. Neusser, Z. Phys. **D 20**, 189 (1991).

[21] H. Krause, B. Ernstberger, and H. J. Neusser, Ber. Bunsenges. Phys. Phys. Chem. **96**, 1183 (1992).

[22] B. Ernstberger, H. Krause, and H. J. Neusser, Ber. Bunsenges. Phys. Phys. Chem. **97**, 884 (1993).

[23] K. Hiraoka, S. Fujimaki, K. Aruga, and S. Yamabe, J. Chem. Phys. **95**, 8413 (1991).

[24] E. Miyoshi, T. Ichikawa, T. Sumi, Y. Sakai, and N. Shida, Chem. Phys. Lett. **275**, 404 (1997).

[25] M. Matsumoto, Y. Inokuchi, K. Ohashi, and N. Nishi, J. Phys. Chem. A **101**, 4574 (1997).

[26] Y. Inokuchi, K. Ohashi, and N. Nishi, Chem. Phys. Lett. **279**, 73 (1997).

[27] K. Kosugi, Y. Inokuchi, and N. Nishi, J. Chem. Phys. **114**, 4805 (2001).

[28] Y. Inokuchi and N. Nishi, J. Chem. Phys. **114**, 7059 (2001).

[29] W. Weltner, J. Am. Chem. Soc. **77**, 3941 (1955).

[30] M. Haurie and A. Novak, J. Chim. Phys. **62**, 137 (1965).

[31] L. Turi and J. J. Dannenberg, J. Phys. Chem. **97**, 12197 (1993).

[32] T. Nakabayashi, K. Kosugi, and N. Nishi, J. Phys. Chem. A **103**, 8595

(1999).

[33] M. D. Taylor, J. Am. Chem. Soc. 73, 315 (1951).

[34] D. J. Frurip, L. A. Curtiss, and M. Blander, J. Am. Chem. Soc. 102, 2610 (1980).

[35] J. Karle and L. O. Brockway, J. Am. Chem. Soc. 66, 574 (1944).

[36] J. L. Derissen, J. Mol. Struct. 7, 67 (1971).

[37] J. K. Wilmshurst, J. Chem. Phys. 25, 1171 (1956).

[38] P. Excoffon and U. Marechal, Spectrochim. Acta Part A 28, 269 (1972).

[39] M. Halupka and W. Sander, Spectrochim. Acta Part A 54, 495 (1998).

Acknowledgement

本研究の遂行ならびに博士論文の作成におきまして，常に適切な御指導御鞭撻を賜りました分子科学研究所・総合研究大学院大学の西信之教授に心より感謝申し上げます．西教授からは，科学研究の技法のみならず，自然を探究することの面白さや研究をする上での心構えなど，研究生活全般にわたって多くのことを学ばせていただきました．ここに重ねて御礼申し上げます．

酢酸およびその水溶液の液体構造に関する研究（Chapter II & III）において，有益な助言と議論をしてくださいました分子科学研究所・総合研究大学院大学の中林孝和博士に心より感謝いたします．中林博士には，特に溶液科学と分子軌道法に関して多くのことを教えていただきました．重ねて御礼申し上げます．

気相における酢酸とベンゼンカチオンとの分子間相互作用に関する研究（Chapter IV & V）において，常に適切な助言をしてくださいました分子科学研究所・総合研究大学院大学の井口佳哉博士に心より感謝いたします．井口博士には，飛行時間型質量分析装置の立ち上げから，光解離スペクトルの測定・解析まで，大変お世話になりました．重ねて御礼申し上げます．

酢酸・ベンゼン２量体カチオンクラスターの電子スペクトルの測定（Chapter V）の際に約１ヶ月もの長い間貴重なマシンタイムを都合してレーザーシステムを使用させていただきました分子科学研究所・総合研究大学院大学の藤井正明教授ならびに藤井研究室の皆様に心より感謝いたします．また，藤井教授には，博士論文の査読をしていただき，有益な助言を頂きました．重ねて御礼申し上げます．

博士論文の提出に際して，ご多忙の中貴重な時間を割いて著者の拙文を懇切丁寧に査読していただきました九州大学の関谷博教授に心より感謝いたします．関谷教授には，学会発表の折にも度々有益な助言を頂きました．重ねて御礼申し上げます．

九州大学の大橋和彦助教授には，飛行時間型質量分析装置の製作に際して，豊富な経験をもとに装置の原案を作成していただきました．心より御礼申し上げます．

分子科学研究所電子構造研究系の皆様には，研究生活全般にわたって大変お世話になりました．心より御礼申し上げます．

最後に，研究生活の精神的支えになってくれた，両親，祖母，そして弟達家族に，感謝いたします．

List of Publications

1. "Charge transfer interaction in acetic acid-benzene cation complex"
Kentaroh Kosugi, Yoshiya Inokuchi, and Nobuyuki Nishi
J. Chem. Phys., **114**, 4805-4816 (2001).

2. "Raman Spectroscopic Study on Acetic Acid Clusters in Aqueous Solutions: Dominance of Acid-Acid Association Producing Microphases"
Nobuyuki Nishi, Takakazu Nakabayashi, and Kentaroh Kosugi
J. Phys. Chem. A **103**, 10851-10858 (1999).

3. "Liquid Structure of Acetic Acid Studied by Raman Spectroscopy and Ab Initio Molecular Orbital Calculations"
Takakazu Nakabayashi, Kentaroh Kosugi, and Nobuyuki Nishi
J. Phys. Chem. A **103**, 8595-8603 (1999).

4. "Low-frequency Raman spectra of crystalline and liquid acetic acid and its mixtures with water. Is the liquid dominated by hydrogen-bonded cyclic dimers?"
Kentaroh Kosugi, Takakazu Nakabayashi, and Nobuyuki Nishi
Chem. Phys. Lett. **291**, 253-261 (1998).

5. "Electronic Spectra of Jet-Cooled Anthracene Dimer: Evidence of Two Isomers in the Electronic Ground State"
Tomohiro Matsuoka, Kentaro Kosugi, Kazuyuki Hino, Masaharu Nishiguchi, Kazuhiko Ohashi, Nobuyuki Nishi, and Hiroshi Sekiya
J. Phys. Chem. A **102**, 7598-7602 (1998).